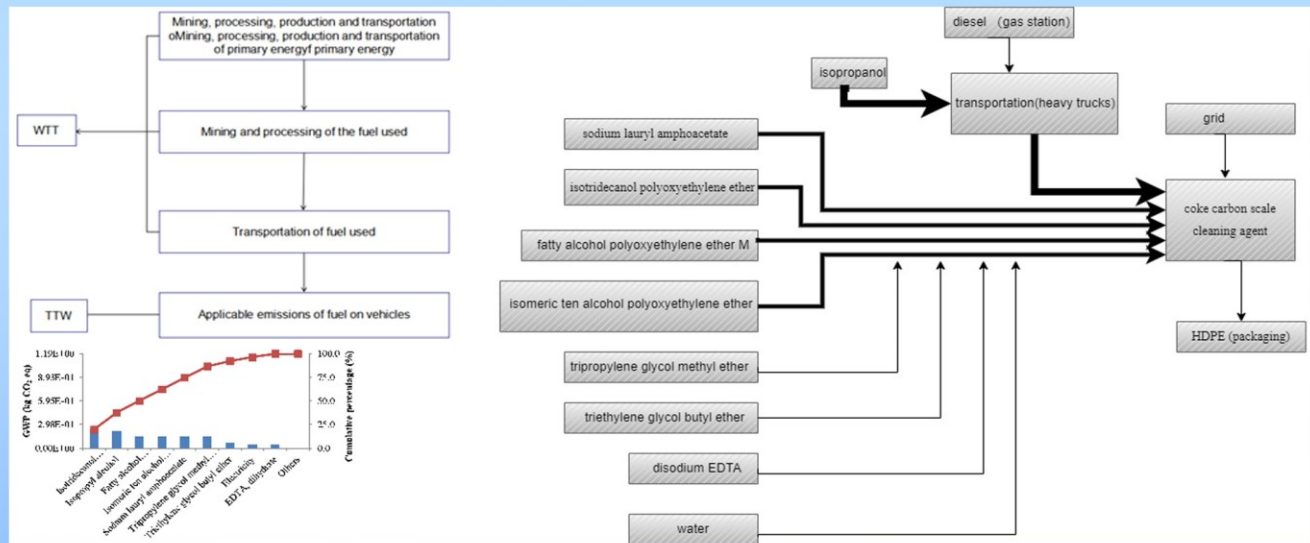


# Trends in Renewable Energy

Volume 8, Issue 1, March 2022



Cover image: Life Cycle Assessment of Hydrogen Internal Combustion Engine Vehicles and Coke Cleaning Agent , see articles by Guo et al. and Gong et al. in this issue, respectively.

# Trends in Renewable Energy

ISSN: 2376-2136 (Print) ISSN: 2376-2144 (Online)

<http://futureenergysp.com/>

---

Trends in Renewable Energy is an open accessed, peer-reviewed semi-annual journal publishing reviews and research papers in the field of renewable energy technology and science.

The aim of this journal is to provide a communication platform that is run exclusively by scientists working in the renewable energy field. Scope of the journal covers: Bioenergy, Biofuel, Biomass, Bioprocessing, Biorefinery, Biological waste treatment, Catalysis for energy generation, Energy conservation, Energy delivery, Energy resources, Energy storage, Energy transformation, Environmental impact, Feedstock utilization, Future energy development, Green chemistry, Green energy, Microbial products, Physico-chemical process for Biomass, Policy, Pollution, Renewable energy, Smart grid, Thermo-chemical processes for biomass, etc.

The Trends in Renewable Energy publishes the following article types: peer-reviewed reviews, mini-reviews, technical notes, short-form research papers, and original research papers.

*The article processing charge (APC), also known as a publication fee, is fully waived for the Trends in Renewable Energy.*

## Editorial Team of Trends in Renewable Energy

### EDITOR-IN-CHIEF

Dr. Bo Zhang

Prof., School of Chemical Engineering & Pharmacy, Wuhan Institute of Technology, China

Dr. Changyan Yang

Prof., School of Chemical Engineering & Pharmacy, Wuhan Institute of Technology, China

### HONORARY CHAIRMEN

Dr. Yong Wang

Voiland Distinguished Professor, The Gene and Linda Voiland School of Chemical Engineering and Bioengineering, Washington State University, United States

Dr. Mahendra Singh Sodha

Professor, Lucknow University; Former Vice Chancellor of Devi Ahilya University, Lucknow University, and Barkatulla University; Professor/Dean/HOD/Deputy Director at IIT Delhi; Padma Shri Award; India Professor of Industrial Chemistry, CEO of Eurochem Engineering srl, Italy

Dr. Elio Santacesaria

### VICE CHAIRMEN

Dr. Mo Xian

Prof., Assistant Director, Qingdao Institute of BioEnergy and Bioprocess Technology, Chinese Academy of Sciences, China

### EDITORS

Dr. Yiu Fai Tsang,

Associate Prof., Department of Science and Environmental Studies, The Education University of Hong Kong

Dr. Melanie Sattler

Dr. Syed Qasim Endowed Professor, Dept. of Civil Engineering, University of Texas at Arlington, United States

Dr. Attila Bai

Associate Prof., University of Debrecen, Hungary

Prof. Christophe Pierre Ménézo

University of Savoy Mont-Blanc, France

Dr. Moinuddin Sarker

MCIC, FICER, MInstP, MRSC, FARSS., VP of R & D, Head of Science/Technology Team, Natural State Research, Inc., United States Associate Prof., Biomass Processing Laboratory, Centre for Biofuel and Biochemical Research, Green Technology Mission Oriented Research, Universiti Teknologi PETRONAS, Malaysia

Dr. Suzana Yusup

Global Technology Development, Monsanto Company, United States

Dr. Zewei Miao

Pfizer Inc., United States

Dr. Hui Wang

North Carolina Agricultural and Technical State University, United States

Dr. Shuangning Xiu

Associate Prof., Institute of Chemical Industry of Forest Products, China

Dr. Junming XU

Academy of Forest, China

Dr. Hui Yang

Prof., College of Materials Science and Engineering, Nanjing Tech University, China

Dr. Ying Zhang

Associate Prof., School of Chemistry and Materials Science, University of Science and Technology of China, China

Dr. Ming-Jun Zhu

Prof., Assistant Dean, School of Bioscience & Bioengineering, South China University of Technology, China

### EDITORIAL BOARD

Dr. Risabh Dev Shukla

Dean and Associate Prof., Department of Electrical Engineering, Budge Budge Institute of Technology Kolkata, India

Dr. Neeraj Gupta

Indian Institute of Technology Roorkee, India

Dr. Elena Lucchi	Politecnico di Milano, Italy
Dr. Muhammad Mujtaba Asad	Faculty of Technical and Vocational Education, Universiti Tun Hussein Onn Malaysia, Malaysia
Dr. Afzal Sikander	Department of Instrumentation and Control Engineering, Dr. B. R. Ambedkar National Institute of Technology, India
Dr. Padmanabh Thakur	Professor and Head, Department of Electrical Engineering, Graphic Era University, India
Dr. K. DHAYALINI	Professor, Department of Electrical and Electronics Engineering, K. Ramakrishnan College of Engineering, Tamilnadu, India
Shangxian Xie	Texas A&M University, United States
Dr. Tanmoy Dutta	Sandia National Laboratories, United States
Dr. Efsthios Stefanos	Pontifical Catholic University of Ecuador, Faculty of Exact and Natural Sciences, School of Physical Sciences and Mathematics, Ecuador
Dr. Xin Wang	Miami University, United States
Dr. Rami El-Emam	Assist. Prof., Faculty of Engineering, Mansoura University, Egypt
Dr. Rameshprabu Ramaraj	School of Renewable Energy, Maejo University, Thailand
Dr. ZAFER ÖMER ÖZDEMİR	Kirklareli University, Technology Faculty, Turkey
Dr. Vijay Yeul	Chandrapur Super Thermal Power Station, India
Dr. Mohanakrishna Gunda	VITO - Flemish Institute for Technological Research, Belgium
Dr. Shuai Tan	Georgia Institute of Technology, United States
Shahabaldin Rezanian	Universiti Teknologi Malaysia (UTM), Malaysia
Dr. Madhu Sabnis	Contek Solutions LLC, Texas, United States
Dr. Qiang Yan	Mississippi State University, United States
Dr. Mustafa Tolga BALTA	Associate Prof., Department of Mechanical Engineering, Faculty of Engineering, Aksaray University, Turkey
Dr. María González Alriols	Associate Prof., Chemical and Environmental Engineering Department, University of the Basque Country, Spain
Dr. Nattaporn Chaiyat	Assist. Prof., School of Renewable Energy, Maejo University, Thailand
Dr. Nguyen Duc Luong	Institute of Environmental Science and Engineering, National University of Civil Engineering, Vietnam
Mohd Lias Bin Kamal	Faculty of Applied Science, Universiti Teknologi MARA, Malaysia
Dr. N.L. Panwar	Assistant Prof., Department of Renewable Energy Engineering, College of Technology and Engineering, Maharana Pratap University of Agriculture and Technology, India
Dr. Caio Fortes	BASF, Brazil
Dr. Flavio Praticco	Department of Methods and Models for Economics, Territory and Finance, Sapienza University of Rome, Italy
Dr. Wennan ZHANG	Docent (Associate Prof.) and Senior Lecturer in Energy Engineering, Mid Sweden University, Sweden
Dr. Ing. Stamatis S. Kalligeros	Associate Prof., Hellenic Naval Academy, Greece
Carlos Rolz	Director of the Biochemical Engineering Center, Research Institute at Universidad del Valle, Guatemala
Ms. Liliash Makashini	Copperbelt University, Zambia
Dr. Ali Mostafaeipour	Assistant Prof., Industrial Engineering Department, Yazd University, Iran
Dr. Camila da Silva	Prof., Maringá State University, Brazil
Dr. Anna Skorek-Osikowska	Silesian University of Technology, Poland
Dr. Shek Atiqure Rahman	Sustainable and Renewable Energy Engineering, College of Engineering, University of Sharjah, Bangladesh
Dr. Emad J Elnajjar	Associate Prof., Department of Mechanical Engineering, United Arab Emirates University, United Arab Emirates
Dr. Seyed Soheil Mousavi Ajarostaghi	Babol Noshirvani University of Technology, Babol, Iran
Dr. Dinesh K. Sharma	National Ecology and Environment Foundation, India
Dr. Lakshmana Kumar Ramasamy	Department of Corporate relations, Hindusthan College of Engineering and Technology, India
Dr. S. Venkata Ramana	SUSU/National Research University, Russian Federation
Dr. Priyanka Marathey	Department of Solar Energy, Pandit Deendayal Petroleum University, India
Osamah Siddiqui	University of Ontario Institute of Technology, Canada

Dr. Rupendra Kumar Pachauri	Assistant Prof., Electrical and Electronics Engineering Department, University of Petroleum and Energy Studies, India
Dr. Jun Mei	School of Chemistry and Physics, Science and Engineering Faculty, Queensland University of Technology, Australia
Dr. Valeria Di Sarli	Institute for Research on Combustion, National Research Council of Italy, Italy
Dr. Utkucan Şahin	Assistant Prof., Department of Energy Systems Engineering, Faculty of Technology, Muğla Sıtkı Koçman University, Turkey
Dr. ALIASHIM ALBANI	School of Ocean Engineering, Universiti Malaysia Terengganu, Malaysia
Dr. Ashwini Kumar	Assistant Prof., College of Engineering, HSBPVT's Parikrama Group of Institutions, India
Dr. Hasan AYDOGAN	Associate Prof., Mechanical Engineering Department, Selcuk University, Turkey
Dr. Jiekang Wu	Professor, School of Automation, Guangdong University of Technology, China
Dr. Ong Huei Ruey	DRB-HICOM University of Automotive, Malaysia
Dr. Miguel Ángel Reyes Belmonte	IMDEA Energy Institute, Spain
Dr. Chitra Venugopal	Associate Professor in Electrical Engineering, University of Trinidad and Tobago, Trinidad
Dr. Amit Kumar Singh	Assistant Prof., Instrumentation & Control Engineering Department, Dr. B.R.A. National Institute of Technology, India
Dr. Suvanjan Bhattacharyya	University of Pretoria, South Africa
Dr. Karunesh Tiwari	Babu Banarasi Das University, India
Dr. Sharadrao A. Vhanalkar	Karmaveer Hire Arts, Science, Commerce and Education College, India
Dr. Prasenjit Chatterjee	Assistant Prof. and Head, MCKV Institute of Engineering, India
Dr. S. Balamurugan	Mindnotix Technologies, India
Dr. Mohammad Nurunnabi	University of Oxford, United Kingdom
Dr. Kenneth Okedu	Caledonian College of Engineering, Oman
Dr. Cheng Zhang	Sr. Materials Engineer, Medtronic, Inc., United States
Dr. Chandani Sharma	Assistant Prof., Department of Electrical Engineering, Graphic Era University, India
Dr. Kashif Irshad	Assistant Prof., Mechanical Engineering Department, King Khalid University, Saudi Arabia
Dr. Abhijit Bhagavatula	Principal Lead Engineer, Southern Company Services, United States
Dr. S. Sathish	Associate Prof., Department of Mechanical Engineering, Hindustan University, India
Mr. A. Avinash	Assistant Prof., KPR Institute of Engineering & Technology, India
Dr. Bindeshwar Singh	Assistant Prof., Kamla Nehru Institute of Technology, India
Dr. Yashar Hashemi	Tehran Regional Electric Company, Iran
Dr. Navanietha Krishnaraj R	South Dakota School of Mines and Technology, United States
Dr. SANDEEP GUPTA	JECRC University, India
Dr. Shwetank Avikal	Graphic Era Hill University, India
Dr. Xianglin Zhai	Poochon Scientific LLC, United States
Dr. Rui Li	Associate Prof., College of Engineering, China Agricultural University, China
Dr. Adam Elhag Ahmed	National Nutrition Policy Chair, Department of Community Services, College of Applied Medical Sciences, King Saud University, Saudi Arabia
Dr. Jingbo Li	Massachusetts Institute of Technology, United States
Dr. Srikanth Mutnuri	Associate Prof., Department of Biological Sciences, Associate Dean for International Programmes and Collaboration, Birla Institute of Technology & Science, India
Dr. Bashar Malkawi	Global Professor of Practice in Law, James E. Rogers College of Law, University of Arizona, United States
Dr. Simona Silvia Merola	Istituto Motori - National Research Council of Naples, Italy
Dr. Hakan Caliskan	Faculty of Engineering, Department of Mechanical Engineering, Usak University, Turkey
Dr. Umashankar Subramaniam	Associate Prof., College of Engineering, Prince Sultan University, Saudi Arabia
Dr. Tayfun GÜNDOĞDU	Faculty of Electrical and Electronic Engineering, Department of Electrical Engineering, Istanbul Technical University, Turkey
Dr. Yukesh Kannah R	Department of Civil Engineering, Anna University Regional Campus, India

Jean Bosco Mugiraneza  
Dr. R. Parameshwaran

Dr. Endong Wang

Dr. Jianxin Xu

Dr. Qingtai Xiao

University of Rwanda, Rwanda  
Assistant Prof., Dept. of Mechanical Engineering, Birla Institute of Technology  
& Science (BITS-Pilani), India  
Associate Prof., Department of Sustainable Resources Management, College  
of Environmental Science and Forestry, State University of New York (SUNY-  
ESF), USA  
Prof., Faculty of metallurgy and energy engineering, Kunming University of  
Science and Technology, China  
Distinguished Associate Prof., Department of Energy and Power Engineering,  
Kunming University of Science and Technology, China

## Table of Contents

### Volume 8, Issue 1, March 2022

#### Articles

##### **Modeling and Performance Investigations of Partially Shaded Solar PV Arrays with Cell Partition**

##### **Technique based Modules**

V Bala Raju, Ch Chengaiah.....1-26

##### **Study of hydrogen internal combustion engine vehicles based on the whole life cycle evaluation method**

Ping Guo, Jianlun Xu, Chuanhao Zhao, Baoliang Zhang.....27-37

##### **Life Cycle Assessment of a Coke Cleaning Agent**

Yu Gong, Changyan Yang, Yinhang Qu, Jiayi Li, Bohan Yang, Yigang Ding, Bo Zhang .....67-83

#### Reviews

##### **Introduction of Abnormal Combustion in Hydrogen Internal Combustion Engines and the Detection**

##### **Method**

Jiahui Liu.....38-48

##### **Energy Conversion and Conservation Technology in Facing Net Zero-Emission Conditions and**

##### **Supporting National Defense**

Abdi Manab Idris, Nugroho Adi Sasongko, Yanif Dwi Kuntjoro.....49-66

# Modeling and Performance Investigations of Partially Shaded Solar PV Arrays with Cell Partition Technique based Modules

V. Bala Raju\*, Dr. Ch. Chengaiah

*Department of Electrical and Electronics Engineering, Sri Venkateswara University College of Engineering, Tirupati, India*

Received September 29, 2021; Accepted October 25, 2021; Published November 25, 2021

Solar photovoltaic (PV) modules consist of solar cells connected in series to provide the required output power. The solar PV system is experiencing major challenges, which are mainly due to the partial shadows on the photovoltaic modules leading to mismatching power loss and hot spot problems. Hotspots have become a major cause of PV module failure. The Cell Partition Technique (CPT) is proposed to reduce hotspots and minimize mismatch losses caused by partial shadings. Specifically, each solar PV cell (Full cell) in a solar PV module is divided or partitioned into two half cells (known as Half-Cut Cells or HC) and three equal cells (known as Tri-Cut Cells or TC) in accordance with the proposed technique. The HC and TC types of cells are connected in a strings of series-parallel connection, and bypass diode is placed in middle of the solar PV module to ensure proper operation. The primary aim of this research is to model, evaluate, and investigate the performance of solar PV arrays using new PV modules are developed based on Cell Partition Technique (PVM-CPT), such as half-cut cell modules (HCM), and tri-cut cell modules (TCM) and compared with full-sized cell modules (FCM). These PVM-CPT are connected in Series-Parallel (SP), Total-Cross-Tied (TCT), and proposed static shade dispersion based TCT reconfiguration (SD-TCTR) for the array sizes of 3x4, 4x3 and 4x4, respectively. The purpose is to select the most appropriate solar PV array configurations in terms of the highest global maximum power and thus the lowest mismatch power losses under short and narrow, short and wide, long and narrow, long and wide type of cell level partial shadings. The Matlab/Simulink software is used to simulate and analyze all of the shading cases. The results show that, when compared to conventional module configurations under different shading conditions, the proposed static SD-TCTR arrangement with TC modules (SDTCTR-TCM) exhibits the lowest mismatch power losses and the greatest improvement in array power.

*Keywords: Solar PV module; Full cell; Half cell; Tri cell; Array configurations; Static reconfigurations; Cell level shading conditions; Mismatch power losses*

## Introduction

Solar PV power generation is universally available, virtually endless, pollution-free, and simple to utilize [1]. The global photovoltaic (PV) market projection (2019–2023) anticipated a demand to rise by 12% to 144 GW in 2020, 10% to 158 GW in

\*Corresponding author: vbrajuu@gmail.com



2021, 7% to 169 GW in 2022, and 6% to 180 GW in 2023. We anticipate that the world's total installed capacity might reach as much as 1,610 GW by the end of 2023 under optimal conditions [2].

While there are a variety of problems that are impeding the advancement of PV generating technology, the inherent generation efficiency of PV cells in partial shadowing conditions is one of the most significant [3-6]. Controlling PV modules with maximum power point tracking (MPPT) technology is a key strategy for maximizing the efficiency of a particular PV array [7-8]. The hotspot effect happens when the maximum current generation capacity of one or more cells in a series-connected solar cell string is dropped to values below the module's operational current. In this situation, reverse bias across cells with lesser current induces heat dissipation. Although bypass diodes are extensively utilised to safeguard the cells, the hotspot effect remains a key failure mode for silicon solar modules. It is possible to reduce resistive losses in a solar module by cutting solar cells into two, and three parts which reduces the amount of current flowing in each cell. That's why PV module efficiency can be improved by reducing the amount of power loss. New technique, to improve efficiency and reduce overall power losses, and a hotspot effect a solar cell is split into two halves or three equal parts using a laser cutting known as the Cell Partition Technique (CPT), is introduced in this work. CPT has been proposed for the development of new solar photovoltaic modules. These solar PV modules have been named as PV modules developed based on the cell partition technique (PVM-CPT). CPT uses conventional solar cells that have been cut in half and one-third to generate electricity (*i.e.*, full cell is equally divided into two and three equal parts). Instead of having a single solar PV module with 36 or 60 or 72 full cells, the module could be divided into 72 or 120 or 144 half-sized cells and 108 or 180 or 216 tri-sized cells while maintaining the same design and dimensions as traditional modules, according to the manufacturer.

Electrical losses are calculated using the formula  $P_{\text{loss}}=I^2 \cdot R_s$ , which is equal to the square of the electrical current multiplied by the resistance [9-10]. If a solar cell is cut into half or one-third, it will produce half or one-third of the current, and the resistance is reduced to half or one-third of the full cell resistance. Due to the fact that the power loss is proportional to the current. The half-cut cell modules minimize the power loss by a factor of four, resulting in an increase in the power produced. However, there will be twice as many of them. As a result, if they are connected to operate in the same manner as a conventional solar module, the current would be the same, but the resistance will be reduced by half. Because of the lower resistance, electrical losses are reduced, and the module efficiency is increased. Thus, half-cut and tri-cut cells improve the performance, longevity, and shade tolerance of the PV module. When a solar cell in a module string is shaded, the energy produced by the un-shaded cells is transferred as heat into the shaded cell. This creates a hot spot that can damage the solar module if it persists. It can use twice as many module cell strings to reduce heat. The lower heat production should reduce damage to the solar PV module from hot spots and boost module longevity. In half-cell and tri-cell modules, bypass diodes are used to prevent power loss from occurring from the shaded area of the module rather than the complete module. It provides a replacement path for the current to travel in the un-shaded portion of the circuit and prevents the current from passing through the shaded portion of the circuit. It minimizes the impact of shade and improves the performance of the solar PV system under shading conditions [11-14].

In a conventional solar PV module, a number of solar cells are connected together to form a solar module with a predetermined wattage. In the Half-cut cell and Tri-cut cell type of partial cell modules, the full cells are cut into half and one-third, respectively, and then assembled to form the module with the specified wattage. Generally, the cells are cut with the help of laser technology. Losses that occur when current is transferred from one cell to another within a module are reduced as a result of this procedure. Cutting a solar cell into half or one-third pieces minimizes the resistance loss across the entire interconnected string of solar cells in a module, resulting in increased efficiency and power output. However, power loss is proportional to the square of the current. As a result, the power loss in a half cell and tri cell is decreased by a factor of four and nine respectively. By lowering the power loss, the fill factor can be raised, which increases the cell's ability to generate more current from the available light [15-17]. By using the proposed CPT, the standard 36, 60, or 72 number of full size cell modules are converted into 72, 120, or 144 number of half cell modules and 108, 180, or 216 number of tri cell modules. The new design decreases internal losses, resulting in enhanced performance in terms of energy yield, particularly during times of high irradiance.

Finally, the standard full-sized cell modules (FCM) and cell partition technique (CPT) based partial cell modules, *i.e.*, half-cut cell modules (HCM) and tri-cut cell modules (TCM) are connected in  $3 \times 4$ ,  $4 \times 3$ , and  $4 \times 4$  array sizes with series-parallel (SP), Total-Cross-Tied (TCT), and proposed static shade dispersion based TCT reconfigurations (SD-TCTR) arrangements, and the performance under various cell level shading conditions is investigated. The “Solar Cell” package component of Matlab/Simulink (version 2018a, MathWorks, USA) was built and proven to operate basic PV modules under normal conditions (STC- Standard Test Conditions). To simulate partial shade of a module comprised of half cut cells, Tri cut cells this study only uses the Matlab/Simulink component “Solar Cell”. The author did not intend to test the component because it was built on the validated double-diode replacement PV cell model. The literature has numerous concepts for modelling PV cells/modules.

The following is the structure of the paper. Section 2 describes the mathematical modeling of double diode solar PV cell and module. Section 3 presents the performance investigations of partial solar cell modules using the cell partition technique under cell level shading conditions, Section 4 discusses the proposed shade dispersion based TCT reconfiguration (SD-TCTR) using PVM-CPT in different arrays under SW, SN, LW and LN shadings. Finally, conclusions are drawn in Section 5.

## Mathematical Modeling of the Solar PV Cell and Module

### Modeling of a Double Diode PV Cell and Module

Figure 1(a) illustrates the equivalent model of the double diode photovoltaic cell. There are two anti-parallel diodes in the model, as well as series resistance and parallel resistance. Figure-1(b) shows the construction of a solar PV array, depicting the number of modules and the number of series-connected solar PV cells in each module in the array.

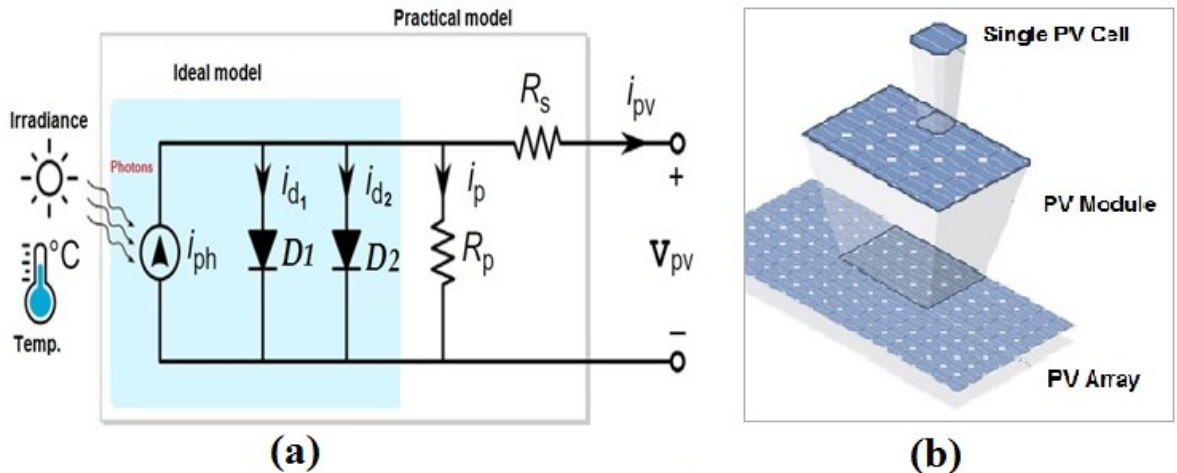


**Figure 1.** (a) Equivalent Double diode PV cell model. (b). Solar PV array with modules and cells

By applying Kirchhoff's current law for the PV cell model, the PV cell current is given in equation (1) [18].

$$i_{pv} = i_{ph} - i_{d1} - i_{d2} - i_p \dots \dots \dots (1)$$

where  $i_{ph}$  is the photocurrent when the PV cell is exposed to sunlight, the anti-parallel diode currents are  $i_{d1}$  and  $i_{d2}$ , and  $i_p$  represents the parallel resistor current. Substitute the expression for  $i_p$ ,  $i_{d1}$  and  $i_{d2}$  in Equation (1). Therefore, the cell current is derived as per Equation (2).

$$i_{pv} = i_{ph} - i_{s1} \left[ \exp\left(\frac{V_{pv} + i_{pv} R_s}{a_1 V_t}\right) - 1 \right] - i_{s2} \left[ \exp\left(\frac{V_{pv} + i_{pv} R_s}{a_2 V_t}\right) - 1 \right] - \left(\frac{V_{pv} + i_{pv} R_s}{R_p}\right) \dots (2)$$

where  $i_{s1}$  and  $i_{s2}$  are the reverse saturation currents of the diode  $D1$  and  $D2$ , respectively.  $V_t$  is the module thermal voltage and calculated as  $V_t = kT/q$ , where  $q$  is the electron charge with a value of  $1.602 \times 10^{-19}$  C, Boltzmann constant as  $k = 1.3806503 \times 10^{-23}$  J/K, and  $T$  is the cell temperature.  $R_p$  and  $R_s$  are parallel and series resistances, respectively. The  $a_1$  and  $a_2$  are the quality factors of the two diodes  $D1$  and  $D2$  used in the two-diode model, respectively.

The PV module is made up of solar PV cells which are connected in series and indicated by the symbol  $N_{se}$ . When  $N_{se}$  cells are linked in series, the output current ( $i_m$ ) of the PV module is expressed in terms of the output voltage ( $V_m$ ). Equation (3) represents the total current drawn from a PV module [12].

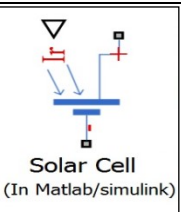
$$i_m = i_{ph} - i_{s1} \left[ \exp\left(\frac{q(V_m + i_m R_s)}{N_{se} a_1 K T}\right) - 1 \right] - i_{s2} \left[ \exp\left(\frac{q(V_m + i_m R_s)}{N_{se} a_2 K T}\right) - 1 \right] - \left(\frac{V_m + i_m R_s N_{se}}{N_{se} R_p}\right) \dots (3)$$

### Solar PV Cell Parameters

The parameters of solar cell are given in Table 1. In this paper, the solar PV modules based on cell partition technique (PVM-CPT) are developed by using two diode solar cells in the MATLAB-Simulink software. For designing a 40 W solar module with 36 number of solar cells (full sized cell), the open circuit voltage  $V_{oc}$  and short circuit

current  $I_{sc}$  of each solar cell is taken as 0.6083 V and 2.45 A, respectively. A solar cell's series resistance ( $R_s$ ) is 0.0079  $\Omega$  and its shunt resistance ( $R_{sh}$ ) is set to infinity (default value) in simulink tool (as shown in Figure 2). Half cut cell (HC) and Tri cut cell (TC) in the MATLAB-Simulink is developed by considering the short circuit current of each partition cell which is half and one third of full sized cell (FC). Characteristics are given in Table 1.

**Table 1.** Characteristics of solar cell used in a FC, HC, and TC PV modules

SNO	Parameters of cell	FC PV Module	HC PV Module	TC PV Module	Solar full cell in simulink
1	Short circuit current, $I_{sc}$ (A)	2.45	1.225	0.8166	 <p>Solar Cell (In Matlab/simulink)</p>
2	Open circuit voltage, $V_{oc}$ (V)	0.6083	0.6083	0.6083	
3	Irradiance used for measurements, $I_{rr}$ ( $W/m^2$ )	1000	1000	1000	
4	Temperature, $T$ ( $^{\circ}C$ )	25 $^{\circ}C$	25 $^{\circ}C$	25 $^{\circ}C$	
5	Quality factor, $N$	1.5	1.5	1.5	

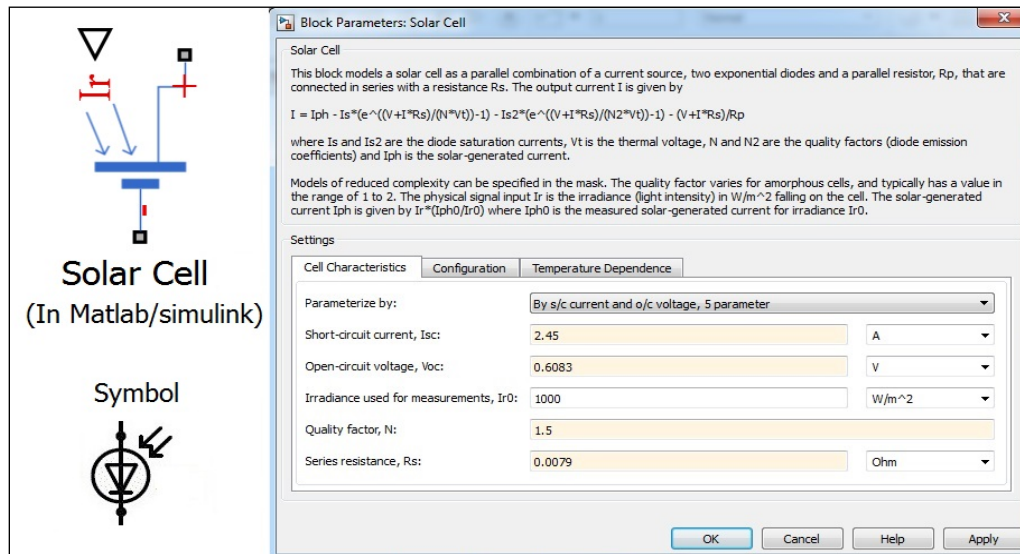


**Figure 2.** Parameters of solar PV full cell in the MATLAB-Simulink software

## Performance Investigations of Partial Solar Cell Modules Using Cell Partition Technique under Cell Level Shading Conditions

### Methodology: Cell Partition Technique (CPT)

In general, a solar PV module is made up of a number of solar cells (full-sized cells) that are connected together in series. A cell string is formed when a number of solar cells are connected in series (creating a so-called cell string), and the sum of the single cell voltages results in a string voltage that is equal to the sum of the single cell currents. As a result, when dividing or partitioning a full-sized cell into two or three equal portions, this technique is referred to as Cell Partition Technique (CPT). This partitioning results in a 1/2 or 1/3 reduction in current, as well as a reduction in ohmic losses. The ohmic loss is dependent on the equation  $P_{ohmic\ loss} = I^2 \cdot R_s$ , which describes the effect of

current on the ohmic loss. Because the squared current has the greatest effect on the ohmic loss, while the series resistivity ' $R_s$ ' has a linear effect. Electrical current ' $I$ ' flowing on bus bar is halved ' $I/2$ ' in HCM and  $I/3$  in TCM, and Resistive losses(ohmic losses) in a HCM and TCM is  $1/4$  and  $1/9$  of a FCM resistive losses, respectively. The Full cell is partitioned into a two and three equal parts using CPT, as shown in Figure 3.

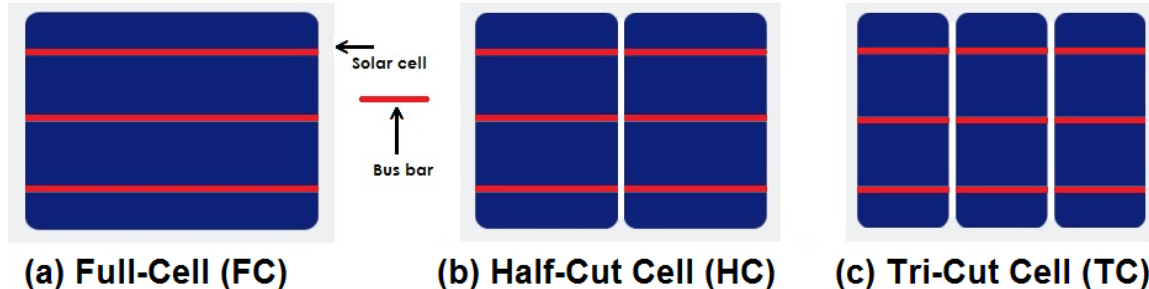


**Figure 3.** Partial solar cells using CPT

Utilizing halved and tri cells in solar photovoltaic modules (i.e. partial cell modules) effectively reduces resistive power loss. Halved and Tri cells are created by laser cutting, the standard full-size cells cut into half and one third, perpendicular to the busbars. The halved and tri cells are then joined and packaged into a single photovoltaic module. We outline the theory underlying the benefits of utilizing HCM and TCM in a silicon wafer-based photovoltaic module and conduct a performance analysis of PV modules developed based on CPT technique using the matlab/simulink software.

### Performance Investigations of proposed partial cell PV modules based on CPT *Solar PV Modules based on CPT(PVM-CPT)*

The standard single PV module with 36 number of series connected Full cells (FC) to form full cell module (FCM) as shown in Figure 4(a). The full sized 36 cells are partitioned into 72 half cells and one part of 36 series connected half cells is connected in parallel to other part of 36 series connected half cells to form Half cell module (HCM) as shown in Figure 4(b). The full sized 36 cells are partitioned into 108 tri cells and one part of 54 series connected tri cells is connected in parallel to other part of 54 series connected tri cells to form a Tri cell module (TCM) as illustrated in Figure 4(c). Bypass diodes (BD's) are connected in each solar PV module to bypass the solar cells under shading cases. The electrical power generated by the FCM, HCM and TCM is approximately 40.02W, 40.75W, and 41W respectively with an open circuit voltage of 0.6083V. Standard FCM and partial cell PV modules, i.e., HCM and TCM, with representative current flow through cell strings (1, 2, 3, 4) and bypass diodes (1, 2), as illustrated in Figs. 5(a), 5(b), and 5(c) [19].

A standard solar module (developed in this paper is a 40W module with 36 full cells) has two internal cell strings. The HCM and TCM, on the other hand, have four internal cell strings, making it a four string module instead of two strings. A single minor spot of shade on a module (such as a leaf or bird dropping) will disable the entire cell string, but will have no effect on the others. This is due to the bypass diodes (shown in white color in Figure 5). Partially shaded cells are less severe in the half-cut and Tri-cut cell modules since they have more strings. The internal cell strings of FCM is 2, while the internal cell strings of HCM and TCM are 4 (with only 2 bypass diodes), resulting in improved partial-shade tolerance. Even if half of the module is shaded, the other half is still capable of operating and generating electricity

### Shading Loss, Resistive Loss and Hotspot-Heating in Partial Cell Modules

Due to the difference in current between the two parts of the cell, the shading loss in half-cut cells and tri-cut cells is insignificant. If half of the string cells are shaded, that region is affected, and the bypass diode for that half of the string cells will be activated. Meanwhile, the other half of the string cells is still in action, and the bypass diode for that half of the string cells will be inactive. The power generated by the other half of the cell is unaffected by this event. With reference to Table 2, which depicts bypass diode 1 and 2 as a white triangle, and internal cell strings as 1, 2, 3, and 4, this becomes evident. As a result, half-cut or tri-cut cells are favoured over conventional cells in order to reduce shading losses. The use of series-parallel-series connections in half-cut and tri-cut cell modules (HCM and TCM) significantly reduces the amount of heat lost. Half-cut and tri-cut cells, for example, have a lower temperature rise in a hotspot cell than full-cut cells, which reduces the degradation caused by such a situation. In partial shading, the module can save up to 50% of its power because the strings are configured in parallel. It is also less likely that there will be hotspots due to shading in the future. With regard to the series resistance of a module made of silicon wafer solar cells, it can be divided into two categories: First, there is the series resistance of the cell (which includes bulk silicon resistance, metal semiconductor contact resistance, and resistance of metal electrodes), and second, there is the series resistance of the ribbons (which includes resistance of the ribbons and metal electrode resistance). The relationship between ohmic loss and current is  $P_{\text{ohmic loss}} = I^2 \cdot R_s$ , and the ohmic loss of partial cell modules is lower than that of a normal full cell PV module.

1	18	19	36
2	17	20	35
3	16	21	34
4	15	22	33
5	14	23	32
6	13	24	31
7	12	25	30
8	11	26	29
9	10	27	28

9	10	27	28
8	11	26	29
7	12	25	30
6	13	24	31
5	14	23	32
4	15	22	33
3	16	21	34
2	17	20	35
1	18	19	36

37	54	55	72
38	53	56	71
39	52	57	70
40	51	58	69
41	50	59	68
42	49	60	67
43	48	61	66
44	47	62	65
45	46	63	64

14	15	41	42
13	16	40	43
12	17	39	44
11	18	38	45
10	19	37	46
9	20	36	47
8	21	35	48
7	22	34	49
6	23	33	50
5	24	32	51
4	25	31	52
3	26	30	53
2	27	29	54
1	81	28	108

55	80	82	107
56	79	83	106
57	78	84	105
58	77	85	104
59	76	86	103
60	75	87	102
61	74	88	101
62	73	89	100
63	72	90	99
64	71	91	98
65	70	92	97
66	69	93	96
67	68	94	95

(a) 36 Full Cells with 2 BD's

(b) 72 Half Cells with 2 BD's

(c) 108 Tri Cells with 2 BD's

**Figure 4.** Illustration of standard 36 full cell module and proposed PV modules using 72 half cells, and 108 tri cells with 2 BD's

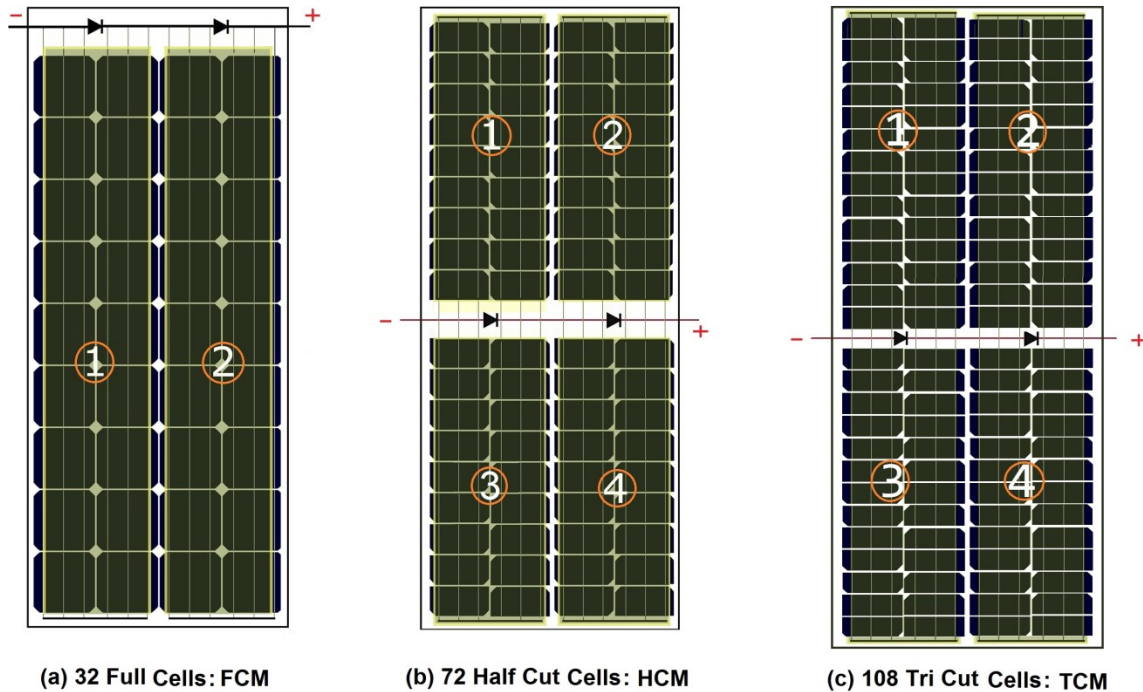


**Figure 5.** Illustration of standard FCM and proposed partial cell modules with 2 BD's

### Effect of Internal Cell String Shading on FCM, HCM and TCM

The amount of power that a single solar PV module can produce in the Simulink software with 36 full cells, 72 half-cut cells and 108 tri-cut cells are approximately 40.02W, 40.75W, and 41W. The standard 40W FCM has two internal strings of cell but HCM, and TCM has four internal strings of cells as exposed in Figure 5. One string is made up of a total of 18 cells that are connected together in a series. The operation of bypass diodes and voltage, current, power of a solar FCM, HCM, and TCM under different internal cell strings shading are given in Table 2.

#### *Operation of FCM, HCM and TCM under Cell String Shadings*

Figure 5 illustrates the 36 full cell module, 72 half-cell module, and 108 tri-cell module. The power output (Wp means watts peak) of standard single full cell module is approximately 40W. The operation of the FCM, HCM and TCM are clearly elaborated in Table 2.

*Under uniform irradiance case (Case-U):* All modules of FCM, HCM and TCM are generating full output power of approximately 40.02W, 40.75W, and 41W respectively. In this case, two diodes 1 and 2 are inactive.

*Under shading case-1:* In this case, first string of half cells is shaded. In FCM, the diode-**a** is active and it bypassing shaded string-1 and diode-**b** is inactive. In HCM and TCM, diode-2 is inactive and diode-**a** is active. So shaded string-3 is bypassed and power is still being produced by top string-1.

*Under shading case-2:* In this case, cells in bottom left string are shaded. The diode- **a** is active, *i.e.*, bypassing shaded string and diode- **b** is inactive in FCM, HCM and TCM.

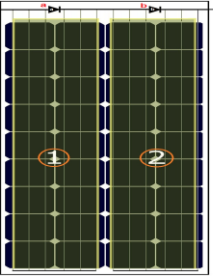
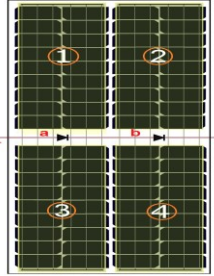
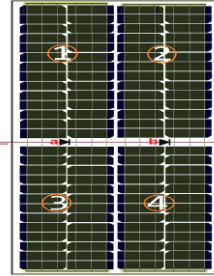
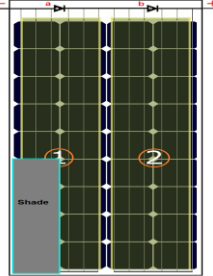
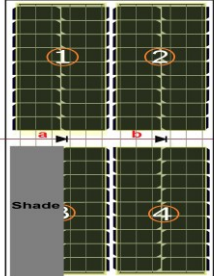
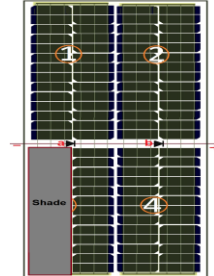
*Under shading case-3:* In this case, half cells shaded in two strings. The diode-**a** is active, diode- **b** is active, and it bypassing shaded strings in FCM, HCM and TCM.

*Under shading case-4:* In this case, bottom module cells are shaded. The diode-**a** is active, diode-**b** is active in FCM, HCM and TCM, and it bypassing shaded strings.

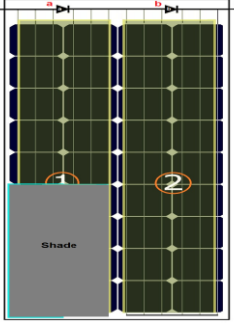
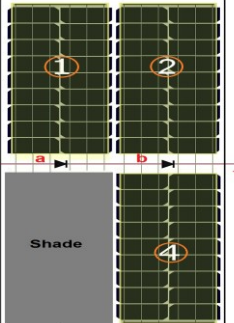
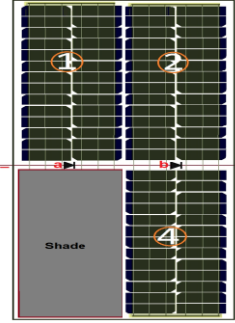
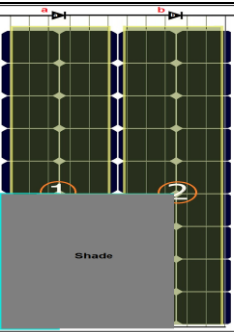
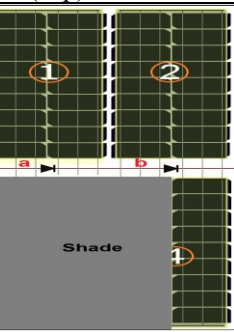
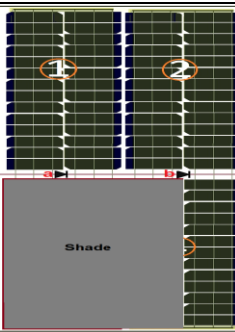
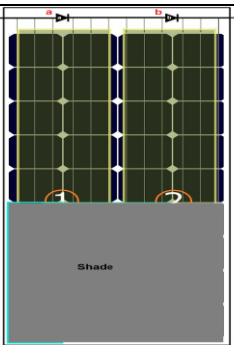
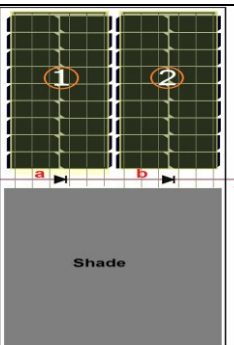
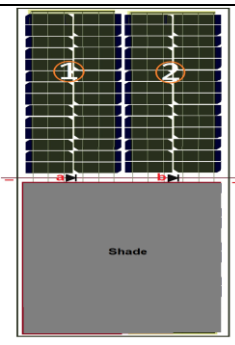
*Under shading case-5:* In this case, one cell shaded in string. The diode-**a** is active: bypassing shaded string and diode-**b** is inactive in FCM, HCM and TCM.

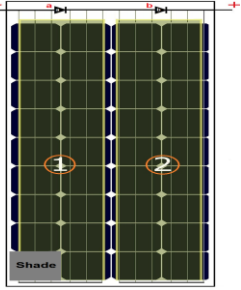
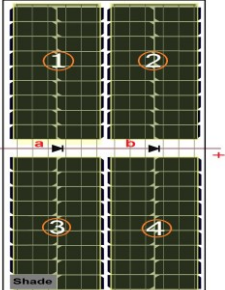
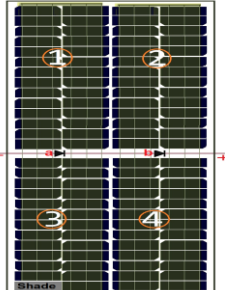
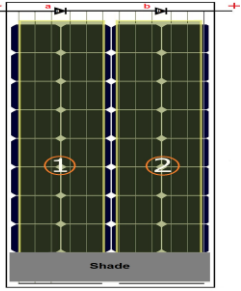
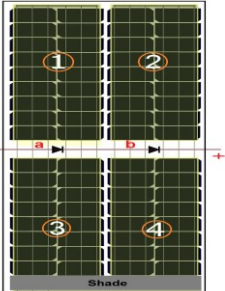
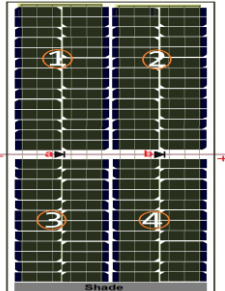
*Under shading case-6:* In this case, bottom cells shaded in solar PV module. Two diodes are active in FCM. The diode-**a** is active: bypassing shaded string and diode-**b** is inactive in HCM and TCM.

**Table 2.** Effect of internal cell string shading on FCM, HCM, and TCM

Shading Cases	Standard PV module with Full Cells: FCM (2 internal strings of cells)	PV module with Half Cut Cells: HCM (4 internal strings of cells)	PV module with Tri Cut Cells: TCM (4 internal strings of cells)
Case-U (Un- Shade)	 <p>Diode-<b>a</b>: inactive Diode-<b>b</b>: inactive</p> <p>Voltage (V) 100% Current (A) 100% Power (Wp) 100%</p>	 <p>Diode- <b>a</b>: inactive Diode-<b>b</b>: inactive</p> <p>Voltage (V) 100% Current (A) 100% Power (Wp) 100%</p>	 <p>Diode- <b>a</b>: inactive Diode- <b>b</b>: inactive</p> <p>Voltage (V) 100% Current (A) 100% Power (Wp) 100%</p>
Shading Case-1:  1/4 Cells Shading in Bottom String	 <p>Diode- <b>a</b>: active, Shaded String is bypassed. Diode- <b>b</b>: inactive</p> <p>Voltage (V) 50% Current (A) 100% Power (Wp) 50%</p>	 <p>Diode- <b>a</b> is active, Shaded String is bypassed. Power is still being produced by top string. Diode- <b>b</b>: inactive.</p> <p>Voltage (V) ~66%* Current (A) 100% Power (Wp) ~66%*</p>	 <p>Diode- <b>a</b>: active Diode- <b>b</b>: inactive</p> <p>Voltage (V) ~66%* Current (A) 100% Power (Wp) ~66%*</p> <p>* Depending on the MPP tracking, the diode will turn on to enable excess current to pass through.</p>



<p>Shading Case-2:  1/2 Cells Shading in Bottom String</p>	 <p>Diode- <b>a</b>: active Diode- <b>b</b>: inactive</p> <p>Voltage (V) 50% Current (A) 100% Power (Wp) 50%</p>	 <p>Diode- <b>a</b>: active Diode- <b>b</b>: inactive</p> <p>Voltage (V) 66% Current (A) 100% Power (Wp) 66%</p>	 <p>Diode- <b>a</b>: active Diode- <b>b</b>: inactive</p> <p>Voltage (V) 66% Current (A) 100% Power (Wp) 66%</p>
<p>Shading Case-3:  3/4 Cells Shading in Bottom Strings</p>	 <p>Diode- <b>a</b>: active Diode- <b>b</b>: active. Shaded Strings Bypassed.</p> <p>Voltage (V) 0% Current (A) 0% Power (Wp) 0%</p>	 <p>Diode- <b>a</b>: active Diode- <b>b</b>: active Shaded String bypassed.</p> <p>Voltage (V) 100% Current (A) 50% Power (Wp) 50%</p>	 <p>Diode- <b>a</b>: active Diode- <b>b</b>: active Shaded Strings bypassed.</p> <p>Voltage (V) 100% Current (A) 50% Power (Wp) 50%</p>
<p>Shading Case-4:  Bottom Half Module Shading</p>	 <p>Diode- <b>a</b>: active Diode- <b>b</b>: active. Shaded Strings Bypassed.</p> <p>Voltage (V) 0% Current (A) 0%</p>	 <p>Diode- <b>a</b>: active Diode- <b>b</b>: active. Shaded Strings Bypassed.</p> <p>Voltage (V) 100% Current (A) 50%</p>	 <p>Diode- <b>a</b>: active Diode- <b>b</b>: active. Shaded Strings Bypassed.</p> <p>Voltage (V) 100% Current (A) 50%</p>

	Power (Wp) 0%	Power (Wp) 50%	Power (Wp) 50%
Shading Case-5: One Cell Shading in A String	 <p>Diode- <b>a</b>: active Diode- <b>b</b>: inactive</p> <p>Voltage (V) 50% Current (A) 100% Power (Wp) 50%</p>	 <p>Diode- <b>a</b>: active Diode- <b>b</b>: inactive</p> <p>Voltage (V) 66% Current (A) 100% Power (Wp) 66%</p>	 <p>Diode- <b>a</b>: active Diode- <b>b</b>: inactive</p> <p>Voltage (V) 66% Current (A) 100% Power (Wp) 66%</p>
Shading Case-6: Bottom Cells Shading in Strings	 <p>Diode- <b>a</b>: active Diode- <b>b</b>: active</p> <p>Shaded Strings Bypassed.</p> <p>Voltage (V) 0% Current (A) 0% Power (Wp) 0%</p>	 <p>Diode- <b>a</b>: active Diode- <b>b</b>: active</p> <p>Shaded Strings Bypassed.</p> <p>Voltage (V) 100% Current (A) 50% Power (Wp) 50%</p>	 <p>Diode- <b>a</b>: active Diode- <b>b</b>: active</p> <p>Shaded Strings Bypassed.</p> <p>Voltage (V) 100% Current (A) 50% Power (Wp) 50%</p>

The simulation results of a single FCM, HCM and TCM under six internal cell string shading conditions (shown in Table 2) with irradiance of  $0 \text{ W/m}^2$  and  $500 \text{ W/m}^2$  are tabulated in Tables 3 to 8. The mismatch loss and fill factor formulas are given below.

$$\text{Mismatch losses } ML(\text{ in watts}) = GMPP_{uni} - GMPP_{SCs} \quad \text{--- (4)}$$

$$\text{Mismatch losses, } ML(\%) = \frac{GMPP_{uni} - GMPP_{sc}}{GMPP_{uni}} \times 100 \quad \text{--- (5)}$$

$$\text{Fill Factor, } FF(\%) = \frac{V_m \cdot I_m}{V_{oc} \cdot I_{sc}} \times 100 \quad \text{--- (6)}$$

Where,  $GMPP_{uni}$  is the global maximum peak power(in watts) at uniform irradiance of  $1000 \text{ W/m}^2$ ,  $GMPP_{sc}$  is the global maximum peak power(in watts) in shading cases.  $V_m$  and  $I_m$  are the maximum voltage(in Volts) and the maximum current(in Amperes), respectively.  $V_{oc}$  is open circuit voltage(in Volts) and  $I_{sc}$  is short circuit current(in Amperes) of solar PV module.

**Table 3.** Performance of 36 cell FCM with 2BD's under irradiance of 0 W/m<sup>2</sup>

Shading Cases	Standard Full Cell Module (FCM) with 36 Full Cells							
	P <sub>max</sub> (W)	V <sub>max</sub> (V)	I <sub>m</sub> (A)	V <sub>oc</sub> (V)	I <sub>sc</sub> (A)	ML (W)	ML (%)	FF
Case-U	40.02	17.72	2.258	21.9	2.45	0	0	0.7457
Case-1	29.82	13.26	2.248	16.72	2.45	10.20	25.49	0.7277
Case-2	18.83	8.402	2.241	10.45	2.45	21.19	52.95	0.7354
Case-3	0	0	0	0	0	40.02	100	0
Case-4	0	0	0	0	0	40.02	100.00	0
Case-5	18.83	8.402	2.241	10.45	2.45	21.19	52.95	0.7354
Case-6	0	0	0	0	0	0	0	0

**Table 4.** Performance of 36 cell FCM with 2BD's under irradiance of 500 W/m<sup>2</sup>

Shading Cases	Standard Full Cell Module (FCM) with 36 Full Cells							
	P <sub>max</sub> (W)	V <sub>max</sub> (V)	I <sub>m</sub> (A)	V <sub>oc</sub> (V)	I <sub>sc</sub> (A)	ML (W)	ML (%)	FF
Case-U	40.02	17.72	2.258	21.9	2.45	0	0	0.7457
Case-1	29.9	13.34	2.242	21.76	2.45	10.12	25.29	0.5610
Case-2	22.94	19.19	1.195	21.61	2.45	17.08	42.68	0.4331
Case-3	22.1	18.68	1.183	21.49	2.45	17.92	44.78	0.4197
Case-4	21.34	18.27	1.168	21.36	1.225	18.68	46.68	0.8155
Case-5	24.88	20.35	1.222	21.86	2.45	15.14	37.83	0.4643
Case-6	0	0	0	0	0	0	0	0

**Table 5.** Performance of HCM with 2BD's under irradiance of 0 W/m<sup>2</sup>

Shading Cases	Half Cell Module(HCM) with 72 Half Cells							
	P <sub>max</sub> (W)	V <sub>max</sub> (V)	I <sub>m</sub> (A)	V <sub>oc</sub> (V)	I <sub>sc</sub> (A)	ML (W)	ML (%)	FF
Case-U	40.75	18	2.264	21.9	2.45	0.00	0.00	0.7595
Case-1	22.28	18.97	1.174	21.6	2.45	18.47	45.33	0.4208
Case-2	21.83	18.54	1.177	21.4	2.45	18.92	46.43	0.4162
Case-3	19.88	17.61	1.129	21.11	1.225	20.87	51.21	0.7688
Case-4	19.46	17.23	1.13	20.92	1.225	21.29	52.25	0.7597
Case-5	22.3	18.98	1.175	21.82	2.45	18.45	45.28	0.4172
Case-6	20.38	18	1.132	21.89	1.225	20.37	49.99	0.7599

**Table 6.** Performance of HCM with 2BD's under irradiance of 500 W/m<sup>2</sup>

Shading Cases	Half Cell Module(HCM) with 72 Half Cells							
	P <sub>max</sub> (W)	V <sub>max</sub> (V)	I <sub>m</sub> (A)	V <sub>oc</sub> (V)	I <sub>sc</sub> (A)	ML (W)	ML (%)	FF
Case-U	40.75	18	2.264	21.9	2.45	0.00	0.00	0.7595
Case-1	33.02	18.71	1.765	21.79	2.45	7.73	18.97	0.6055
Case-2	32.33	18.42	1.755	21.69	2.45	8.42	20.66	0.6083
Case-3	30.62	17.93	1.708	21.58	1.838	10.13	24.86	0.7721
Case-4	30.02	17.71	1.695	21.49	1.838	10.73	26.33	0.7803
Case-5	33.12	18.82	1.759	21.88	2.45	7.63	18.72	0.6175
Case-6	20.38	18	1.132	21.89	1.225	20.37	49.99	0.7599

**Table 7.** Performance of TCM with 2BD's under irradiance of 0 W/m<sup>2</sup>

Shading Cases	Tri Cell Module(TCM) with 108 Tri Cells							
	P <sub>max</sub> (W)	V <sub>max</sub> (V)	I <sub>m</sub> (A)	V <sub>oc</sub> (V)	I <sub>sc</sub> (A)	ML (W)	ML (%)	FF
Case-U	41	27.27	1.503	32.84	1.633	0.00	0.00	0.7643
Case-1	22.37	28.61	0.782	32.42	1.633	18.61	45.41	0.4226
Case-2	21.89	27.96	0.783	32.11	1.633	19.09	46.58	0.4175
Case-3	19.98	26.38	0.757	31.7	0.816	21.00	51.24	0.7717
Case-4	19.52	25.75	0.758	31.38	0.816	21.46	52.37	0.7618
Case-5	22.39	28.62	0.782	32.74	1.633	18.59	45.36	0.4188
Case-6	20.5	27.05	0.757	32.84	0.816	20.48	49.97	0.7641

**Table 8.** Performance of TCM with 2BD's under irradiance of 500 W/m<sup>2</sup>

Shading Cases	Tri Cell Module(TCM) with 108 Tri Cells							
	P <sub>max</sub> (W)	V <sub>max</sub> (V)	I <sub>m</sub> (A)	V <sub>oc</sub> (V)	I <sub>sc</sub> (A)	ML (W)	ML (%)	FF
Case-U	41	27.27	1.503	32.84	1.633	0	0	0.7643
Case-1	33.17	27.91	1.188	32.66	1.633	7.81	19.06	0.6217
Case-2	32.48	27.62	1.176	32.52	1.633	8.50	20.74	0.6116
Case-3	30.78	26.89	1.145	32.38	1.225	10.20	24.89	0.7762
Case-4	30.16	26.62	1.133	32.22	1.225	10.82	26.40	0.7641
Case-5	33.27	28.47	1.169	32.83	1.633	7.71	18.81	0.6208
Case-6	20.5	27.05	0.757	32.84	0.816	20.48	49.97	0.7641

Based on the findings of the simulations presented above, it can be deduced that the performance of HCM and TCM is better compared to FCM under internal cell strings shading conditions.

### Effects of Cell Level Shadings on PVM - CPT

Shading occurs due to several factors like clouds, trees, nearby buildings, etc. It effects the output power of an solar PV module. In the literature, all researchers elucidated module level partial shading conditions only not cell level shading conditions. The novelty of this research is in the investigation of the performance of PVM-CPT under various cell level shading conditions. Figures 6, 7, and 8 display the FCM, HCM, and TCM modules, which represent different cell level shading cases. The performance of PVM-CPT are analyzed under twelve cell level shadings with different irradiances and one uniform case (Case-U) with irradiance of 1000 W/m<sup>2</sup>. The performance of a standard FCM with 36 cells is studied using 12 shadings at the cell level, as exposed in Figure 6.

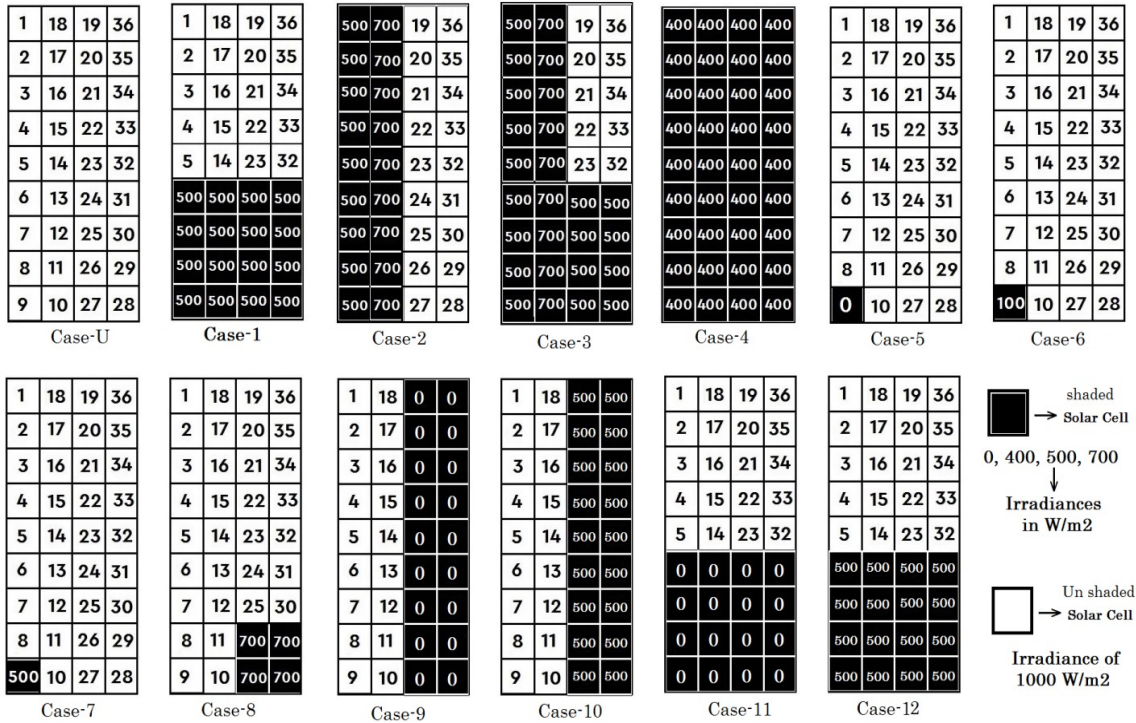


Figure 6. Different cell level shadings considered in a 36 full cells module

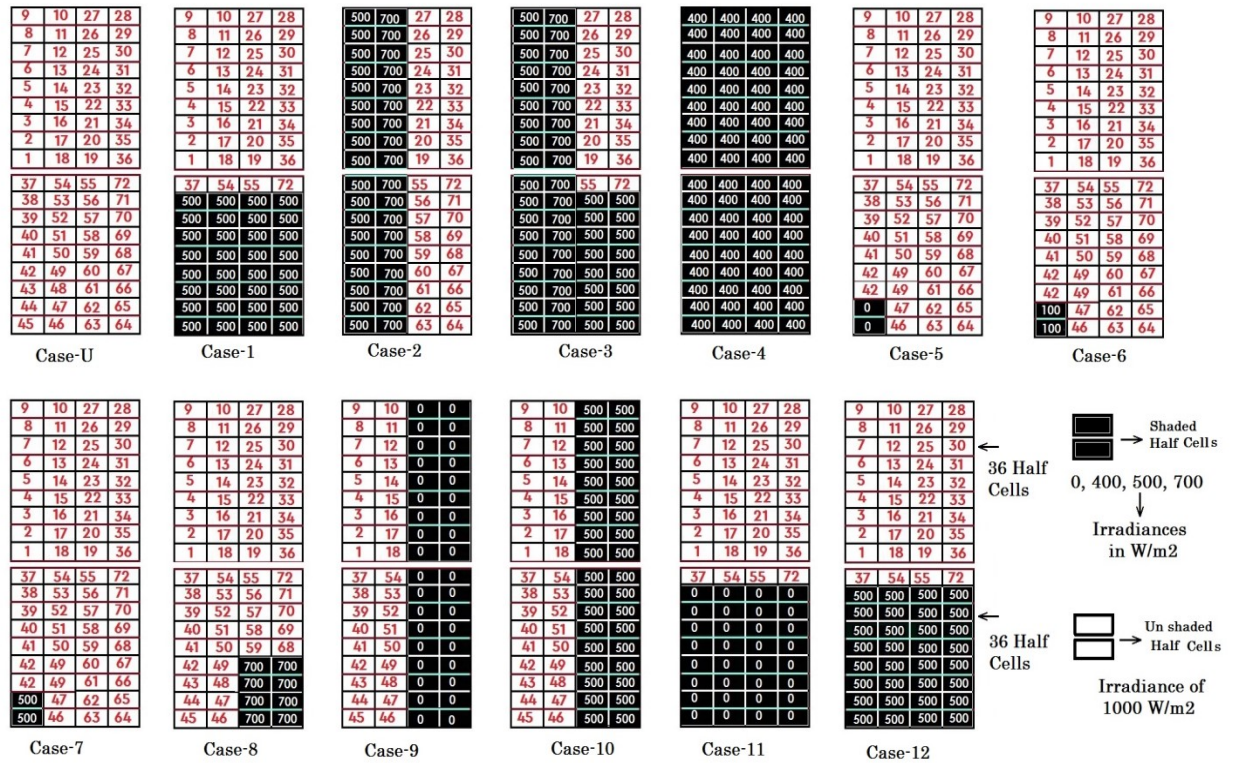


Figure 7. Different cell level shadings considered in a 72 half cells module

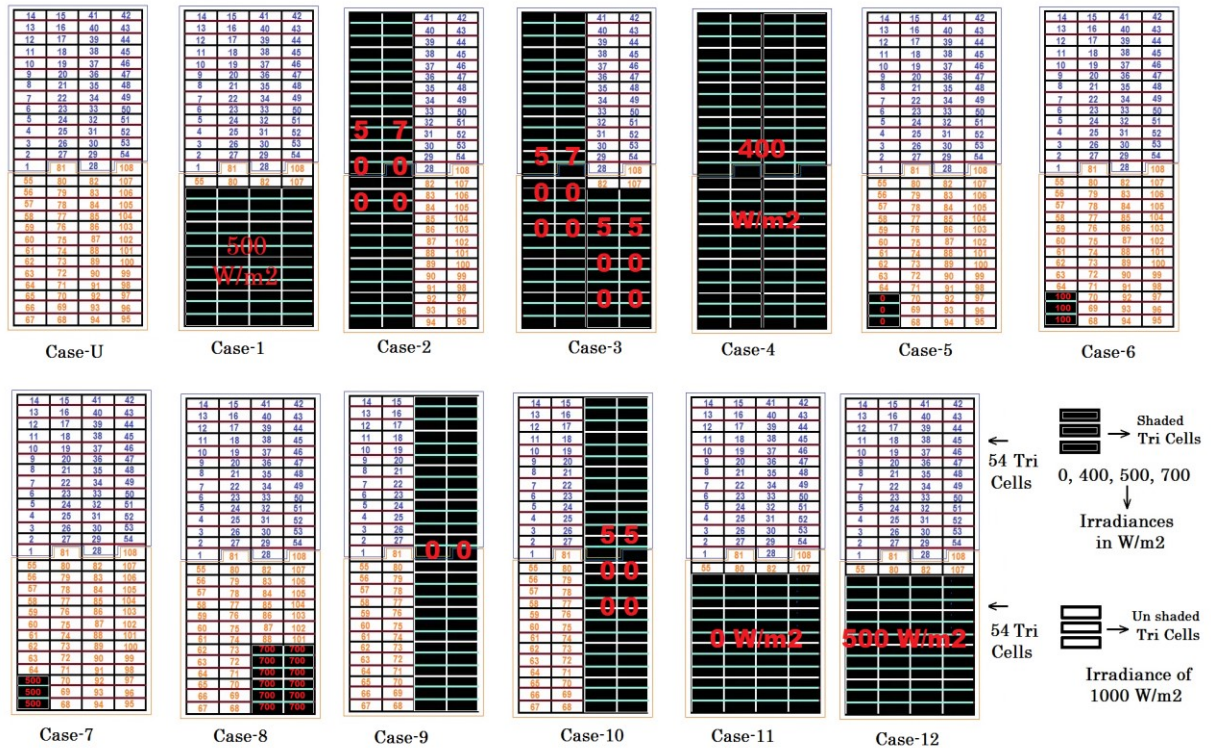


Figure 8. Different cell level shadings considered in a 108 tri cells module

MATLAB-Simulink model of PVM-CPT

The MATLAB-Simulink model of a standard full cell module (FCM) for shading case-1 (shown in Figure 6: case-1) is depicted in Figure 9. As illustrated in Figure 6, the 36 cells of an FCM are shaded in accordance with the shadings addressed at the cell levels. The PVM-CPT subsystem1 consists of conventional FCM and partial cell modules such as HCM and TCM, which is shown in Figure 9. The terms V, I and P are the solar PV module voltage(V), current(A) and power(W), respectively. The output (V-I and P-V) characteristics of PVM-CPT and FCM are obtained from V, I, and W.

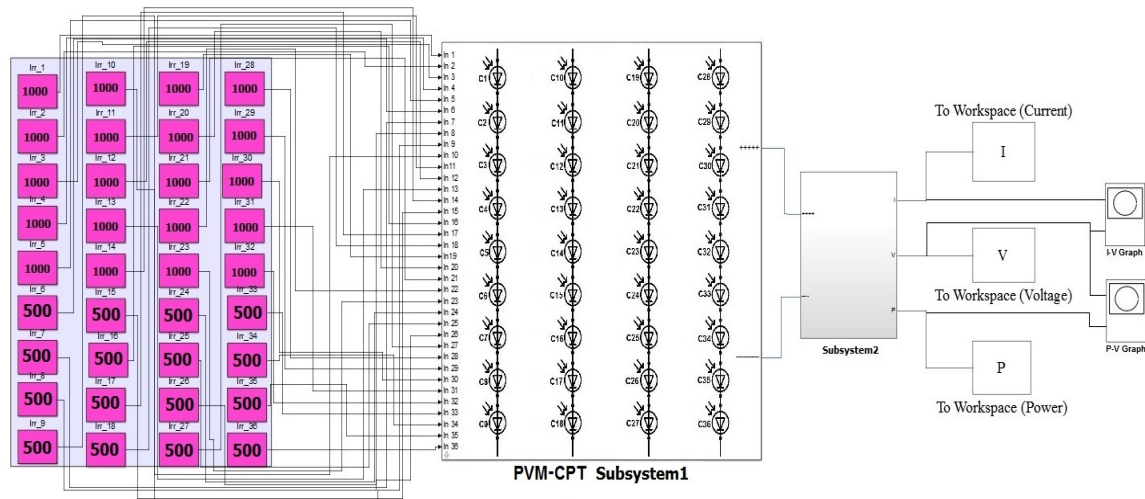


Figure 9. Matlab-Simulink model of a single PV Module with 36 full cells under Case-1

## Results and Discussions

In order to explain various shading cases, we first describe the case of uniform irradiance, (*i.e.*, no shading) which means that all cells in a PV module get standard irradiance of  $1000 \text{ W/m}^2$ . In uniform irradiance case (case-U), the power output of single FCM, HCM and TCM is equal to 40.02W, 40.75W, and 41W respectively. The simulation results of a single standard FCM and PVM-CPT (*i.e.*, HCM, and TCM) under different cell level shadings are presented in Tables 9, 10, and 11, respectively.

**Table 9.** Performance of single solar PV 36 full cells module with 2 BD under cell level shadings

Shading Cases	Series Connected 36 Full Cells in a Single PV Module							
	$P_{\max}$ (W)	$V_{\max}$ (V)	$I_m$ (A)	$V_{oc}$ (V)	$I_{sc}$ (A)	ML (W)	ML (%)	FF
Case-U	40.02	17.72	2.258	21.9	2.45	0	0	0.746
Case-1	21.94	18.62	1.178	21.47	1.225	18.08	45.18	0.834
Case-2	22.75	18.99	1.198	21.53	2.45	17.27	43.15	0.431
Case-3	21.43	18.25	1.174	21.31	1.225	18.59	46.45	0.821
Case-4	15.21	16.91	0.8993	20.62	0.98	24.81	61.99	0.753
Case-5	18.83	8.402	2.241	10.44	2.45	21.19	52.95	0.736
Case-6	18.84	8.348	2.256	21.8	2.45	21.18	52.92	0.353
Case-7	24.88	20.35	1.222	21.86	2.45	15.14	37.83	0.464
Case-8	32.59	19.19	1.698	21.84	2.45	7.43	18.57	0.609
Case-9	18.83	8.402	2.241	10.44	2.45	21.19	52.95	0.736
Case-10	21.64	18.4	1.176	21.42	2.45	18.38	45.93	0.412
Case-11	0	0	0	0	0	40.02	100.0	0
Case-12	21.94	18.62	1.178	21.47	1.225	18.08	45.18	0.834

**Table 10.** Performance of single solar PV 72 half cells module with 2 BD under cell level shadings

Shading Cases	Parallel Connected Two Half of 36 HC in a Single PV modules							
	$P_{\max}$ (W)	$V_{\max}$ (V)	$I_m$ (A)	$V_{oc}$ (V)	$I_{sc}$ (A)	ML (W)	ML (%)	FF
Case-U	40.75	18	2.264	21.9	2.45	40.75	0	0.7595
Case-1	30.31	17.8	1.703	21.52	1.838	10.44	25.62	0.7664
Case-2	22.96	19.13	1.2	21.53	2.45	17.79	43.66	0.4352
Case-3	22.44	18.77	1.195	21.35	1.837	18.31	44.93	0.5719
Case-4	15.32	17.08	0.8966	20.62	0.98	25.43	62.40	0.7573
Case-5	22.3	18.98	1.175	21.84	2.45	18.45	45.28	0.4168
Case-6	24.52	18.95	1.294	21.86	2.45	16.23	39.83	0.4579
Case-7	33.12	18.82	1.759	21.88	2.45	7.63	18.72	0.6175
Case-8	36.94	18.5	1.993	21.84	2.45	3.81	9.35	0.6891
Case-9	19.19	8.539	2.247	10.45	2.45	21.56	52.91	0.7494
Case-10	21.83	18.6	1.174	21.4	2.45	18.92	46.43	0.4165
Case-11	19.46	17.23	1.13	20.92	1.225	21.29	52.25	0.7597
Case-12	30.02	17.71	1.695	21.5	1.838	10.73	26.33	0.7596

**Table 11.** Performance of single solar PV 108 tri cells module with 2 BD under cell level shadings

Shading Cases	Parallel Connected Two Half of 54 TC in a Single PV modules							
	$P_{max}(W)$	$V_{max}(V)$	$I_m(A)$	$V_{oc}(V)$	$I_{sc}(A)$	ML(W)	ML (%)	FF
Case-U	41	27.09	1.513	32.82	1.633	0	0	0.7648
Case-1	30.45	26.75	1.139	32.3	1.225	10.55	25.73	0.7700
Case-2	23.02	28.67	0.8029	32.29	1.633	17.98	43.85	0.4366
Case-3	22.55	27.99	0.8036	32.02	1.225	18.5	45.12	0.5734
Case-4	15.56	25.61	0.5998	30.92	0.653	25.64	62.54	0.7608
Case-5	22.45	28.62	0.7823	32.77	1.633	18.61	45.39	0.4184
Case-6	24.83	28.55	0.8627	32.8	1.633	16.37	39.93	0.4598
Case-7	33.27	28.47	1.169	32.83	1.633	7.73	18.85	0.6208
Case-8	37.14	27.84	1.334	32.76	1.633	3.86	9.41	0.6942
Case-9	19.72	13.1	1.505	15.91	1.633	21.28	51.90	0.7588
Case-10	21.89	27.96	0.783	32.08	1.633	19.11	46.61	0.4179
Case-11	19.52	25.75	0.7581	31.38	0.816	21.48	52.39	0.7618
Case-12	30.16	26.62	1.133	32.23	1.225	10.84	26.44	0.7639

From the simulation results, it can be concluded that:

- In uniform irradiance case (case-U), the power output of single FCM, HCM and TCM is equal to 40.02W, 40.75W, and 41W respectively.
- When compare to the conventional FCM, the power output of HCM and TCM is improved under the consideration of 12 cell level shading scenarios.
- In one cell shading case (case-5), the maximum power of FCM, HCM and TCM is 18.83 W, 22.3 W and 22.45 W, respectively.
- Hotspot temperature and cell damage impact area in PVM-CPT are reduced due to smaller currents, so the risk of micro-crack propagation is less. Diode temperature also reduced.

### Proposed Static SD-TCTR Array with PVM-CPT

Reconfiguration techniques are used to reduce the effects of partial shading on solar PV arrays. Reconfiguration is the process of changing the structure of an existing PV system, which can be accomplished either by modifying the physical positions i.e., physical relocation of PV modules or electrical connections i.e., electrical array reconfiguration. In order to decrease mismatch losses in partial shading conditions, reconfiguration techniques has been proposed by several authors[20-23] to reposition of PV modules inside the PV array. This work proposes a static reconfiguration technique to reduce mismatch losses and increase array power under different cell level shading conditions. The proposed shade dispersion based total cross tied reconfiguration (SD-TCTR) is a static reconfiguration method and is used to distribute the shading effectively throughout a PV array.

### General Rule for the Proposed Static SD-TCTR Array Connection [24]

The proposed Static Shade dispersion based Total Cross Tied reconfiguration (SD-TCTR) array arrangement adaptable to shading patterns of any size, *i.e.*, row and column sizes can be odd or even. The rule for configuring a general solar array can be defined as:



$$n_{rc}, \text{ Where } \begin{cases} r = \text{Row number} & (r = 1, 2, 3, 4, \dots) \\ c = \text{Column number} & (j = 1, 2, 3, 4, \dots) \end{cases} \quad (7)$$

where  $n_{rc}$  is written for the  $n^{\text{th}}$  element of the  $r^{\text{th}}$  row and  $c^{\text{th}}$  column of a shading pattern. The following equations can be considered for determining the logic number in a column:

$$c = \begin{cases} c & , \text{ if } r = 1 \\ c + (r - 1) \cdot \text{floor}\left(\frac{c_{\max}}{3}\right) & , r > 1 \end{cases} \quad (8)$$

$$\begin{aligned} & \text{if } c < c_{\max}, \quad c = c \\ & \text{else } c = c - c_{\max} \end{aligned}$$

If any number is repeated in a column, just add 1 to the corresponding column, *i.e.*,  $c = c_0 + 1$  ( $c_0$  is the repeated column number). Alternatively, create a column with the same number( $c$ ).

### Formation of Proposed Static SD-TCTR Array Connection [13]

The primary objective of an Static SD-TCTR design is to distribute shadows throughout the array under shadings by arranging a  $r \times c$  array column location with the numbers 1 to  $c$  as illustrated in Figure 10. The proposed Static SD-TCTR array is implemented using Number Logic (NL) method and this method is developed for  $r = \text{odd}$  or even for the column location arrangement of the  $r \times c$  solar PV array. A unique solution is obtained by adding 1 to the preceding logic number in a specific column ( $c$ ) and row ( $r$ ) of a solar PV array in order to avoid the numbers repeating in that column and row. The proposed number logic method is applied for any array size, which is used in this paper for  $3 \times 4$ ,  $4 \times 3$ , and  $4 \times 4$  solar PV arrays shown in Figure 10. The 1st number in the box represents a logic number, and the 2nd number denotes the column number. The row and column positions in a  $4 \times 4$  array are arranging with the numbers 1 to 4 in the proposed arrangement, as shown in Figure 10(a). R1, R2, R3 and R4 represent the rows numbers, while C1, C2, C3 and C4 represents the column numbers.

	C1	C2	C3	C4		C1	C2	C3		C1	C2	C3	C4	
R1	11	22	33	44	R1	11	22	33		R1	11	22	33	14
R2	31	42	13	24	R2	31	42	13		R2	31	12	23	34
R3	21	32	43	14	R3	21	32	43		R3	21	32	13	24
R4	41	12	23	34	R4	41	12	23						
	<b>(a) 4x4 Array modules with Proposed NL method</b>					<b>(b) 4x3 Array modules with Proposed NL method</b>				<b>(c) 3x4 Array modules with Proposed NL method</b>				

**Figure 10.** SD-TCTR Arrangement of  $4 \times 4$ ,  $4 \times 3$  and  $3 \times 4$  arrays with Number Logic (NL) method

### Performance Investigation of $3 \times 4$ , $4 \times 3$ and $4 \times 4$ SPV Arrays with Cell Level Shading

#### *Cell Level Shading (CLS) Conditions*

In order to investigate the performance of PVM-CPT, we have conducted the tests on  $3 \times 4$ ,  $4 \times 3$ , and  $4 \times 4$  solar PV arrays under cell level shading (CLS) conditions. In this section, total four shading cases mainly Short Narrow (SN), Short Wide (SW), Long Narrow (LN), Long Wide (LW) type under cell level are considered for analyzing the

performance of solar PV arrays. Figures 11 and 12 illustrate the various partial shading conditions that were investigated in this study. Figure 11 illustrates the 3×4, 4×3, and 4×4 SPV arrays with different cell level partial shading cases such as SW, SN, LW, LN (case:1 to case: 4) and Figure 12 represents the shaded cells positions in PVM-CPT of different PV arrays.

1000 1000 1000 1000 1000 1000 1000 1000 SW SW SW SW	1000 1000 1000 1000 SN SN 1000 1000 SN SN 1000 1000	LW1 1000 1000 1000 LW1 1000 1000 1000 LW2 LW3 LW3 LW3	1000 1000 1000 1000 LN LN LN 1000 LN LN LN 1000
Case-1: 3x4 Array with SW Shading	Case-2: 3x4 Array with SN Shading	Case-3: 3x4 Array with LW Shading	Case-4: 3x4 Array with LN Shading
1000 1000 1000 1000 1000 1000 SW SW SW	1000 1000 1000 1000 1000 1000 SN SN 1000 SN SN 1000	LW1 1000 1000 LW1 1000 1000 LW2 LW3 LW3	1000 1000 1000 1000 1000 1000 LN LN LN LN LN LN
Case-1: 4x3 Array with SW Shading	Case-2: 4x3 Array with SN Shading	Case-3: 4x3 Array with LW Shading	Case-4: 4x3 Array with LN Shading
1000 1000 1000 1000 1000 1000 1000 1000 1000 1000 1000 1000 SW SW SW SW	1000 1000 1000 1000 1000 1000 1000 1000 SN SN 1000 1000 SN SN 1000 1000	LW1 1000 1000 1000 LW1 1000 1000 1000 LW1 1000 1000 1000 LW2 LW3 LW3 LW3	1000 1000 1000 1000 1000 1000 1000 1000 LN LN LN 1000 LN LN LN 1000
Case-1: 4x4 Array with SW Shading	Case-2: 4x4 Array with SN Shading	Case-3: 4x4 Array with LW Shading	Case-4: 4x4 Array with LN Shading

**Figure 11.** Illustration of solar irradiance levels in 3×4, 4×3 and 4×4 SPV arrays under SW, SN, LN and LW shadings in cell level

1000 350 350 350 350 350 350 350 350 350 350 350 350 350 350 350 350	600 1000 1000 1000 1000 1000 1000 1000 1000 1000 1000 1000 1000 1000 1000 1000 1000	450 1000 1000 1000 450 1000 1000 1000 450 1000 1000 1000 450 1000 1000 1000 450 1000 1000 1000 450 1000 1000 1000 450 1000 1000 1000 450 1000 1000 1000 450 1000 1000 1000
SW: Shaded Cells position	SN: Shaded Cells position	LN: Shaded Cells position
700 700 1000 1000 700 700 1000 1000 700 700 1000 1000 700 700 1000 1000 700 700 1000 1000 700 700 1000 1000 700 700 1000 1000 700 700 1000 1000	700 700 1000 1000 700 700 1000 1000 700 700 1000 1000 700 700 1000 1000 700 700 500 500 700 700 500 500 700 700 500 500 700 700 500 500	1000 500 500 500 500 500 500 500 500 500 500 500 500 500 500 500 500
LW1: Shaded Cells position	LW2: Shaded Cells position	LW3: Shaded Cells position

**Figure 12.** Number of cells shaded in a single PVM-CPT used in 3×4, 4×3 and 4×4 solar PV arrays under SW, SN, LN and LW shading cases

### Solar PV Arrays with TCT and Static SD-TCTR arrangements

The solar PV modules are connected in several ways, there are series-parallel (SP), Series (S), total cross tied (TCT), bridge link (BL) and honey comb (HC) type of configurations. In this paper, only SP and TCT configurations are considered for simulation and compared with static SD-TCTR array under different cell level shading cases. In Figure 13: Cases 1(a), 2(a), 3(a), and 4(a) represent the shaded modules in TCT configuration. In Figure-14: Cases 1(b), 2(b), 3(b), and 4(b) represent the shaded modules in static SD-TCTR arrangement using proposed NL method discussed in the above section. In Figure 15: Cases 1(c), 2(c), 3(c), and 4(c) represent the shade dispersion of

modules in TCT configuration for  $3 \times 4$ ,  $4 \times 3$  and  $4 \times 4$  arrays. Partial shading cases 1, 2, 3 and 4 are short wide (SW), long-wide (LW), short narrow (SN), and long narrow (LN) shadings in cell level, respectively.

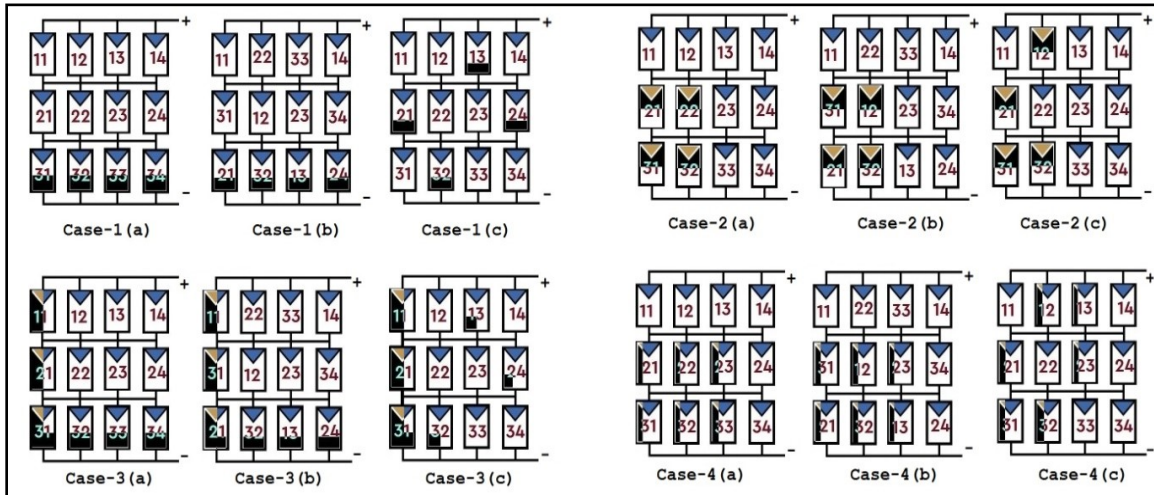


Figure 13.  $3 \times 4$  SPV Array with TCT and SD-TCTR arrangements under 4 shading cases

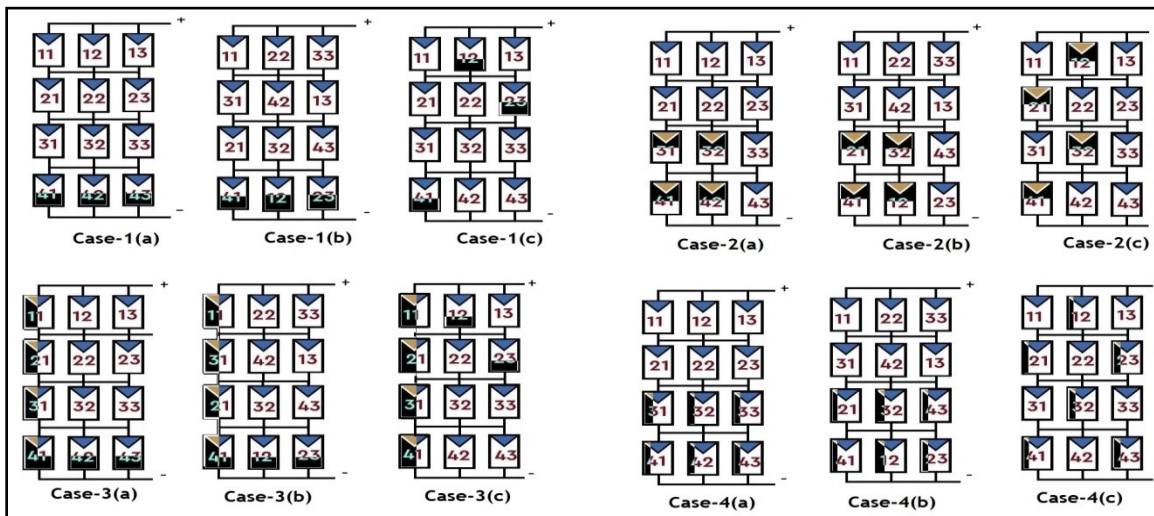
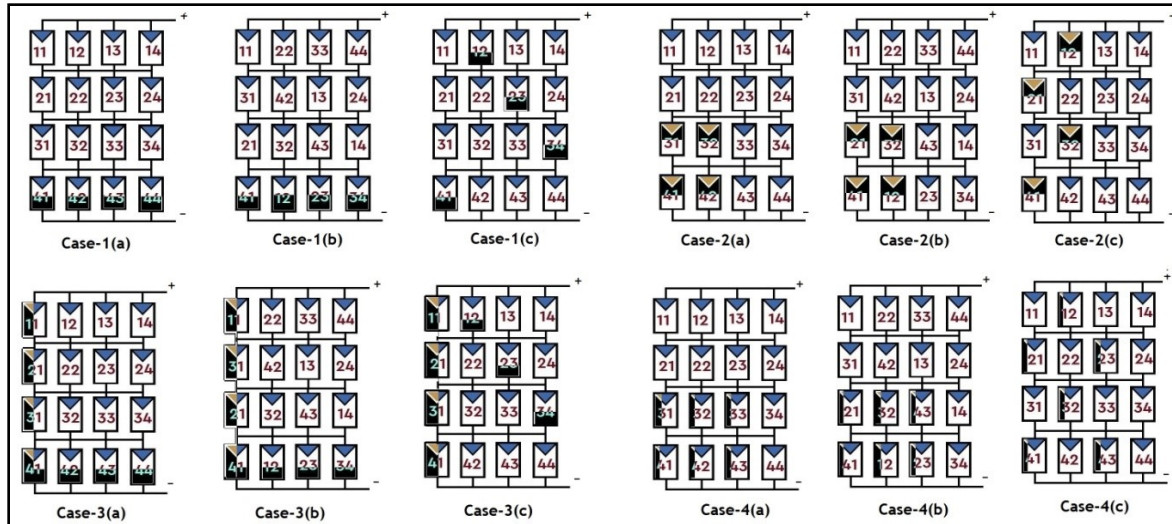


Figure 14.  $4 \times 3$  SPV Array with TCT and SD-TCTR arrangements under 4 shading cases



**Figure 15.** 4×4 SPV Array with TCT and SD-TCTR arrangements under 4 shading cases

### MATLAB/Simulink model of SP, TCT and static SD-TCTR Array Connections

The developed 40 W solar PV modules using number of solar cells, which are connected in series-parallel (SP), total-cross-tied (TCT) and proposed static SD-TCTR connections, are modeled and simulated in MATLAB/Simulink software. Figure 16 shows the Simulink model of 3×4 static SD-TCTR array with CPT based modules (PVM-CPT) under shading case-4. Each solar PV module in a 3×4 array is PVM-CPT and connected in static SD-TCTR array connection (discussed in previous section). The static SD-TCTR array with PVM-CPT is modeled under Short Narrow (SN), Long Narrow (LN), Short Wide (SW), and Long Wide (LW) type in cell level shadings. The power output of each PVM-CPT under uniform case-U is approximately 40.75W, and 41W. The different array sizes 3×4, 4×3 and 4×4 are modeled and simulated under cell level shadings in MATLAB/Simulink software. Moreover, all shading cases are carried out at constant temperature of 25°C. The standard FCM, HCM and TCM type PV modules are used to develop 3×4, 4×3 and 4×4 array configurations.

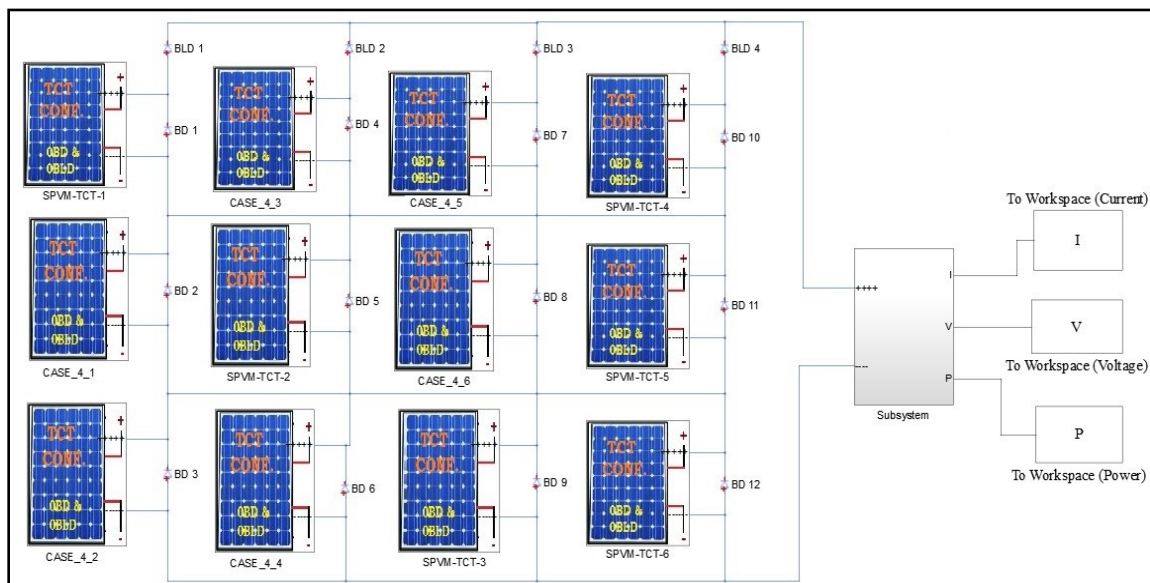


**Figure 16.** Simulink model of a 3×4 static SD-TCTR array with FCM, HCM, and TCM

## Results and Performance Evaluation of Proposed Static SDTCTR with PVM-CPT

The obtained global maximum powers of SP and TCT configuration with FCM (Full cell module), HCM (Half cell module), TCM (Tri cell module) and proposed static SD-TCTR array with PVM-CPT under different cell level shadings (CLS) for an array sizes of 3×4, 4×3 and 4×4 are tabulated in Tables 12, 13 and 14, respectively. SP\_FCM represents the series parallel configuration with FCM, TCT\_FCM represents the Total Cross Tied configuration with FCM, SP\_HCM represents the series parallel configuration with HCM, TCT\_HCM represents the Total Cross Tied configuration with HCM, SP\_TCM represents the series parallel configuration with TCM, and TCT\_TCM represents the Total Cross Tied configuration with TCM. Prop\_FCM represents the proposed static SD-TCTR array with FCM, Prop\_HCM represents the proposed static SD-TCTR array with HCM, Prop\_TCM represents the proposed static SD-TCTR array with TCM.

**Table 12.** Comparison of FCM, HCM, and TCM with 2 BD's under CLS for a 3×4 array

CASES	Global maximum powers of a 3x4 array in Watts									BEST
	3×4 array with FCM			3×4 array with HCM			3×4 array with TCM			
	SP_FCM	TCT_FCM	Prop_FCM	SP_TCM	TCT_TCM	Prop_HCM	SP_TCM	TCT_TCM	Prop_TCM	
Case-U	475.5	475.5	475.5	484.3	484.3	484.3	488.8	488.8	488.8	<i>Prop_TCM</i>
Case-1	306.2	306.2	352.3	361.8	361.8	423.7	364.3	364.3	427.4	<i>Prop_TCM</i>
Case-2	393.2	401.6	408.3	396.2	404	411.8	399.5	407.3	415.3	<i>Prop_TCM</i>
Case-3	275	281	366.6	365.7	365.5	397.5	368.5	368.2	401	<i>Prop_TCM</i>
Case-4	313.7	310	355.3	319.3	315.7	361.4	326	322.4	364.6	<i>Prop_TCM</i>

**Table 13.** Comparison of FCM, HCM, and TCM with 2 BD's under CLS for a 4×3 array

CASES	Global maximum powers of a 4x3 array in Watts									BEST
	4×3 array with FCM			4×3 array with HCM			4×3 array with TCM			
	SP_FCM	TCT_FCM	Prop_FCM	SP_TCM	TCT_TCM	Prop_HCM	SP_TCM	TCT_TCM	Prop_TCM	
Case-U	476.7	476.7	476.7	485.5	485.5	485.5	489.5	489.5	489.5	<i>Prop_TCM</i>
Case-1	349.1	349.7	387.8	369.2	369.2	439.6	371.3	371.3	443.1	<i>Prop_TCM</i>
Case-2	370.4	382.3	418.7	465.9	383	422.7	375	385.6	434.5	<i>Prop_TCM</i>
Case-3	296.9	296.9	347.1	360.5	360.4	383.4	362.8	362.8	386.3	<i>Prop_TCM</i>
Case-4	349.7	349.7	332.2	356.3	356.3	337.1	362	362	339.4	<i>SP_TCM or TCT_TCM</i>

**Table 14.** Comparison of FCM, HCM, and TCM with 2 BD's under CLS for a 4×4 array

CASES	Global maximum powers of a 4x4 array in Watts									BEST
	4×4 array with FCM			4×4 array with HCM			4×4 array with TCM			
	SP_FCM	TCT_FCM	Prop_FCM	SP_TCM	TCT_TCM	Prop_HCM	SP_TCM	TCT_TCM	Prop_TCM	
Case-U	635.6	635.6	635.6	647.3	647.3	647.3	652.8	652.8	652.8	<i>Prop_TCM</i>
Case-1	466.2	466.2	536.6	492.3	492.3	593	494.8	494.8	597.8	<i>Prop_TCM</i>
Case-2	527.4	546.6	577.6	556.4	550.6	584.6	537.3	555.7	589.3	<i>Prop_TCM</i>
Case-3	413.3	413.3	499.1	495.5	495.4	538.6	498.4	498.3	542.8	<i>Prop_TCM</i>
Case-4	477.2	470.1	495.1	485.7	478.7	503.1	493.3	486.4	506.8	<i>Prop_TCM</i>

The analysis results so far have demonstrated what advantages are available in terms of power output and least mismatch power loss, when using half-cells and tri-cells

instead of full-size cells (FC) for solar PV modules. Figures 17, 18 and 19 represent the global maximum powers of  $3 \times 4$ ,  $4 \times 3$  and  $4 \times 4$  solar PV arrays, respectively.

From the above obtained results it can be concluded that:

- The amount of power that a  $3 \times 4$ ,  $4 \times 3$  and  $4 \times 4$  array can produce under uniform irradiance case-U is 475.5 W, 476.7 W and 635.6 W, respectively.
- In a  $3 \times 4$  array, the obtained maximum power of proposed SDTCTR with TCM (Prop\_TCM) is superior than that of FCM and HCM under considered shadings cases.
- In a  $4 \times 3$  array, the obtained maximum power of SDTCTR with TCM (Prop\_TCM) is superior than that of FCM and HCM under four shading cases.
- In a  $4 \times 4$  array, the obtained maximum power of SDTCTR with TCM (Prop\_TCM) is superior than that of FCM and HCM under four shading cases.

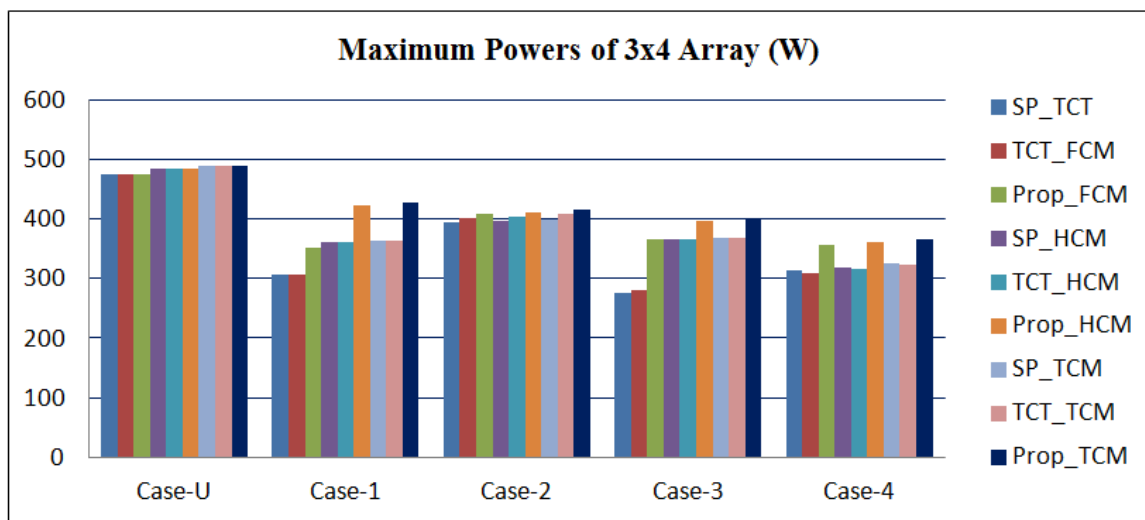


Figure 17. Power output from a  $3 \times 4$  solar PV array under cell level shading cases

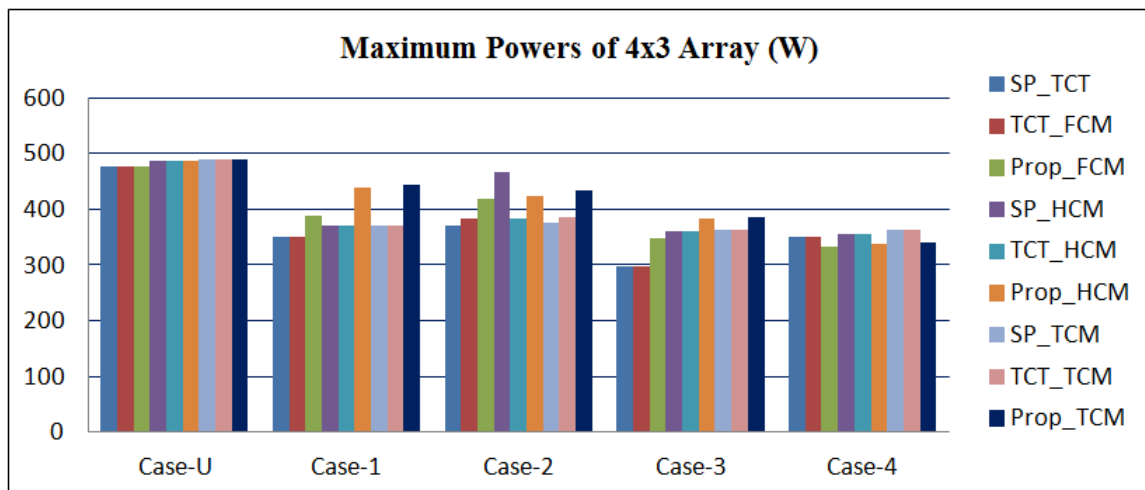
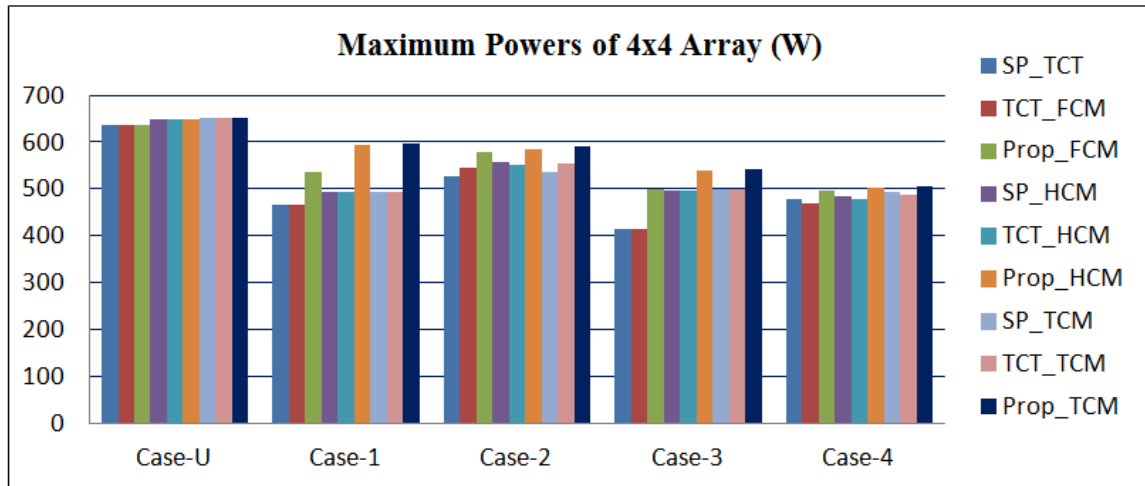


Figure 18. Power output from a  $4 \times 3$  solar PV array under cell level shading cases



**Figure 19.** Power output from a 4×4 solar PV array under cell level shading cases

## CONCLUSIONS

In this study, a simulation model for solar photovoltaic modules based on cell partition technique (PVM-CPT) was developed. The use of PVM-CPT can provide a significant advantage as well as increased performance in cell level shadowed conditions. Aligned with other energy generation advancements in half-cut and tri-cut cells, it is possible to achieve a large improvement in overall energy yield, making the new module based on CPT, a more attractive option for rooftop as well as grid connected energy generation. When the PVM-CPT is used, the current flow in a cell is reduced, which helps to eliminate the hotspot problems and a reduction in mismatch power loss while also improving overall performance. When comparing the Matlab/simulation results of HCM and TCM to full-size cell modules (FCM), we noticed an increase in fill factor and an increase in the maximum power. The HCM and TCM have a reduced power loss than a full-size-cell module with the same shade area. For solar cells with high short circuit current density of FCM, our modeling results demonstrate that employing PVM-CPT rather than FCM is even more advantageous. Finally, the performance of FCM, HCM and TCM connected in a 3×4, 4×3, and 4×4 array sizes with SP, TCT and proposed SD-TCTR connections are investigated, and the results show that the proposed SD-TCTR with TCM is superior to standard full cell module (FCM) under all possible cell level shading conditions.

## Conflict of Interest

The authors declare that there is no conflict of interests regarding the publication of this paper.

## REFERENCES

- [1] Mekhilef, S., Saidur, R., and Safari, A. (2011). A review on solar energy use in industries. *Renewable and Sustainable Energy Reviews*, 15(4), 1777-1790. DOI: 10.1016/j.rser.2010.12.018
- [2] SolarPower Europe. (2019) *Global Market Outlook For Solar Power / 2019 – 2023*, [https://www.solarpowereurope.org/wp-content/uploads/2019/07/SolarPower-Europe\\_Global-Market-Outlook-2019-2023.pdf](https://www.solarpowereurope.org/wp-content/uploads/2019/07/SolarPower-Europe_Global-Market-Outlook-2019-2023.pdf) (accessed on 11/25/2021)
- [3] Kalogirou, S. (Ed.). (2017). *McEvoy's handbook of photovoltaics: fundamentals and applications*. Academic Press
- [4] Seyedmahmoudian, M., Mekhilef, S., Rahmani, R., Yusof, R., and Renani, E. T. (2013). Analytical Modeling of Partially Shaded Photovoltaic Systems. *Energies*, 6(1), 128-144. DOI: 10.3390/en6010128
- [5] Teo, J. C., Tan, R. H. G., Mok, V. H., Ramachandaramurthy, V. K., and Tan, C. (2018). Impact of Partial Shading on the P-V Characteristics and the Maximum Power of a Photovoltaic String. *Energies*, 11(7), 1860. DOI: 10.3390/en11071860
- [6] ESRAM, T., and Chapman, P. L. (2007). Comparison of Photovoltaic Array Maximum Power Point Tracking Techniques. *IEEE Transactions on Energy Conversion*, 22(2), 439-449. DOI: 10.1109/TEC.2006.874230
- [7] Belhachat, F., and Larbes, C. (2018). A review of global maximum power point tracking techniques of photovoltaic system under partial shading conditions. *Renewable and Sustainable Energy Reviews*, 92, 513-553. DOI: 10.1016/j.rser.2018.04.094
- [8] Belhachat, F., and Larbes, C. (2015). Modeling, analysis and comparison of solar photovoltaic array configurations under partial shading conditions. *Solar Energy*, 120, 399-418. DOI: 10.1016/j.solener.2015.07.039
- [9] Roeth, J., Facchini, A., and Bernhard, N. (2017). Optimized Size and Tab Width in Partial Solar Cell Modules including Shingled Designs. *International Journal of Photoenergy*, 2017, 3609109. DOI: 10.1155/2017/3609109
- [10] Guo, S., Singh, J. P., Peters, I. M., Aberle, A. G., and Walsh, T. M. (2013). A Quantitative Analysis of Photovoltaic Modules Using Halved Cells. *International Journal of Photoenergy*, 2013, 739374. DOI: 10.1155/2013/739374
- [11] Qian, J., Thomson, A., Blakers, A., and Ernst, M. (2018). Comparison of Half-Cell and Full-Cell Module Hotspot-Induced Temperature by Simulation. *IEEE Journal of Photovoltaics*, 8(3), 834-839. DOI: 10.1109/JPHOTOV.2018.2817692
- [12] Sarniak, M. T. (2020). Modeling the Functioning of the Half-Cells Photovoltaic Module under Partial Shading in the Matlab Package. *Appl. Sci.*, 10(7), 2575. DOI:10.3390/app10072575
- [13] Chiodetti, M., Dupuis, J., Boublil, D., Radouane, K., and Dupeyrat, P. (2019). Half-Cell Module Behaviour and Its Impact on the Yield of a PV Plant, in *36th European Photovoltaic Solar Energy Conference and Exhibition*. pp. 1444 - 1448. DOI: 10.4229/Eupvsec20192019-5do.3.3
- [14] Rooij, D.D. (2016). Half cut solar cells: new standard in product differentiation? <https://sinovoltaics.com/solar-cells/half-cut-solar-cells-the-new-standard/> (accessed on 11/25/2021)



- [15] Hanifi, H., Schneider, J., and Bagdahn, J. (2015). Reduced shading effect on half-cell modules—Measurement and simulation. In *31st European Photovoltaic Solar Energy Conference and Exhibition*. pp. 2529-2533
- [16] Qian, J., Clement, C. E., Ernst, M., Khoo, Y. S., Thomson, A., and Blakers, A. (2019). Analysis of Hotspots in Half Cell Modules Undetected by Current Test Standards. *IEEE Journal of Photovoltaics*, 9(3), 842-848. DOI: 10.1109/JPHOTOV.2019.2898209
- [17] Mittag, M., Pfreundt, A., Shahid, J., Wöhrle, N., and Neuhaus, D. H. (2019). Techno-Economic Analysis of Half Cell Modules: The Impact of Half Cells on Module Power and Costs. In *36th European Photovoltaic Solar Energy Conference and Exhibition (EU PVSEC)*.
- [18] Bala Raju, V. and Chengaiah, C. (2020). Mathematical Analysis of Solar Photovoltaic Array Configurations with Partial Shaded Modules. *Trends in Renewable Energy*, 6, 121-143. DOI: 10.17737/tre.2020.6.2.00115
- [19] REC Solar Pte. Ltd. (2015). The REC Twin Peak Series: Innovative module design gives improved yield performance in shaded conditions, [https://www.recgroup.com/sites/default/files/documents/whitepaper\\_twinpeak\\_shading\\_properties\\_eng.pdf](https://www.recgroup.com/sites/default/files/documents/whitepaper_twinpeak_shading_properties_eng.pdf) (accessed on 11/04/2021)
- [20] Ajmal, A. M., Sudhakar Babu, T., Ramachandaramurthy, V. K., Yousri, D., and Ekanayake, J. B. (2020). Static and dynamic reconfiguration approaches for mitigation of partial shading influence in photovoltaic arrays. *Sustainable Energy Technologies and Assessments*, 40, 100738. DOI: 10.1016/j.seta.2020.100738
- [21] Bala Raju, V. and Chengaiah, C. (2020). A Comprehensive Study on Re-arrangement of Modules Based TCT Configurations of Partial Shaded PV Array with Shade Dispersion Method. *Tr Ren Energy*, 6(1), 37-60. DOI: 10.17737/tre.2020.6.1.00111
- [22] Vicente, P. d. S., Pimenta, T. C., and Ribeiro, E. R. (2015). Photovoltaic Array Reconfiguration Strategy for Maximization of Energy Production. *International Journal of Photoenergy*, 2015, 592383. DOI: 10.1155/2015/592383
- [23] Parlak, K. Ş. (2014). PV array reconfiguration method under partial shading conditions. *International Journal of Electrical Power & Energy Systems*, 63, 713-721. DOI: 10.1016/j.ijepes.2014.06.042
- [24] Bala Raju, V. and Chengaiah, C. (2021). Enhance the Output Power of a Shaded Solar Photovoltaic Arrays with Shade Dispersion based TCT Configuration. *Trends in Renewable Energy*, 7, 1-23. DOI: 10.17737/tre.2021.7.1.00128

**Article copyright:** © 2022 V. Bala Raju, Dr. Ch. Chengaiah. This is an open access article distributed under the terms of the [Creative Commons Attribution 4.0 International License](https://creativecommons.org/licenses/by/4.0/), which permits unrestricted use and distribution provided the original author and source are credited.



# Study of Hydrogen Internal Combustion Engine Vehicles Based on the Whole Life Cycle Evaluation Method

Ping Guo,\* Jianlun Xu, Chuanhao Zhao and Baoliang Zhang

*School of Mechanical Engineering, North China University of Water Resources and Electric Power, Zhengzhou, Henan 450045, China*

Received January 1, 2022; Accepted January 22, 2022; Published February 2, 2022

In order to better achieve the goal of low carbon emissions from vehicles, a whole life cycle assessment of hydrogen-fueled internal combustion engine vehicles has been conducted in recent years. Based on the study of hydrogen use around the world, we studied the emission and economic performance of hydrogen-fueled internal combustion engine vehicles from the beginning of hydrogen production to the end of use (Well-to-Wheel, WTW) based on the whole life cycle evaluation method. The results show that the overall environmental impact of hydrogen production by steam reforming of natural gas is the smallest, and that the rational use of "abandoned electricity" for hydrogen production from electrolytic water in the western part of China significantly reduces the overall environmental impact and the cost of hydrogen production. In the use phase, the emissions are less, which not only can meet the National 6 emission standard, but also can reach higher emission standard after adding exhaust gas recirculation (EGR). From the whole life cycle point of view, hydrogen-fueled internal combustion engine has a very good development prospect.

*Keywords: Whole Life Cycle; Hydrogen Fuel Internal Combustion Engine; Emission; Economy*

## Introduction

By 2020, the number of cars in China has reached 281 million [1], which results in the problem of pollutant emissions and energy consumption. According to 2020 data, China's dependence on imported oil has reached 69.84% in 2020 [2]. Hydrogen, as a clean and renewable new energy source, can not only reduce the emission of pollutants from vehicles, but also alleviate the problem of transitional dependence on traditional energy sources.

In this study, a comprehensive evaluation of new energy vehicles fueled by hydrogen is conducted from the whole life cycle of the energy source. Most studies on the whole life cycle evaluation of hydrogen have focused on hydrogen fuel cell vehicles. Lin *et al.* [3] used the GREET model to comprehensively evaluate the CO<sub>2</sub> emissions of hydrogen fuel cell vehicles under various routes of hydrogen fuel production and concluded that the energy consumption and CO<sub>2</sub> emissions could be reduced by 90% under the clean way of hydrogen production. Chen [4], Andrew [5], and Kong *et al.* [6] studied the emissions during the production of different hydrogen production methods, and obtained the most economical and least emitting method through comparative analysis. Changing the power generation structure not only reduces the overall

\*Corresponding author: Ping Guo (1999—), female (Han nationality), master's degree student, the main research direction is the combustion and optimization of clean energy vehicle engines. E-mail:

13180614001@qq.com.

Tr Ren Energy, 2022, Vol.8, No.1, 27-37. doi: 10.17737/tre.2022.8.1.00135

environmental impact value of electrolytic water hydrogen production, but also reduces the cost of hydrogen production. Daniele *et al.* [7] evaluated the life-cycle performance of three different types of vehicles based on wind power electrolysis of water for hydrogen production and the results showed that hydrogen fuel is an excellent decarbonization solution. Both Dong *et al.* [8] and Huang *et al.* [9] performed life cycle analysis of the environmental impact of fuel cell vehicle energy under different fossil fuel-based hydrogen fuel paths. The results showed that supplying fuel cell vehicles with hydrogen from natural gas reforming is the most advantageous in terms of energy saving and emission reduction.

Hydrogen-fueled internal combustion engines are another way to use hydrogen as an alternative energy source. Hydrogen fuel cells are hampered by materials and technology, which provides an opportunity for the development of hydrogen-fueled internal combustion engines. The use of hydrogen fuel cells involves electrochemical reactions which require the purity of the hydrogen used (usually greater than 99.99%) to minimize the impact of impurities in the hydrogen on the catalyst and electrolyte, while hydrogen-fueled internal combustion engines require low purity of hydrogen. In contrast, hydrogen internal combustion engines have a definite advantage in terms of manufacturing and fuel purification costs. There are no reports on the life cycle of hydrogen-fueled internal combustion engine vehicles in China, and few studies have been done by other countries. Halim *et al.* [10] compared gasoline doped hydrogen with pure gasoline engine and analyzed the investment cost planning of two different combustion modes in five and ten years, and the results showed that after the fourth year, the investment cost of gasoline doped hydrogen car is lower than that of pure gasoline car, and the gap increases gradually with the increase of service life. However, the main study focuses on the consumption in the hydrogen production phase, and does not analyze the emissions and energy consumption in the combustion phase, which is not a comprehensive evaluation. In summary, the study of the whole life cycle of hydrogen fueled internal combustion engines not only reveals the application prospects of hydrogen fueled internal combustion engines, but also makes the evaluation of hydrogen fuel in vehicles more comprehensive.

## Research Methods and Contents

### Whole Life Cycle Evaluation Method

Life cycle evaluation method is a method of aggregating and evaluating one or more specific indicators of a product (service) system throughout its life cycle in terms of all inputs, outputs, and their direct or indirect impacts on the external environment [11]. The life cycle assessment of vehicles can be described as a well-to-wheel (WTW) process, which can be divided into two stages: well-to-tank (WTT) and tank-to-wheel (TTW). The hydrogen-fueled internal combustion engine can be described as the stages of hydrogen production, transportation, and use of hydrogen fuel in the internal combustion engine. The system boundary is shown in Figure 1.

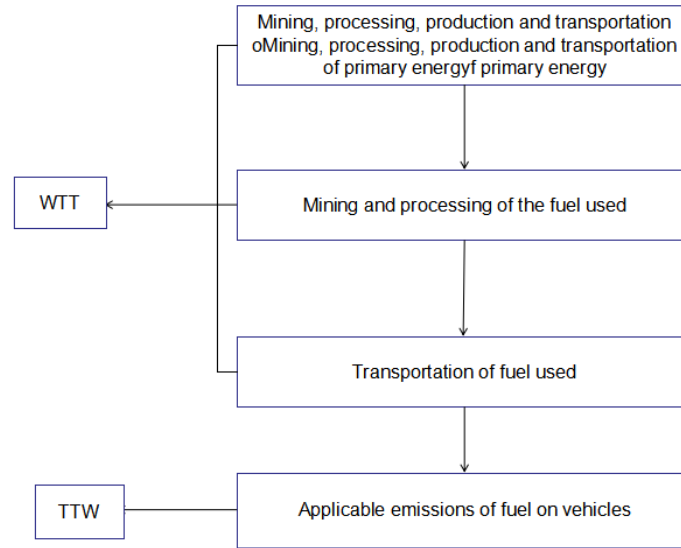


**Figure 1.** Hydrogen fuel system boundary

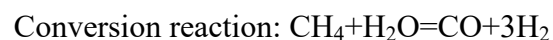
## Research Content

This study focuses on the whole life cycle analysis of a hydrogen-fueled internal combustion engine by selecting the two most and least energy-consuming and emission-consuming ways to produce hydrogen from a variety of hydrogen production methods, and considering the whole life cycle of hydrogen from the generation of hydrogen to the end of its emission after use in a hydrogen-fueled internal combustion engine, focusing on the production, manufacturing, and use costs (*i.e.*, understood the economics) and the emission of pollutants (mainly  $\text{NO}_x$  and  $\text{CO}_2$ -based emissions). Because only a simple modification of a conventional gasoline engine is needed to burn hydrogen and the weight of the vehicle manufacturing process itself is less than 1% [12], in order to study the main content, the vehicle manufacturing process is ignored and only the energy consumption and pollutant emissions during the production and manufacturing costs of hydrogen fuel and its use in the vehicle are focused.

## Two-stage Energy Consumption and Emissions

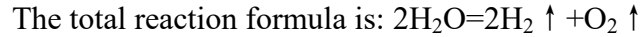
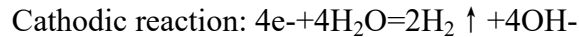
### Hydrogen Production Method

1. Hydrogen production by steam reforming of natural gas: The basic principle of producing hydrogen from natural gas is to use natural gas, high-temperature steam and synthetic reaction to form a mixture of hydrogen ( $\text{H}_2$ ), carbon monoxide ( $\text{CO}$ ) and a small amount of carbon dioxide ( $\text{CO}_2$ ).  $\text{CO}$  reacts with water again to produce additional hydrogen. Hydrogen production by steam reforming of natural gas is the most effective and common hydrogen production technology. The chemical reaction formula are as follows:



2. Hydrogen production by water electrolysis: The principle of hydrogen production by water electrolysis is electrochemical reaction which uses direct current to

electrolyze the electrolyte, and chemical reactions that occur at the two ends of different electrodes, thereby producing hydrogen and oxygen at the cathode and anode, respectively. The chemical reaction formula is as follows:



3. Coke oven gas hydrogen production method: Coke oven gas is a hydrogen-rich combustible gas. Using coke oven gas after removing impurities, the pressure swing adsorption separation method can be used to produce hydrogen.

In order to study the value of the entire hydrogen energy production range, this research selects hydrogen production by steam reforming of natural gas and electrolysis water hydrogen production methods for research.

## Energy Consumption and Emissions in WTT Phase

### *Energy Consumption for Hydrogen Production*

The consumption of one cubic meter of hydrogen produced under standard conditions (the quantities of reactants and products involved in the following are standard conditions) is analyzed. The cost of hydrogen production mainly includes natural gas costs, deionized water costs, cooling water costs, and electricity costs. For the four parts, the prices of raw materials are based on the relevant standards and related documents [13-14] announced by Beijing in 2021:

**Table 1.** Consumption and unit price of raw materials for producing 1 cubic meter of hydrogen (Unit : Yuan ¥)

	Natural gas steam Reforming hydrogen production	Electrolyte Hydrogen production	Unit price
Natural gas/m <sup>3</sup>	0.48	0.00	4.25
Deionized water/kg	1.30	0.88	0.069
Cooling water/kg	6.00	3.00	0.003
Electricity/degree	0.40	5.50	0.25
Equipment depreciation	0.1583	0.1286	-

Based on the data in Table 1, the costs for producing 1 cubic meter of hydrogen via steam reforming of natural gas and electrolysis of water are 2.37604 and 2.14474 yuan, respectively. From the perspective of production costs, the cost of hydrogen production from electrolysis of water is lower, which is 9.61% lower than that of natural gas reforming.

### *Hydrogen Production Emissions*

#### (1) Emissions from hydrogen production by steam reforming of natural gas

Natural gas is a primary energy source. The main components are methane and a small amount of olefins. There is no harmful gas emission during the acquisition process, but CO<sub>2</sub> is emitted during the hydrogen production process.

#### (2) Discharge of hydrogen production by electrolysis of water

There will be no emissions of pollutants in the process of electrolysis of water to produce hydrogen. But if considering that thermal power generation accounts for 73.32%

of the total power generation of china, pollutants are emitted during the power generation process.

### *Comparison of Two Hydrogen Production Schemes*

**Table 2.** Energy consumption and emissions of the two hydrogen production schemes

	Natural gas reforming to produce hydrogen	Hydrogen production by electrolysis of water
Coal/kg	0.000	0.320
CH <sub>4</sub> /m <sup>3</sup>	0.480	0.000
CO/kg	0.005	0.136
CO <sub>2</sub> /kg	0.491	1.030
NO <sub>x</sub> /kg	0.007	0.015
SO <sub>2</sub> /kg	0.007	0.030
PM2.5/kg	0.001	0.081

Table 2 shows the energy consumption and emissions of two different hydrogen production schemes to produce 1 cubic meter of hydrogen. Using CML2001 [15] to normalize and quantify the above data, the comprehensive environmental impact value is shown in Table 3:

**Table 3.** Comprehensive environmental impact values of the two hydrogen production schemes

Plan	Natural gas reforming to produce hydrogen	Hydrogen production by electrolysis of water
Comprehensive environmental impact value	$4.8 \times 10^{-11}$	$2.99 \times 10^{-9}$

The comprehensive environmental impact value of hydrogen production by steam reforming of natural gas is only 1.6% of that of hydrogen production by electrolysis of water, and its impact on the environment is much smaller than that of hydrogen production by electrolysis of water, mainly because the electricity consumed comes from thermal power generation.

### *Scenario Simulation*

The proportion of thermal power generation in western china is less than 15%. Table 4 shows the power generation structure of the four western regions in China in 2020.

**Table 4.** Power generation structure of Sichuan, Yunnan, Tibet and Qinghai in China in 2020

Source Province	Sichuan	Yunnan	Tibet	Qinghai
Thermal power	13.69%	9.51%	3.62%	13.5%
Hydropower	83.78%	81.97%	89.31%	65.78%
wind power	1.99%	7.54%	0.88%	6.53%
Solar energy	0.54%	0.98%	6.09%	14.19%
total	100%	100%	100%	100%

For different power generation structures, the comprehensive environmental impact values of the above four places can be calculated through the GaBi model. The comprehensive environmental impact results of the electrolytic water method in different power generation structures are shown in Table 5.

**Table 5.** Comprehensive environmental impact value of electrolyzed water in four provinces

Province	Sichuan	Yunnan	Tibet	Qinghai
Comprehensive environmental impact value	$3.2 \times 10^{-10}$	$2.9 \times 10^{-10}$	$1.6 \times 10^{-10}$	$3.1 \times 10^{-10}$

The use of electrolyzed water to produce hydrogen in western china has less impact on the environment than the use of electrolyzed water to produce hydrogen in other cities in China. As can be seen from Tables 3 and 5, although there is still a gap compared with hydrogen production by steam reforming of natural gas, the overall environmental impact has been reduced from 62 times to 3.3 times. Since the unstable power generation of renewable energy has impacted the grid, causing grid fluctuations and insecurity, this part of the power that cannot be connected to the grid has caused a large amount of "power abandonment". Table 6 shows the statistics of china's "abandonment of electricity" in recent years.

**Table 6.** 2017-2020 National abandoned electricity in China

Type Years	Abandon water	Abandon light	Abandon the wind
2017	4%	6%	12%
2018	5%	3%	7.2%
2019	4%	2%	4%
2020	3.39%	2%	3%

### Energy Consumption and Emissions in TTW Phase

Starting from the hydrogen fuel internal combustion engine, the energy consumption and emissions of the TTW phase are analyzed. The AVL-Fire three-dimensional simulation software is used for simulation. The model is based on a hydrogen-fueled internal combustion engine modified from the Jialing JH-600 single-cylinder engine. In order to ensure the reliability of the test simulation, the experimental data and the simulation data were compared at 3000 r/min and the equivalent ratio of 0.4. The simulated value is slightly higher than the experimental value, mainly because the simulated working conditions are relatively ideal. It is believed that the cylinder is fully enclosed, and there will be some deviations in the experiment. The maximum difference is 1.2%. It can be considered that this model can well reflect the actual working conditions of the hydrogen fuel internal combustion engine.

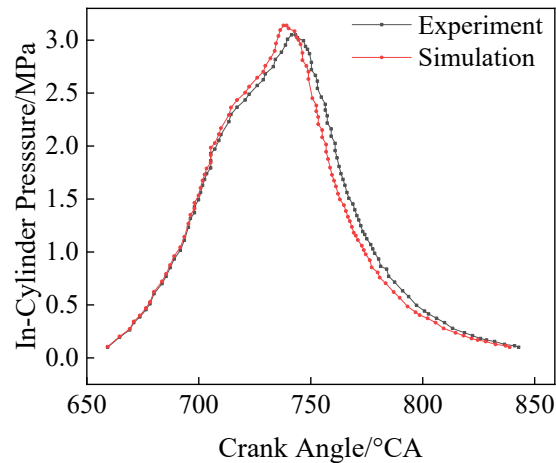


**Figure 2.** Model validation

### *Energy Consumption*

Hydrogen has high thermal efficiency whether used as the power source of hydrogen fuel cell or hydrogen fuel internal combustion engine. The low calorific value of hydrogen is 119.64 MJ/kg, which is 2.72 times that of gasoline. The combustion speed of hydrogen is fast, and high thermal efficiency [16]. BMW was the first company to develop hydrogen-fueled internal combustion engine vehicles. As early as 2004, BMW Motor Company conducted tests. The test result is that the hydrogen consumption per 100 kilometers is 3.7 kg, which is equivalent to 13.8 L gasoline/100-km. The hydrogen consumption can be reduced to 2.1 kg hydrogen/100-km at high speed, which is equivalent to 7.8 L gasoline/100-km [17]. Based on a 2.0-L gasoline engine modified hydrogen fuel internal combustion engine test, Beijing Institute of Technology Sun Baigang and others found that when the vehicle speed reaches 80 km/h, the hydrogen consumption per 100 kilometers is 1.43 kg. When the vehicle speed decreases, the hydrogen consumption per 100 kilometers drops to 1.27 kg, equivalent to 4.7 L gasoline/100-km, which is 18.9% lower than the original engine fuel consumption [18].

Through simulation, the fuel consumption and indicated thermal efficiency of hydrogen-fueled internal combustion engines under different operating conditions are studied. Figure 3 shows that the maximum power speed of the modified hydrogen fuel internal combustion engine is 6000 r/min. From the simulation results, it can be seen that at a hydrogen injection pressure of 4.5 bar, the maximum power at an equivalent ratio of 1.05 can reach 25 kW, and the maximum hydrogen consumption is 2.124 kg Hydrogen/h which is equivalent to 7.86 L gasoline/h. It can be seen from Figure 3 that as the engine speed increases, the indicated thermal efficiency of the hydrogen fuel internal combustion engine first increases and then decreases. The maximum indicated thermal efficiency can reach 43.2% at 3000 r/min. Compared with the maximum output power of 30 kW of the original engine, the maximum power of the modified hydrogen fuel internal combustion engine is reduced by 16.7%, but the indicated thermal efficiency can reach up to 43.2%, which is a great improvement compared with the traditional gasoline engine.



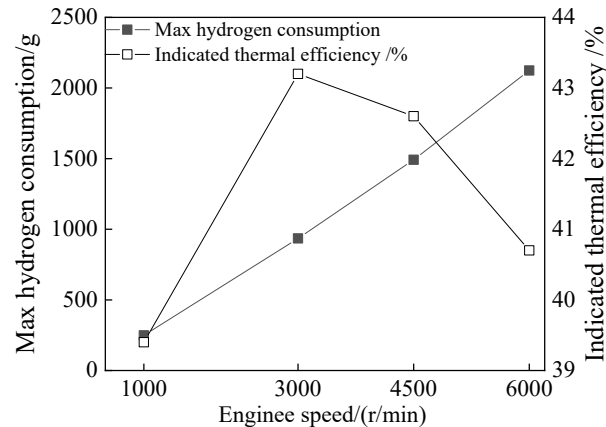


**Figure 3.** Maximum hydrogen consumption and indicated thermal efficiency at different speeds

### Emissions

Hydrogen is a clean energy source. There are few pollutant emissions during the combustion process. Compared with traditional internal combustion engines, the emissions of unburned hydrocarbon are almost negligible. Compared with traditional internal combustion engines, the emission of greenhouse gases can be reduced by 90%. The main pollutant is nitrogen oxides. In recent years, research on technologies for reducing nitrogen oxide emissions has become more and more mature, usually using exhaust gas recirculation (EGR) technology and in-cylinder water injection.

The simulation simulates the combustion emissions of the engine at 4 speeds and 5 loads. Table 7 shows the specific parameter levels:

**Table 7.** Simulation scheme

parameter	level				
Rotating speed rpm	1000	3000	4500	6000	
Load	10%	30%	50%	70%	100%
Equivalent ratio	0.5	0.6	0.7	0.84	1.05

Table 8 shows the simulation results of nitrogen oxide emissions at different speeds and loads.

**Table 8.** The mass fraction of NO under different working conditions (unit: ppm)

Equivalent ratio \ Rotational Speed	0.5	0.6	0.7	0.84	1.05
1000r/min	6	32	956	1969	195
3000r/min	60	895	4064	4985	365
4500r/min	159	2362	6256	6958	569
6000r/min	269	3025	6589	7846	695

The data in Table 8 are NO emissions under all operating conditions. When the normal working speed is below 3000 r/min and the equivalent ratio is lower than 0.5 and higher than 1.05, the NO emission is below 500ppm. At high speed and medium and high load (0.67-0.84), NO emission increases sharply. Compared with traditional internal combustion engine exhaust gas treatment devices that need to reduce CO, unburned hydrocarbons (HC) and NO emissions, the exhaust gas treatment of hydrogen fuel internal combustion engines only needs to reduce NO emissions. The simplest technology to reduce high-load NO emissions is the EGR Technology. Table 9 shows the NO

emission after adopting the EGR technology, in which 1000 r/min adopts 5% EGR, and the remaining speed is 10% EGR.

By comparing Table 8 and Table 9, it can be found that the highest reduction in NO emissions after the use of EGR technology has reached 94.1%. At 1000 r/min and 3000 r/min speeds, it is lower than 50 ppm at full load and low load, which is close to zero emission. The main reasons for the reduction of NO emissions are: increasing EGR reduces the fresh charge in the combustible mixture, the maximum combustion temperature in the cylinder decreases, the high temperature duration decreases, and the optimal NO generation conditions are changed. 4500 r/min and 6000r/min are the highest torque speed and the highest power speed. The NO emission is higher under medium and high loads, but the frequency of use is low. If you need to work at this speed for a short time, you can appropriately sacrifice the output power and the use of 15% EGR can reduce NO emissions by 92.6%, and it is also less than 500 ppm under medium and high loads.

**Table 9.** NO emissions (ppm) under different working conditions after using EGR

Rotational Speed	Equivalent ratio				
	0.5	0.6	0.7	0.84	1.05
1000r/min	0.4	1.9	58.7	210.3	11.7
3000r/min	3.5	53.7	243.6	485.6	21.9
4500r/min	39.8	590.5	1564	1739.5	142.2
6000r/min	67.2	756.3	1647.3	1961.5	173.8

**Table 10.** Emission test of hydrogen fuel internal combustion engine

Projects	Emissions/(g/km)		
	CO	HC	NOx
CHINA 6	0.7	0.068	0.05
Simulation results	0.09	0.033	0.042

Table 10 shows the various emissions after increasing EGR. According to limits and measurement methods for emissions from light-duty vehicles (CHINA 6). Carbon monoxide emissions are only 12.8% of the regulations, HC emissions are 48.5% of the regulations, and nitrogen oxides emissions are slightly higher, at 84% of the regulations.

In addition to adding exhaust gas treatment equipment, there are many ways to reduce nitrogen oxides. (1) Hydrogen has a wide range of flammable limits, and controlling the equivalent ratio below 0.5 or above 1.05 can effectively reduce NO emissions; (2) It is possible to mix hydrogen and natural gas to reduce nitrogen oxides at the expense of low carbon emissions Emissions.

## CONCLUSIONS

(1) The comprehensive environmental impact of hydrogen production by steam reforming of natural gas is only 1.6% of that of hydrogen production from electrolyzed water; in western china, "abandonment of electricity" is used to produce hydrogen from electrolyzed water, and the cost of hydrogen production from electrolyzed water is only 1/10 of that from natural gas reforming.

(2) The hydrogen consumption per hundred kilometers of the modified hydrogen internal combustion engine is 12.3% lower than the fuel consumption of the original gasoline engine without modification.

(3) The NO<sub>x</sub> emission of hydrogen fuel internal combustion engine is greatly reduced under the working conditions of equivalent ratio less than 0.5 and higher than 1.05. Under the coordination of EGR technology under medium and high loads, it can easily reach the national VI emission standards and there is room for further improvement.

### Conflict of Interest

The authors declare that there is no conflict of interests regarding the publication of this paper.

### ACKNOWLEDGMENTS

This research was supported by Special support plan for high-level talents of Henan Province- “ZHONGYUAN Thousand Talent Program” (ZYQR201810075).

### REFERENCES

- [1] Jiang, C., Wang, X., and Wang, Z. (2021). Research on automobile sales forecasting methods based on consumer attention. *Data Analysis and Knowledge Discovery*, 5(1), 128-139
- [2] Liu, C., and Jiang, X. (2019). The overall recovery of the oil and gas order reconstruction industry-an overview of the development of the domestic and foreign oil and gas industry in 2018 and the outlook for 2019. *International Petroleum Economics*, 27(1), 27-33+60
- [3] Lin, T., Wu, Ye., He, X., Zhang, S., and Hao, J. (2018). Fossil energy consumption and CO<sub>2</sub> emissions during the fuel life cycle of hydrogen fuel cell vehicles in China. *Environmental Science*, 39(8), 3946-3953
- [4] Chen, Y., Ding, Z., Wang, W., and Liu, J. (2019). Full life cycle assessment and scenario simulation of different hydrogen production schemes for hydrogen fuel cell vehicles. *Chinese Journal of Highways*, 32(5), 172-180
- [5] Simons, A., and Bauer, C. (2015). A life-cycle perspective on automotive fuel cells. *Applied Energy*, 157, 884-896. DOI: <https://doi.org/10.1016/j.apenergy.2015.02.049>
- [6] Kong, D., Tang, W., Liu, W., and Wang, M. (2018). Energy consumption, emission and economic evaluation of fuel cell vehicles. *Journal of Tongji University (Natural Science Edition)*, 46(4), 498-503+523
- [7] Candelaresi, D., Valente, A., Iribarren, D., Dufour, J., and Spazzafumo, G. (2021). Comparative life cycle assessment of hydrogen-fuelled passenger cars. *International Journal of Hydrogen Energy*, 46(72), 35961-35973. DOI: <https://doi.org/10.1016/j.ijhydene.2021.01.034>

- [8] Dong, J., Liu, X., Xu, X., and Zhang, S. (2016). Comparative life cycle assessment of hydrogen pathways from fossil sources in China. *International Journal of Energy Research*, 40(15), 2105-2116. DOI: <https://doi.org/10.1002/er.3586>
- [9] Huang, Z., and Zhang, X. (2006). Well-to-wheels analysis of hydrogen based fuel-cell vehicle pathways in Shanghai. *Energy*, 31(4), 471-489. DOI: <https://doi.org/10.1016/j.energy.2005.02.019>  
DOI:10.1016/j.energy.2005.02.019.DOI:10.1016/j.energy.2005.02.019.
- [10] Razali, H., Sopian, K., and Mat, A. S. (2013). Hydrogen as an Alternative: Life Cycle Cost Analysis between Hydrogen Internal Combustion Engine (AI+Hci) and Gasoline Engine Based on Brake Specific Fuel Consumption. *Applied Mechanics and Materials*, 315, 423-427. DOI: 10.4028/www.scientific.net/AMM.315.423
- [11] Xie, X., Yang, W., Shi, W., Zhang, S., Wang, Z., and Zhou, J. (2018). Research progress in life cycle assessment of hydrogen production technology. *Progress in Chemical Industry*, 37(6), 2147-2158
- [12] Meng, X., Wen, H., Zeng, A., and Shao, Y. (2020). Post-war material recovery vehicle path optimization based on improved ACO. *Firepower and Command Control*, 45(9), 47-51
- [13] Zhang, X., Wei, X., Han, J., Chou, Q., and Chen, J. (2010). Talk about the use of deionized water in hydrogen production by water electrolysis. *Science and Technology Information*, 25, 86
- [14] Guo, X., Huang, X., Zhang, K., Han, G., and Han, P. (2020). Research on the development status and price of natural gas power generation in China. *Zhejiang Electric Power*, 39(9), 109-117
- [15] Chen, Y., Yang, Y., Li, X., Dong, H., and Bai, R. (2014). Life cycle resource consumption of automotive power seats. *International Journal of Environmental Studies*, 71(4), 449-462
- [16] Fu, H., Chai, H., Sun, B., and Bao, L. (2020). Effects of Oxygen-Enriched Combustion on Performance of PFI Hydrogen Engine. *Vehicle Engine*, 2020(4), 1-6. DOI: 10.3969/j.issn.1001-2222.2020.04.001
- [17] Wallner, T., Lohse-Busch, H., Gurski, S., Duoba, M., Thiel, W., Martin, D., and Korn, T. (2008). Fuel economy and emissions evaluation of BMW Hydrogen 7 Mono-Fuel demonstration vehicles. *International Journal of Hydrogen Energy*, 33(24), 7607-7618. DOI: <https://doi.org/10.1016/j.ijhydene.2008.08.067>
- [18] Sun, B., Xiang, Q., and Liu, F. (2012). Hydrogen fuel internal combustion engine and vehicle performance test research. *Journal of Beijing Institute of Technology*, 32(10): 1026-1030

**Article copyright:** © 2022 Ping Guo, Jianlun Xu, Chuanhao Zhao and Baoliang Zhang. This is an open access article distributed under the terms of the [Creative Commons Attribution 4.0 International License](https://creativecommons.org/licenses/by/4.0/), which permits unrestricted use and distribution provided the original author and source are credited.



# Introduction of Abnormal Combustion in Hydrogen Internal Combustion Engines and the Detection Method

Jiahui Liu \*

North China University of Water Resources and Electric Power, Zhengzhou, Henan 450045, China

Received January 28, 2022; Accepted February 13, 2022; Published February 26, 2022

As a clean, environmentally friendly and renewable energy source, hydrogen as an alternative engine fuel can greatly reduce atmospheric pollution and alleviate the shortage of oil resources, and is the most promising alternative fuel for vehicles among new fuels. However, due to its fast combustion rate and wide ignition limit, hydrogen often shows abnormal combustion phenomena (such as pre-ignition, backfire and knock), when it is used in the engine, thus affecting the performance and normal use of engines. In this paper, the advantages and disadvantages of hydrogen as an alternative fuel for the engine are summarized according to the characteristics of hydrogen. On this basis, the mechanism, influence factors and harm of abnormal combustion in the hydrogen internal combustion engine are analyzed and summarized, which provides a theoretical basis for solving abnormal combustion problems. Finally, several commonly used abnormal combustion detection methods are summarized.

*Keywords:* Hydrogen internal combustion engine; Abnormal combustion; Detection method; Clean energy

## Introduction

Energy plays an equally important role in the economic development of all countries in the world, and is an important measure of a country's comprehensive national power, economic development strength, people's basic living and social and cultural civilization level and its essential embodiment. The most widely used conventional energy sources in the global energy industry today are coal, oil, natural gas and other fossil fuels, which have greatly contributed to the progress of socio-economic. With the rapid development of global society and economy, the per capita energy consumption level has been rising significantly and rapidly. People are increasingly dependent on energy in their normal production activities and daily life, and energy plays an increasingly significant role and importance productivity in developed countries [1]. Most of the traditional energy sources such as coal, oil, natural gas and other fossil energy sources are non-renewable. Excessive exploitation and use will reduce energy storage, and the low efficiency of recovery and conversion of traditional conventional energy will cause energy consumption and waste in the conversion process. Traditional energy also causes a lot of pollution to the environment. These pollutants can directly enter our body through human breathing, which also causes harm to human physical and mental health.

As China's population and economy continue to grow and society continues to develop in recent years, the transport industry is gaining momentum and the automotive

\*Corresponding author: 15152025721@163.com

industry is growing rapidly. Although the popularity of the automobile has brought great convenience to people's lives, the problems of pollution and the consumption of oil resources due to exhaust emissions are also becoming more and more serious, so the search for renewable and clean energy sources to replace traditional petroleum-fueled vehicles has become a priority in the automotive sector. The development of clean and non-polluting alternative energy sources has become an inevitable trend, which has led to the transformation of the traditional automotive industry and the development of clean energy vehicles, which has also led to the development of hydrogen-fueled engines.

Therefore, this paper analyzes the advantages and disadvantages of hydrogen as an alternative fuel for vehicles, summarizes several common abnormal combustion phenomena in hydrogen internal combustion engines, lists their generation mechanisms, influencing factors and hazards, and finally summarizes several methods for detecting abnormal combustion in engines, in response to this current situation.

## Properties of Hydrogen as a Fuel

Hydrogen as a fuel is the most promising alternative fuel for vehicles among all new fuels due to its high combustion efficiency, zero emissions and renewability [2]. The value of hydrogen energy applications has been widely recognized worldwide and there has been significant progress in its use. The continuous development of hydrogen storage technology has led to the use of hydrogen in a wide range of applications such as transportation, various engines, fuel cells and power stations.

Hydrogen is a clean and renewable energy source and does not contain CH, CO or carbon particles in its emissions during combustion in engines. It is considered as a good solution to the problem of environmental pollution from conventional engine emissions [3]. Hydrogen can be used as an alternative engine fuel for the following reasons [4].

(1) Hydrogen burns quickly with high thermal efficiency.

(2) Hydrogen has a wide ignition limit and a wide combustible range, allowing for thin combustion and improved economy, while reducing the maximum combustion temperature and significantly reducing NO<sub>x</sub> emissions.

(3) Hydrogen has good diffusion performance. The diffusion coefficient of hydrogen is 12 times that of gasoline, which can be mixed more fully with air during premixed combustion and help combustion.

(4) The low ignition energy of hydrogen makes it less prone to misfires and reduces the cyclic changes in the cylinder. But it is also prone to abnormal combustion phenomena such as premature ignition and backfires, when it is ignited by hot exhaust gases and hot surfaces.

(5) Hydrogen has a higher ignition point in general. Engines can use a larger compression ratio, thus increasing the thermal efficiency of combustion.

## Common Abnormal Combustion

### Premature Combustion

#### *Mechanisms of Generation*

Early ignition means that before the normal ignition of the spark plug, the mixture in the cylinder is ignited by the higher temperature of the incandescent point. As the

mixture is heated in the intake and compression process for a long time by the incandescent surface, the ignition area is also larger. Once ignited, the flame spreads quickly and the pressure rise rate is also larger. So the compression stroke at the end of the negative work is very large and increases the heat dissipation to the cylinder wall, which further promotes the incandescent point temperature rise and earlier ignition mixture [5]. Because of the low ignition energy of hydrogen and hydrogen flame propagation speed, hydrogen internal combustion engines are more prone to pre-ignition phenomenon. Generally speaking, the hot spots in the cylinder that cause pre-ignition are the spark plug insulator, electrode, exhaust valve and some deposits in the cylinder. Pre-ignition is likely to occur in the external mixture formation method of hydrogen internal combustion engine. It is more likely to occur at the high compression ratio of high load.

### *Influencing Factors*

The main factors affecting the pre-ignition of the engine are the compression ratio of the mixture, the engine speed, the temperature of the mixture when entering the cylinder through the intake pipe, the intake and exhaust gas distribution phase and the spark plug [6]. As the compression ratio increases, the temperature of the combustible mixture in the compression process will also continue to rise, resulting in the heat of the hot surface of the cylinder is not easy to dissipate and maintain a higher temperature. Therefore, the mixture into the cylinder is more likely to be ignited by the high temperature hot spot, increasing the tendency of pre-ignition. The higher the temperature of the hydrogen air mixture entering the cylinder, the more likely it is to ignite prematurely by the hot exhaust gas or hot surface in the cylinder. Because the ignition energy of hydrogen is low, the higher the temperature of the mixture, the higher the energy, and the easier it will be ignited. Increasing the overlap angle of the inlet and exhaust valves is conducive to removing the residual exhaust gas in the cylinder, increasing the fresh charge into the cylinder, which is conducive to reducing the heat load in the cylinder, the temperature of the combustion chamber wall and the tendency of pre-ignition. But the overlap angle of the inlet and exhaust valves should not be too large, it may cause some gas backflow phenomenon. The spark plug in the compression and work stroke will absorb the heat generated by the combustion of the mixture (known as the hot surface). Under high temperature conditions, part of the lubricating oil volatilizes and adheres to the surface of the spark plug to form carbon, and the heat is not easy to dissipate. The difference in the structure and material of the spark plug will affect its thermal conductivity. The worse the thermal conductivity, the easier it is to cause premature ignition.

### *Hazards*

When premature ignition is relatively mild, it increases the noise of the hydrogen internal combustion engine and causes a slight vibration of the hydrogen internal combustion engine. In general, premature ignition will cause the hydrogen internal combustion engine to stop running, affecting the normal operation of the vehicle. In severe cases, this may cause damage to components such as intake pipes, spark plugs and cylinders.

## **Backfire**

### *Mechanisms of Generation*

Backfire is a phenomenon where the hydrogen-air mixture in the intake port is ignited prematurely before the intake valve has been closed. There are several different views on the mechanism of backfire. Some researchers believe that the flame of the unburned hydrogen gas in the cylinder ignites the combustible mixture in the intake port, but most believe that the backfire is caused by the high temperature residual exhaust gas in the combustion chamber and hot spots in the cylinder [7]. When the intake valve is first opened, the backfire is mainly caused by the high temperature exhaust gas, afterburning mixture and high temperature hot spots. When the intake valve is almost closed, the backfire is mainly caused by the continuous advance of pre-ignition.

### *Influencing Factors*

Backfire is a type of abnormal combustion, where combustion occurs only under certain conditions. The following conditions are required for backfire to occur in the intake port: Firstly, there must be a suitable concentration of hydrogen in the intake port. Secondly, there must be a high temperature exhaust gas in the vicinity of the intake valve that is capable of igniting the hydrogen. The analysis of the high temperature exhaust gas includes the concentration and temperature of the exhaust gas and its location in the intake port. These parameters are closely related to the occurrence of backfire, so all the structural factors and operation factors that can affect the concentration, temperature of the exhaust gas and the change of the position of the exhaust gas in the intake are factors affecting the backfire. Backfire is related to the combustion rate and the concentration of the mixture. If the mixture is too lean, the combustion rate will be slow and the combustion of the mixture will continue until the exhaust gas end. When the intake valve is opened, the still-burning mixture can easily ignite the mixture in the intake port. [8].

### *Hazards*

When the backfire phenomenon is slight, the noise of hydrogen internal combustion engine will increase rapidly or the intake port will misfire locally. In general, the hydrogen internal combustion engine cannot operate normally. In serious cases, the temperature and pressure in the intake port are too high, and the fresh charge cannot enter, causing the engine misfire and even the damage of the intake port and hydrogen supply system.

## Knock

### *Mechanisms of Generation*

The cause of knock can be attributed to the spontaneous combustion of the final combustion mixture. Before the ignition of a hydrogen internal combustion engine, the mixture is spontaneously combusted at a distance from the flame before the flame front surface reaches it. After the spark ignition, the flame propagates forward at the normal speed propagation rate (30~70 m/s), making part of the final combustion mixture in the final combustion position further compressed and thermally radiated. It accelerates the prior reaction and releases some heat, making the temperature of the final combustion mixture rise continuously. So, before the normal flame arrives, the most suitable part of the final combustion mixture inside has already appeared one or more flame centre, resulting in flame from these centres to 100~300 m/s (slight knock) to 800~1000 m/s or higher rate (strong knock accompanied by shock waves) propagation and rapid combustion of the final mixture of gas burned out. Therefore, the phenomenon of knock is the final combustion mixture of spontaneous combustion phenomenon [9].



### *Influencing Factors*

The main operating factors affecting knock are ignition advance angle, speed, load, mixture concentration and combustion chamber deposits. The main structural factors are cylinder diameter, spark plug position, cylinder head and piston material, and combustion chamber structure. In order to analyze the effects of various factors on knocking more concisely and clearly, two times are defined. The time required from the flame centre to the normal flame propagation to the final combustion mixture is  $t_1$ , while the time required from the formation of the flame center to the spontaneous combustion of the final combustion mixture is  $t_2$ .

Operating factors [10]:

(1) Ignition advance angle: With the increase of ignition advance angle, the time  $t_1$  from flame center formation to flame propagation to the whole combustion chamber decreases. As the ignition advance angle increases, the pressure in the cylinder increases, the extrusion effect on the final fuel mixture increases, the temperature increases, and the delay period  $t_2$  of the final fuel mixture decreases. According to the test, within the range of the practical ignition advance angle, the decrease of  $t_2$  plays a decisive role, so the knock tendency increases with the increase of the ignition advance angle.

(2) Speed: With the increase of rotational speed, the propagation speed of flame increases and  $t_1$  decreases. As the rotational speed increases, the charge coefficient decreases, the pressure in the cylinder decreases,  $t_2$  increases, and the knock tendency increases.

(3) Load: At a certain speed and when the throttle is closed (*i.e.*, the load is reduced), the residual exhaust gas coefficient increases, the in-cylinder pressure drops,  $t_2$  increases, and the propensity for deflagration decreases.

(4) Mixture concentration: The change of the mixture concentration will affect the flame propagation velocity and the ignition delay period of final combustion mixture. When the excess air coefficient is 0.8 to 0.9, the flame propagation speed is the fastest and  $t_1$  is the smallest, but the ignition delay period  $t_2$  of the final combustion mixture is also the smallest. The test shows that the reduction of  $t_2$  plays a decisive role, and thus when the excess air coefficient is 0.8 to 0.9, the knock tendency is the largest. Too thick or too thin mixture of gas can reduce the tendency of knock.

(6) Combustion chamber deposits: During engine operation, a layer of deposits, generally known as carbon, is produced on the walls of the combustion chamber. The temperature of the carbon deposit is higher. The intake compression process constantly heats the mixture, and the deposit is a poor conductor of heat, therefore increasing the temperature of the final combustion mixture. The deposit itself occupies a certain volume, therefore increasing the compression ratio of the engine. In summary, the presence of deposits makes the knock tendency increased.

Structural factors [11]:

(1) Cylinder diameter: When the diameter of the cylinder increases, the propagation distance of the flame becomes longer, that is,  $t_1$  becomes longer. As the ratio of the cooling area of the combustion chamber to the volume means that the surface to volume ratio decreases, the heat dissipation area per unit volume decreases, and the temperature increases. So,  $t_2$  decreases and the knock tendency will increase.

(2) Spark plug position: Spark plug position will affect the flame propagation distance and also affect the final combustion mixture in the cylinder, thus affecting the temperature of the final combustion mixture. For example, the spark plug is located in the

exhaust valve is the least likely to cause knock. But if the distance from the intake valve is too large, then the spark plug gap in the exhaust gas is not easy to remove, and the spark plug will affect the stability of the engine running under low load.

(3) Cylinder head and piston material: The thermal conductivity of cylinder head and piston will affect the tendency of knock. Aluminum alloy has good thermal conductivity, so using aluminum alloy piston and cylinder head can inhibit the occurrence of knock and improve the compression ratio of engine.

(4) Combustion chamber structure: Combustion chamber structure is the most important structural parameter affecting knock. The shape of the combustion chamber will affect the flame propagation distance, turbulence intensity, heat dissipation to the cooling water and the number and temperature of the final combustion mixture. Any combustion chamber structure that allows for a shorter flame spread distance, higher turbulence and flame spread rate will help to reduce the knock tendency.

### *Hazards*

(1) Engine overheating: When bursting into flames, the destruction of the boundary layer, cylinder head, the piston top surface temperature rise. Combustion chamber local overheating will cause surface ignition, thus further overheating, which eventually leads to light alloy cylinder head, piston softening, melting or burning. Local overheating in the cylinder will also cause high temperature decomposition of combustion products and thermal decomposition of the oil film on the cylinder wall. The reoxidation of the decomposed products is incomplete, resulting in exhaust smoke.

(2) Increased stress on parts: During knock, the pressure rise rate and the maximum combustion pressure both rise, making it easy to damage the stressed parts.

(3) Output power (*i.e.*, thermal efficiency is reduced): Knock will lead to a sudden increase in local pressure and temperature in the engine cylinder, and it is too late to make the cylinder pressure equilibrium. The chemical reaction rate is greater than the rate of gas expansion, and thus will produce a pressure wave. When the shock wave hits the cylinder wall, it will destroy the laminar boundary layer, thus increasing the heat transfer coefficient and the cooling loss and reducing the output power. At the same time the thermal efficiency decreases due to the increased cooling losses and the appearance of carbon slag as a combustion product.

(4) The pressure wave generated by knock damages the oil film and cooling water film on the inner and outer surface of the cylinder wall, resulting in accelerated wear of parts [12].

## **Abnormal Combustion Detection Methods**

In the study of engine fault diagnosis, the detection signals are mostly vibration signals, speed fluctuation signals, sound intensity signals, oil parameters, pressure signals, temperature signals and image signals. Most of the signals are processed using amplitude domain analysis, frequency domain analysis, fractal geometry, neural network, wavelet analysis, and combinations of these methods [13]. When abnormal combustion occurs, there may be macroscopic phenomena such as vibration, noise increase and temperature rise, and microscopic changes in the ion current signal, based on which different methods can be used to detect abnormal combustion.

## Ion Current Method

The mixture in the cylinder will produce a large number of charged particles such as free electrons, positive and negative ions and free radicals in the combustion process of spark ignition, fire core formation and flame propagation. Because they exist in the flame front area and burned area, the gas has certain conductivity. When a DC bias voltage is added to the two poles of the spark plug, an electric field is formed in the spark plug gap, with positive ions moving in the direction of the cathode and electrons and negative ions moving in the direction of the anode, forming a spark plug ion current [14].

In the paper [14], for example, a spark plug type ion current sensor was installed in a turbocharged PFI engine and the ion current signal was compared with the cylinder pressure signal and combustion characteristic values under different combustion conditions. By analyzing the ion current waveform, misfire cycles caused by spark plug failure to ignite or injector failure to inject fuel or lean mixture could be identified, respectively. The relationship between the ion current signal and the pre-ignition cycle was further analyzed experimentally. When the normal combustion cycle occurs, the ion current signal is generated in the order of the 1st peak - charging disturbance, 2nd peak - discharging disturbance, 3rd peak - ion current signal. But in the pre-ignition cycle as shown in Figure 1, the ion current signal generation order has changed significantly, when the spark plug ignition accumulation occurs (generate the 1st peak - charging disturbance signal). Due to the pre-ignition phenomenon in the cylinder and the mixture produces spontaneous combustion, the ion current signal is generated in the early stage of spontaneous combustion. As the cylinder pressure rises, the cylinder temperature rises and the ion current signal strength rises (3rd peak - early ignition ion current signal). The duration of the pre-ignition ion current signal  $t_d$  is also significantly greater than the 1st and 2nd peak signals. The pre-ignition ion current signal  $t_d$  value detected in this test is  $25^\circ$ . Therefore, for this engine, when ion current is used to detect pre-ignition, pre-ignition is considered to have occurred when the  $t_d$ -value is greater than  $20^\circ$ . The analysis in this paper shows that the ion current method can detect the occurrence of pre-ignition very well.

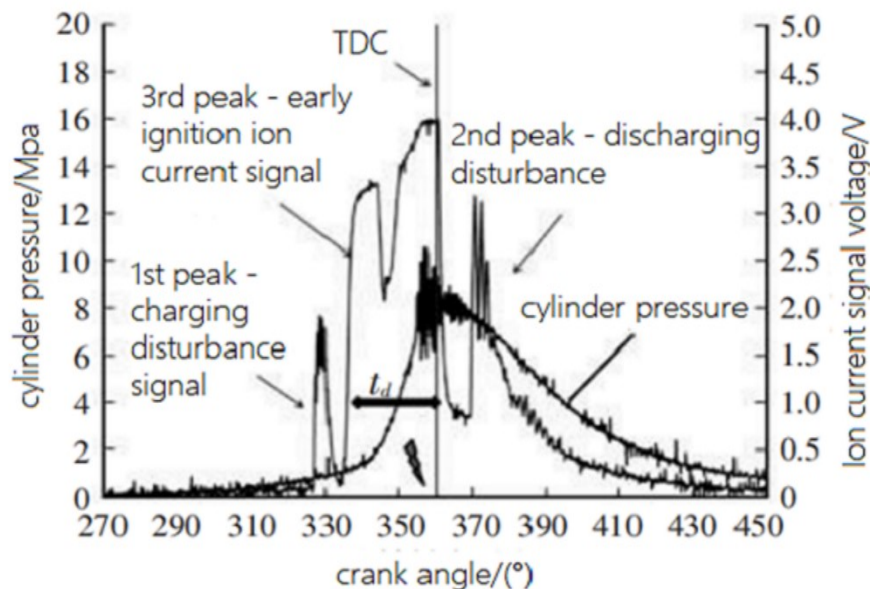


**Figure 1.** Schematic representation of ion current signal detection for pre-ignition [14]

The ion current method can also detect the occurrence of knock. When knock occurs, the pressure wave generated by the knock propagates repeatedly at a high frequency in the cylinder, causing the local gas density in the cylinder to vibrate at a high frequency. In the combustion zone, the ion and free electron density in the gas also vibrates and changes. Thus, the pressure wave caused by the knock is superimposed on the spark plug ion current signal, and the frequency characteristics of the knock pressure wave can be obtained by a reasonable analysis of the spark plug ion current signal [15]. The literature [15] compares the effect of using the ion current method and the body vibration method for detecting engine detonations. It can be seen from Figure 2 that there are obvious differences between the ion current signals and vibration signals of the body under knock and non-knock conditions. The ion current signals in knock and non-knock conditions are smooth and regular, while the ion current signals in knock conditions are not smooth with superposition of high-frequency signals on the waveform. Similarly, the vibration amplitude of the body in the condition of no knock is small, but the vibration signal of the body in the condition of knock appears obvious large oscillation.

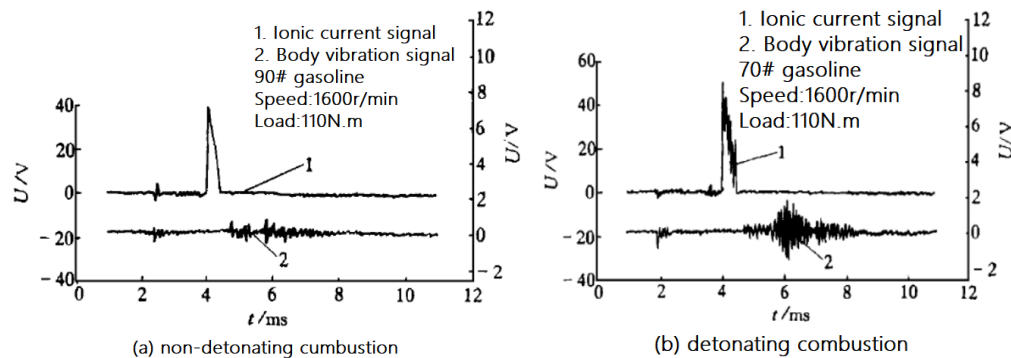


**Figure 2.** Without and with knock signal [15]

The ion current method is an emerging technology that is completely different from the traditional body vibration method. Compared to the body vibration method, it has the advantages of simple signal processing, accurate measurement and low cost, making it a new technology with great market potential.

### Body Vibration Method

The body vibration method uses vibration sensors to detect detonations. During a knock, as the pressure wave is reflected by the cylinder wall, it causes the engine block to vibrate and the magnitude of this vibration varies depending on the position of the engine block. The frequency characteristics of the burst pressure wave can be obtained through a reasonable analysis of the vibration sensor signal at the appropriate location on the engine block. A vibration-based pre-ignition and knock detection system and its detection method can be used [16] to differentiate between pre-ignition and normal knock, depending on the vibration range of the two. This detection system includes vibration sensor and controller. The vibration sensor is mounted on the engine for detecting the vibration signal within a specific crankshaft angle range of the engine, and the detected vibration signal will be transmitted to the controller. The controller calculates and records the peak magnitude of the combustion cycle vibration signal and the phase corresponding to the peak. The vibration signal is used to determine whether pre-ignition and knock have occurred. The specific steps for the detection using this system are:

(1) Pre-calibrate the engine and calibrate the knock threshold and pre-ignition threshold.

(2) Calculation of the vibration signal over a specific range of crankshaft angles, filtering of the signal and calculation of the peak and phase of the signal oscillation.

(3) Comparison of the detected peak and phase with the pre-calibrated knock threshold and pre-ignition threshold.

(4) Comparison of the detected peak and phase with the pre-calibrated knock threshold and pre-ignition threshold.

(5) This system detects pre-ignition and knocks based on vibrations in a simple and easy to use way, and is simple to operate and can be used in real vehicles without the need for additional equipment.

### Wide Domain Oxygen Sensor Method

On Board Diagnostics (OBD) systems require the ability to monitor the components or systems that cause emissions exceedances. It is therefore of great practical value to study abnormal engine combustion in OBD systems and to analyze the emission status through the oxygen sensor signal. While conventional step-type oxygen sensors do not detect sudden changes in oxygen concentration under lean mixture conditions due to their non-linear output characteristics, the Universal Exhaust Gas Oxygen Sensor (UEGO) can measure air-fuel ratios between 10 and 20 in an infinite manner. As a result, the use of wide area oxygen sensors in recent years in lean-burn engines has made it possible to detect abnormal cylinder combustion conditions at full operating conditions.

Qi *et al.* [17] actively and rapidly adjusted the fluctuation range of closed-loop fuel regulating factor under specific working conditions to quickly change the exhaust gas composition of the exhaust system, and calculated the voltage jump frequency and jump amplitude of the oxygen sensor within a reasonable sampling interval to test the response performance of the voltage signal of the oxygen sensor. Dong *et al.* [18] designed a natural gas engine oxygen sensor fault simulation system with the technical support of LabVIEW software, and analyzed the influence of the oxygen sensor fault on engine power economy and various emission indicators. Fang *et al.* [19] studied the use of Bosch LSU ADV wide domain oxygen sensor with fast transient response characteristics to measure oxygen concentration in the exhaust pipe in real time to detect abnormal combustion conditions in the cylinder by identifying different abnormal combustion phenomena and determining abnormal combustion causes through different mutation values on the signals of the wide domain oxygen sensor.

The literature [19] shows that abnormal oxygen sensor signal waveforms, if not caused by engine control strategies under certain special operating conditions, generally indicate abnormal engine combustion and a fault in the associated system. These faults cause abnormal combustion of the mixture in the cylinder, which in turn causes the oxygen content in the exhaust to vary and the signal waveform of the oxygen sensor to become abnormal. For fuel injection system, ignition system faults and vacuum leaks caused by the oxygen sensor's signal waveform serious noise waveform, the pattern will be somewhat different. By distinguishing the faults corresponding to the different spurious waves and analyzing the signal voltage waveform of the oxygen sensor, the fault area causing the abnormal combustion can be further pinpointed. It is therefore feasible to use an oxygen sensor to detect abnormal engine combustion.

## CONCLUSIONS

Based on the current situation of energy shortage and environmental pollution in China, the feasibility and superiority of hydrogen as an alternative fuel for engines are analyzed in this paper. However, due to some inherent characteristics of hydrogen, it is easy to cause abnormal combustion phenomenon of pre-ignition, backfire and knock when used as automobile fuel. Based on this, this paper summarizes the generation mechanism, influence factors and the harm of several abnormal combustion conditions. By analyzing the domestic and foreign researches on engine fault and abnormal combustion detection methods, three commonly used detection methods, including ion current method, body vibration method and wide area oxygen sensor method, are summarized.

## Conflict of Interest

The author declares that there is no conflict of interests regarding the publication of this paper.

## REFERENCES

- [1] Liu, Z. (2019). *Research on flow field and hydrothermal management of proton exchange membrane fuel cells*. South China University, Thesis.
- [2] Verhelst, S. (2014). Recent progress in the use of hydrogen as a fuel for internal combustion engines. *International Journal of Hydrogen Energy*, 39(2), 1071-1085. DOI: <https://doi.org/10.1016/j.ijhydene.2013.10.102>
- [3] Yuan, K. (2017). An introduction to early combustion in abnormal combustion of hydrogen internal combustion engines. *Automotive Practical Art*, 19, 162-164.
- [4] Zhang, F. (2017). *Effect of split-section injection method on the combustion and performance of hydrogen internal combustion engine*. North China University of Water and Electric Power, Thesis.
- [5] Ren, T. (2014). *Influence of in-cylinder operation parameters on the pressure rise rate and early ignition of hydrogen-fueled engines*. North China University of Water Resources and Hydropower, Thesis.
- [6] Yuan, K. (2017). An introduction to early combustion in abnormal combustion of hydrogen internal combustion engines. *Automotive practical arts*, 19, 162-164.
- [7] Duan, J., Liu, F., and Sun, B. (2013). Research on the mechanism and control of tempering in inlet tract fuel-injected hydrogen internal combustion engines. *Journal of Agricultural Machinery*, 44(3), 1-5+37.
- [8] Yamin, J. A. A. (2006). Comparative study using hydrogen and gasoline as fuels: combustion duration effect. 30(14), 1175-1187. DOI: <https://doi.org/10.1002/er.1213>
- [9] Zhou, L. (2011). *Internal Combustion Mechanics*. 3rd edition. Mechanical Industry Press.
- [10] Jiang, D. (2001). *Combustion and emission of internal combustion engines*. Xi'an Jiaotong University Press.

- [11] Jiang, D. (2002). *Principles of Higher Internal Combustion Engines*. Xi'an Jiaotong University Press.
- [12] Zhao, S. (2015). Abnormal combustion of gasoline engines. *Agricultural machinery use and maintenance*, 2015(1), 40.
- [13] Duan, J., Zheng, J., and Yang, Z. (2010). Diagnosis of abnormal combustion in hydrogen engines using radial basis function networks. *Journal of North China University of Water Resources and Hydroelectricity (Natural Science Edition)*, 31(2), 55-58.
- [14] Tong, S., Li, H., Y, Z., Hu, Z., and Li, L. (2016). Diagnosis of abnormal in-cylinder combustion based on ion current. *Automotive Technology*, 2016(9), 18-21+26.
- [15] Wu, X., Wang, Y., and Li, F. (2001). A comparison of the ion current method and the body vibration method for the detection of burst vibration. *Journal of Xi'an Jiaotong University*, 2001(10), 1059-1061+1066.
- [16] Wei, H., Hua, J., Feng, D., Pan, M. (2016). *A kind of early combustion and Knocking detection and its detection method based on vibrations*, CN106762133A, China Patent.
- [17] Qi, Z., Zeng, G., Gary, S., Xu, Y., Wang, C., and Zan, X. (2015). Research on active diagnosis strategy for front oxygen sensor response performance of gasoline vehicles. *Automotive Engineering*, 37(10), 1195-1201.
- [18] Dong, Q., Yuan, H., Jian, X., Li, Y., and Jiao, S. (2013). Simulation test of natural gas engine oxygen sensor failure. *Journal of Transportation Engineering*, 13(3), 62-70.
- [19] Fang, W., Ma, Y., Li, Z., and Zhang, C. (2017). Research on detecting abnormal combustion of gasoline engine based on UEGO signal level. *Journal of Gansu Agricultural University*, 52(4), 188-192.

**Article copyright:** © 2022 Jiahui Liu. This is an open access article distributed under the terms of the [Creative Commons Attribution 4.0 International License](https://creativecommons.org/licenses/by/4.0/), which permits unrestricted use and distribution provided the original author and source are credited.



# Energy Conversion and Conservation Technology in Facing Net Zero-Emission Conditions and Supporting National Defense

Abdi Manab Idris,<sup>1\*</sup> Nugroho Adi Sasongko,<sup>1,2</sup> and Yanif Dwi Kuntjoro<sup>1,3</sup>

1: Energy Security Department, Defence Management Faculty, Indonesia Defense University, Bogor, Indonesia

2: Agency for The Assessment and Application of Technology, M.H Thamrin Street No. 8, Jakarta., 10340

3: Mathematics Department, Mathematics and Natural Science Military Faculty, Indonesia Defense University

Received February 14, 2022; Accepted March 5, 2022, Published March 13, 2022

Conversion technology is a solution that was born to solve energy problems and human needs. Without energy, all human activities ranging from households and jobs to the industry cannot work as they should, but energy conversion that uses conventional fuels will cause new issues such as climate changes. Therefore, energy conservation is very important for sustainability and energy saving. So, by reducing energy use, the pollution produced will decrease. This paper focuses on the introduction of energy conversion and conservation technology based on a qualitative literature review to deal with net-zero emission conditions. The conversion technology is environmentally friendly and efficient, and is committed to following the international Net Zero Emissions (NZE) agreement, renewable energy conversion technology and new technologies (fuel cells) to meet Indonesia's defense equipment and defense needs. Indonesia's energy use (2019) consists of oil 35%, coal 37.3%, gas 18.5%, hydropower 2.5%, geothermal 1.7%, biofuel 3%, and other renewables at nearly 2%. In 2013 Indonesia's recoverable shale resources obtained a value of 8 Billion Barrels. Because of that the total CO<sub>2</sub> emissions resulting from energy use in Indonesia are 581 MtCO<sub>2</sub> in 2019. Efforts to fulfil Indonesia's Nationally Determined Contribution (NDC) continue to be carried out, so that Indonesia's target is to enter a state of net-zero emission by 2060. Fuel cell technology has the potential to be applied in the Indonesian National Army, because of its relatively small size, light weight, zero-emission, high specific energy and zero-noise.

*Keywords: Energy Conservation; Conversion Technology; Net Zero Emission; Supporting National Defense; Fuel Cells Technology.*

## Introduction

The main challenges facing the world today are energy security, sustainability, pollution, and the impact of climate change. Energy security includes affordability, acceptability, accessibility and availability. The main focus of energy security in Indonesia today is the availability of energy evenly and comprehensively [1]. According to the Ministry of Energy and Mineral Resources of the Republic of

\*Corresponding author: amanabidris@gmail.com



Indonesia, hundreds of villages have not received electricity service 24 hours a day [2]. Not to mention that the current energy mix is still dominated by fossil-based power plants (coal, oil and gas) [3]. Many authors and organizations advocate the transition to 100% renewable energy with an eye on the country's economic recovery. The choice was based on the fact that renewable energy is a technology that has been proven to be rapidly developing and has the potential to have a zero-carbon footprint [4]. These benefits are a very appropriate solution to overcome climate change, which is perhaps the most pressing challenge facing the global community, so that the awareness of every country holds an international meeting to discuss a simultaneous solution on an international scale [5].

At the end of 2015, an international meeting was held in Paris to produce an international agreement (The Paris Agreement). This Convention was attended by 196 parties from various countries because it is very important in fighting global climate change and adapting to its impacts. The meeting resulted in an international agreement that is legally binding as an effort to fight climate change. The Paris Convention aims to discuss the maximum limit for global warming of 2 to 1.5 °C concerning the conditions of the earth before the industrial revolution. Efforts to implement these long-term goals by minimizing Greenhouse Gas (GHG) emissions to zero net so that the target of a neutral climate in 2050 can be achieved [6]. Global warming is influenced by several indicators, such as GHG, pollutants, forest burning and use of fossil fuel engines/technology. The Paris Agreement provides a long term framework for financial support, capacity building and technology [7].

One of the visions of the Paris Agreement is about development, transfer and conversion technology. Future technologies will focus on increasing resilience to climate change and reducing GHG emissions. Establishment of a technology framework to provide comprehensive guidance regarding environmentally friendly technology mechanisms (conversion technology) through policy tools and forms of implementation. Conversion technology is an integrated process in achieving the goal of zero waste. This technology not only creates useful products but also has the potential to reduce emissions of greenhouse gases and other air pollutants. Conversion technology refers to a variety of advanced technologies that can convert solid waste that cannot be recycled into useful products, such as green fuels and environmentally friendly renewable energy [8].

The technology diversification used in the conversion is thermal, chemical, biological, mechanical, or mixed processes. In general, the conversion technology consists of three separate and distinct components: (1) a solid waste separation and recycling process [9], (2) a conversion unit [10], and (3) an energy/chemical production system [11]. Preprocessing is used to prepare solid waste for treatment by separating and disposing of non-recyclable waste [12]. The preprocessing process (such as tearing, grinding, and/or drying [13]) varies depending on the technology. This process is required to make more homogeneous raw materials for some thermal technologies. Alternatively, water-based separation techniques can be used in biological processes [14]. The energy production module can be a gas turbine, a boiler, or a propulsion engine for the production of electric power [15]. The production module is fully subject to energy conservation, *i.e.*, energy cannot be destroyed but can be converted into other forms [16]. The utilization of electrical energy from upstream to downstream is fully subject to energy conversion and conservation technology, for example, water drives turbines to produce electricity and electrical energy is used to

drive electric cars [17]. Therefore, this paper will focus on the introduction of energy conversion and conservation technology based on a qualitative literature review to deal with net-zero emission conditions.

## Methods

This article uses a qualitative descriptive literature review method. According to Onwuegbuzie and Weinbaum in Miles and Huberman [18], descriptive qualitative method is research that describes the state of the object being studied as it is, in accordance with the situation and conditions at the time the research was conducted suggesting that activities in qualitative data analysis are carried out continuously until complete so that data literacy has been repeated/already saturated. According to Sugiyono [19], the qualitative approach is a non-statistical subjective assessment, where the measure of value used in this study does not assess numbers but categorizes values or quality. Qualitative methods aim to describe the state or condition of the phenomenon of the focus of the study, especially with regard to the theme of the study being taken. Further exploration is carried out based on theories that support arguments, statements and limited searches related to the theme of conversion technology and clean (green)energy conservation. The search results generated include reviews and opinions by experts in their fields and a good scientific background.

## Results and Discussion

### Technology of Conventional Energy

Conventional energy is non-renewable energy, because energy sources come from nature but the amount is quite limited [20]. Two types of conventional energy can be distinguished into fossil fuels and nuclear fuels [21]. Fossil fuels are classified into coal, oil and natural gas. From 1962 to 2009, Indonesia was one of the oil-exporting countries. But Indonesia has ceased to be an oil-exporting country in 2009, because the country's internal demand for oil has increased, so Indonesia had to leave the Organization of the Petroleum Exporting Countries (OPEC) [22]. World oil reserves are quite limited, only 500 Bb in 1970 which is estimated to be exhausted in 1995. But due to continuous exploration, in the last 20 years, the world had 900 Bb of oil, and currently consumption is around 600 Bb [23]. The growth rate of oil and gas reserves due to massive exploration was 0.11 Mb or 7.4 trillion cubic meters (TCM) in 2010, as shown in Figure 1 [24].

So far, global oil, gas and coal reserves have continued to increase with no immediate threat of depletion, but fossil fuels are a finite resource. Apart from climate change, population growth, inflation and living standards increase over time. The oil reduction scenario is related to supply chain cuts as a result of the oil embargo in the 1970s, resulting in a decrease in oil demand as a result of the clean energy transition, (*i.e.*, cars using electric energy). Many energy experts have different views regarding the rate of decline after peak oil production occurred between 2000-2030 with peak rates ranging from 75 to 120 Mbpd. A significant decrease in oil production will determine the scarcity of goods. The phenomenon of scarcity of goods will be related to ultimate resources (UR) and ultimate recovery resources (URR), which are used to

show the size of oil and gas reserves on earth. Total oil and gas resources are often referred to as contingent and prospective resources. Based on the results of a statistical review of BP world energy, it shows that world oil reserves in 2013 were 1,687.9 Bb. As a result, there is currently a peak in oil prices when prices fall, but will continue to increase since some have reduced the use of oil and gas-based fossil [24].

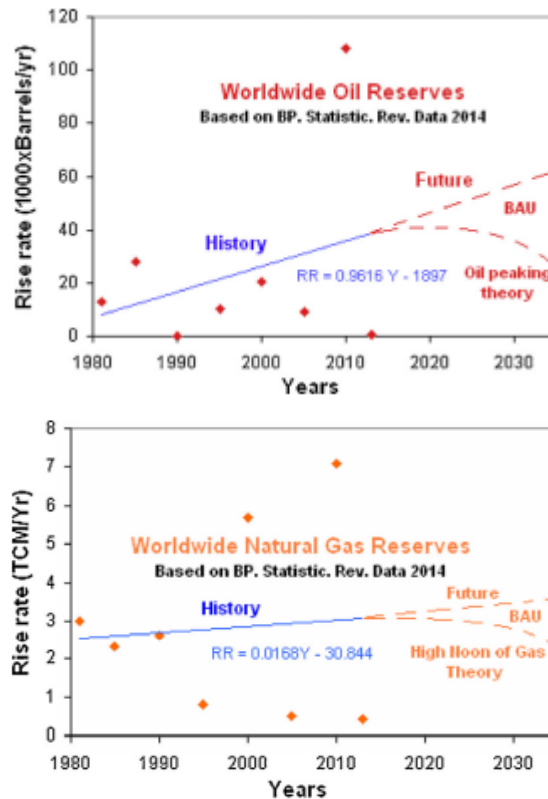


**Figure 1.** Oil and gas reserves increase from 1980-2013 [24]

Environmentalists advise minimizing the use of fossil fuels because of their adverse effects on nature regardless of depletion or non-depletion. Environmentalists attribute peak oil and gas production to peak CO<sub>2</sub> emissions, which have so far increased by 402 ppm in 2014 [25]. Until now, there is no known chemical reaction that can clean the buildup of CO<sub>2</sub> (gas) in the atmosphere. There are several authors who describe sustainable hydrocarbon fuels by recycling H<sub>2</sub>O and CO<sub>2</sub> with renewable energy sources [26]. But there is a concrete solution, namely CO<sub>2</sub> capture and absorption (CCS). It can contribute to converting CO<sub>2</sub> back into hydrocarbon fuels in the presence of H<sub>2</sub>O. The working principle of hydrocarbon fuels is to convert dead vegetation and animals into fossil fuels from tens of millions of years to hundreds of millions of years ago [27]. The energy conversion technology for environmentally friendly coal-based power plants is Integrated Gasification Combined Cycle (IGCC).

IGCC is a coal-fired power plant technology that utilizes a high-pressure gasifier to convert coal or other hydrocarbon fuels into pressurized gas/synthesis gas (syngas). Conversion of solid coal to gas is possible to be applied in combined cycle generators, which will lead to the high efficiency of the engine. The IGCC process can also be used as a pollutant removal system, because it has become clean energy (syngas) before entering the power generation cycle. However, a difficult challenge for

developing countries is that the IGCC technology is quite expensive when compared to other (conventional) hydrocarbon and coal-fired power plants. The IGCC scheme can be seen in Figure 2 [28].

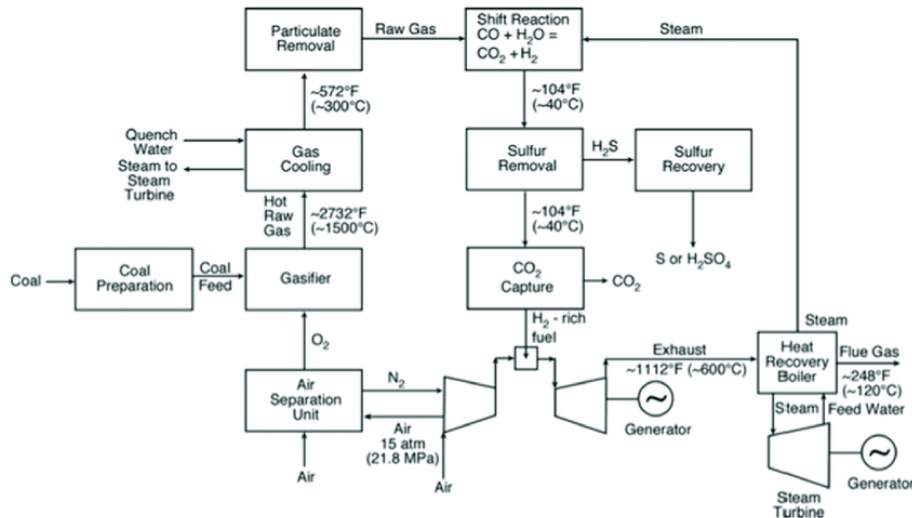


**Figure 2.** Coal-based Integrated gasification combined cycle (IGCC) scheme [28]

The working principle of IGCC is to separate oxygen from the air in the factory using cryogenic separation [29]. The oxygen passes through a gasifier where the coal is gasified at high pressure to produce syngas at a relatively high temperature. Next phase is the cooling and pre-cleaning phase, in which the syngas is transferred through a water gas displacement reaction in a water gas reactor so that it is later converted into  $H_2S$ ,  $H_2$ , and  $CO_2$ . Cleaning is carried out by several steps to remove mercury, water, sulphur, and other impurities. This is because the composition of syngas only consists of  $CO_2$  and  $H_2$ . The final cleaning stage of this gas mixture is passing through a  $CO_2$  removal process where  $CO_2$  is captured by CCS. Hydrogen is then used to generate power and drive electric turbines. Please note that most of the technologies developed today (commercial) utilize physical solvents to separate  $CO_2$  from syngas. In the future, better technology is needed to separate  $CO_2$  from syngas [28].

### Technology of Renewable Energy

Renewable Energy Technology is divided into 2, namely New Energy and Renewable Energy. New energy is energy that utilizes technology that is relatively new in Indonesia, while renewable energy is energy that utilizes "sustainable and clean natural processes". Because in general renewable energy does not produce pollutants and greenhouse gases, it does not contribute to climate change. However, behind its environmentally friendly nature, several issues arise. For example, renewable energy is intermittent (not continuous). Because every year there will be a change in seasons which causes the energy source to change, it is rather difficult to function to meet peak energy needs [30]. Many efforts have been made to produce environmentally friendly and renewable energy-producing technologies, so it is necessary to know the types of technologies that have been developed at this time.

### Solar Cell Technology

The solar panel is a series of photovoltaic cells that convert sunlight into electricity. Photovoltaic cells are semiconductor devices consisting of p-n (positive-

negative) junction diodes. The junction electrons are directly transferred from the n-type semiconductor (electrons being the dominant current carrier) to the p-type semiconductor (Hole being the dominant current carrier) and vice versa for the pole movement. The movement of electrons occurs as a result of the high temperature of the sun's heat to the solar panel [29]. Based on this explanation, the electrons and the movement of the poles result in photogeneration (as shown in Figure 3).

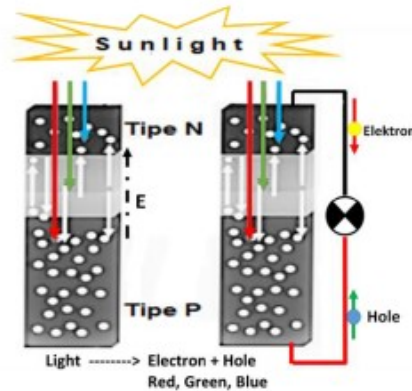


**Figure 3.** Solar cell photogeneration process [31]

High enough waste heat is generated by the absorption of solar radiation, causing the solar panel temperature to be quite high. The amount of radiation that can be converted into electricity in Photovoltaic (PV) panels is only 20% of the total incoming radiation. Therefore, the entire system has a fairly high temperature. As a result, the accumulation of thermal energy increases the operating temperature in the PV panels, therefore resulting in a decrease in the efficiency of the PV system. PV panels decrease by about 0.40 to 0.50% for each degree increase in temperature. The maximum power output can be calculated by equation (1).

$$P_{\max} = V_{oc} I_{sc} FF \quad (1)$$

Description:

$P_{\max}$  = Maximum Power

$V_{oc}$  and  $I_{oc}$  = open circuit electricity

FF = fill factor

The fill factor or can be said to be the ratio of the maximum power produced by the image sensor to the open circuit voltage circuit. Based on equations (1) and (2), the fill factor can be described as follows

$$FF = \frac{P_{max}}{V_{oc} I_{sc}} \quad (2)$$

$$\frac{V_{mpp} I_{mpp}}{V_{oc} I_{sc}} FF = \frac{V_{mpp} I_{mpp}}{V_{oc} I_{sc}} \frac{P_{max}}{V_{oc} I_{sc}} \quad (3)$$

where the voltage ( $V_{mpp}$ ) and  $I_{mpp}$  are the maximum voltage and current, respectively. So that the resulting final power equation is shown by equation (4)

$$P = V \cdot I \quad (4)$$

Description: P = Power (watt), V = voltage (volt), and I = electric current (ampere)

In the previous 1-decade, commercial solar panel technology had an efficiency of around 15% and in 2020 at least the efficiency of commercial solar panels was around 20%. This is one of the main reasons why the solar industry is still struggling to compete with fossil fuels. In general, commercial solar panels rarely exceed 20%

efficiency, because it requires a fairly high cost to use advanced semiconductor materials with high efficiency. Photovoltaic cells produce a direct current which is generally used for small loads (electronic equipment). If the Direct Current (DC) from photovoltaic cells is used for remote home applications, but the electric utility uses an alternating current network, it must use an inverter or solid-state device to convert it to alternating current (AC) [31].

Many efforts to optimize solar cell systems have taken advantage of the factors of solar cell performance. The solar panel factors in question are inverters, batteries, and solar charge controllers that are used to support the electric power system. One of the interesting issues discussed is to find a model of a power generation system using solar cells for a house and the optimal arrangement to improve the performance of solar cell panels.

#### *Turbine-based Hydroelectric Power*

Hydroelectric Power Plant is a generator that relies on the potential and kinetic energy of water with a certain height difference to produce electrical energy. Hydropower is a power plant that Indonesia relies on at this time. Hydropower is more reliable, inexpensive and easy to build in the tropics and subtropics than power plants with other raw materials and is included in renewable energy. To see the electric potential generated is to calculate the potential output power [32]. Potential measurements are carried out like the calculation of Hydro Potential in general, namely using equation (5)

$$P = g \times h \times Q \times \eta \quad (5)$$

Description:

P = Output Power (kW)

g = gravitation ( $9.8 \text{ m/s}^2$ )

h = Falling water level (m)

Q = Debit ( $\text{m}^3/\text{s}$ )

$\eta$  = Efficiency

The classification of hydropower types are distinguished based on the output power produced. The classification of hydropower is summarized in Table 1

**Table 1.** Hydropower is divided into several types of generating scales [4]

Classification Hydro-based Power Plant	Power Estimate
Giga	>100 MW
Mega	15-100 MW
Small	1-15 MW
Mini	100 kW-1 MW
Micro	5-100 kW
Piko	<5kW

Small hydropower plants have recently been developed and have become an alternative to fulfil electrical energy, especially in difficult, affordable and remote areas. Hydropower plants are built in areas that have river potential throughout the year. Small-scale hydropower is the most common generator in Indonesia. The advantages of small-scale hydropower are (1) hydropower plants can be built, managed independently, and owned by local consumers/communities. (2) System operation, maintenance and repair can be done by local technicians. (3) The generator can use a runoff river system with the dam height of < 2 m, without a dam or narrow dam. (4)

Constructed with components commonly used in engineering construction and available in the local market, namely generators, cables, transmission belts, pipes and others. (5) This type of turbine can be made by a local workshop (Crossflow turbine). (6) Emission-free, sustainable (sustainable/long life) and low maintenance [33].

### Geothermal Power Plant (GPP)

Geothermal Power Plant is a power plant that uses geothermal energy as its energy source. Electricity from geothermal power is currently used in several countries that cover the ring of fire. Geothermal Power Plants (GPP) can produce a constant power output based on the installed capacity in geothermal power plants [34]. GPP generally consists of three types of geothermal systems, namely:

- (1) a binary system is characterized by a fluid-dominated flow,
- (2) a flash system characterized by a two-phase flow-form,
- (3) a dry system characterized by a vapour-dominated flow [35].

One of the geothermal power plants (GPP) in Indonesia is the Dieng Geothermal Power Plant in Dieng, Central Java, Indonesia. Geothermal Power Plant (GPP) utilizes single-flash steam system technology, which is indicated by the large-scale use of brine found in geothermal wells [36]. The process flow diagram for the single-flash system at the Dieng Geothermal Power Plant is shown in Fig. 4

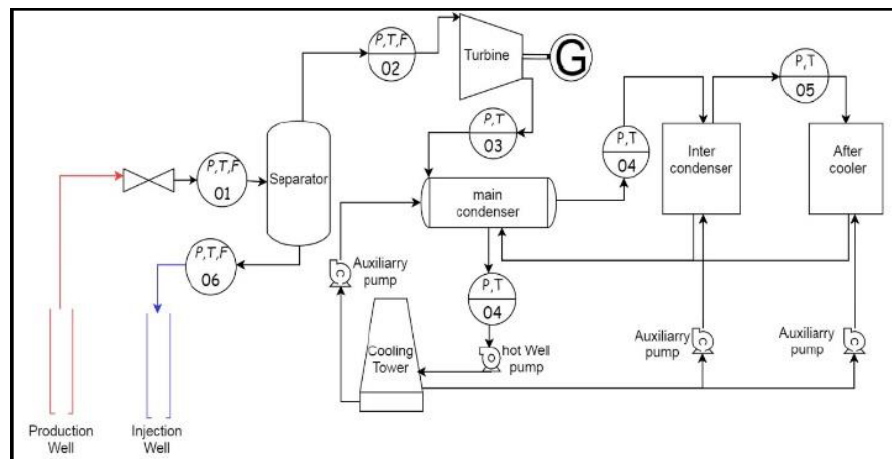


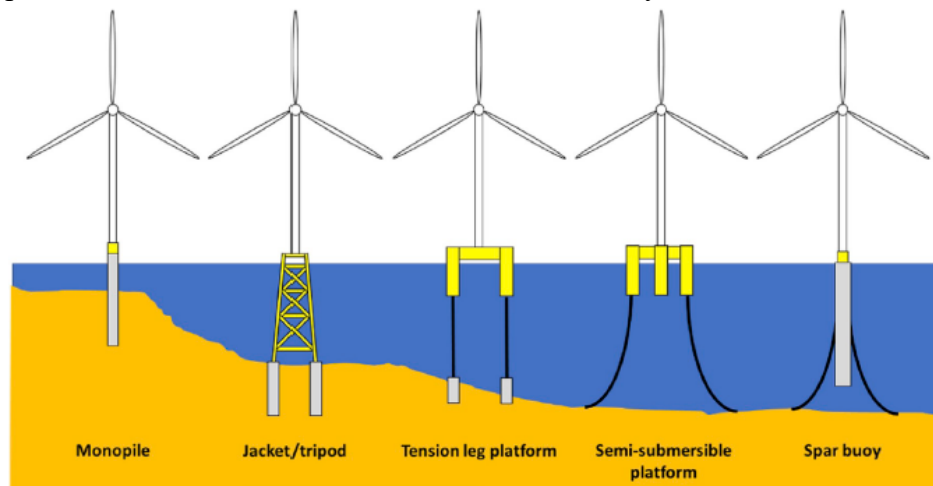
Figure 4. Dieng geothermal power plant schematic diagram [36]

Figure 4 shows a component flow diagram of the Dieng Geothermal Power Plant single-flash system. The figure shows data collection points for the pressure, temperature, and flow rate parameters for each component. There are five injection wells and seven production wells. The flow rate (F) is measured using a flow meter in a distributed control system (DCF). The temperature parameter (T) is measured using a variety of temperature instruments, including element temperatures, bimetals, temperature gauges, and temperature transmitters. The pressure (P) in the power plant is measured using a pressure gauge and a pressure transmitter. Parameters (pressure, temperature, and flow rate) are measured in the production section (well to the separator). Under normal circumstances, the measured temperature, pressures and flow rates are 100–190 °C, 9–10 bar and 70–250 tons/hour, respectively. These parameters are derived from the two flow phases in each well. The flow rate from the separator to the turbine is obtained from a steam flow of 20–150 tons/hour. In the power plant

section, the parameters recorded are flow rate of 250–350 kg/s, the pressure of 8–29 bar, and temperature of 40–140°C. Each parameter mentioned is the value of Geothermal Power Plant under normal conditions for operation [36].

### Wind Energy Turbine

A wind power plant is a power plant that uses wind as a source to generate electrical energy. This plant can convert wind energy into electrical energy using wind turbines or windmills. In general, the wind power plant is divided into 2, namely on-shore wind power plant (wind power plant which is installed in inland areas, both high and low land) and off-shore (wind power plant which is installed in coastal or sea areas). According to Watson *et al.* [37], the offshore wind power plant has greater efficiency in generating electricity than on-shore one, because of the tendency for continuous wind movement to occur in coastal areas. Figure 5 shows the types of wind power plant-offshore which are often found commercially.



**Figure 5.** Off shore wind power plant [37]

Figure 5 shows the shape and type of wind power plants, and it can be seen that the farther the windmill is located from the coastline, the longer the supports and cables are required. But it should be noted that the effective distance of the wind is the best and is continuous. Most of it is not directly on the shoreline, but slightly closer to mid-ocean [37].

### Biomass Energy

Biomass's Power Plant is a power plant that uses fuel converted from biological and organic materials by thermochemical and biochemical processes such as combustion, gasification, pyrolysis and anaerobic/aerobic digestion. The utilization of wastes for power generation can also avoid the production of methane gas if the waste is disposed in a landfill. Biomass-based energy technology consists of briquettes, biogas, biodiesel, biofuels, and microbial technology. If sufficient biomass resources are available, biomass is a clean and reliable resource for electricity generation. The conversion of chemically bound energy from fuel to electricity takes place in a plant called CHP (combined heat and electricity) [38].

The report presented will provide an overview of the technology available for power generation from biomass sources, because it has been widely used in Germany





consumption and activities that use energy. Energy savings lead to cost reductions, this will result in increased environmental sustainability, national and personal security and safety. As a result, industries that require large amounts of energy (commercial users) can increase efficiency and profits by saving energy [40]. One of the big problems related to energy conservation occurs in the combustion process of fossil fuel engines.

Modern Internal Combustion (IC) engines have very high efficiency. About 98% of the energy contained in the fuel is released during combustion in diesel engines and 95-98% in gasoline engines. However, the energy used leaving the engine (called 'brake work') is usually only 40% of the fuel energy. The energy used to provide drive to the wheels is much less than the work of the brakes. This is because a small part of the energy needs to be used for other things such as alternators and water pumps. The system's inability to convert all the chemical energy into brake work is termed "gross indicated thermal efficiency" [41]. The magnitude of the overall efficiency of the engine is called the 'fuel conversion efficiency and is defined in Eq. (6):

$$E_f = EP \times ET \quad (6)$$

Description:  $E_f$  = Fuel conversion efficiency

$EP$  = Combustion efficiency

$ET$  = Gross Indicated Thermal Efficiency

The best efficiency is produced by lubricants with good characteristics. Lubricating properties are quite dependent on temperature. The most efficient engine oils can operate at steady temperatures/conditions ranging from 100 C to 110 C. The high viscosity of the lubricant at low temperatures results in high friction losses. During the preheat stage there is friction loss in the engine or engines at a temperature of 20 C. This can be up to 2.5 times higher than that observed when the lubricant is completely warm. If the engine temperature is lowered to the cold-start scenario (0 C), this can lead to an increase in fuel consumption of up to 13.5% of the course will result in less efficiency value [41].

## Future Challenges and Opportunities

### *Efforts to Prevent Climate Change with a Net Zero Emission (NDC Indonesia) Scenario*

The use of fuel from petroleum, coal and natural gas produces exhaust emissions in the form of carbon dioxide (CO<sub>2</sub>), carbon monoxide (CO), sulphite/sulphur oxide (SO<sub>x</sub>), nitrogen oxides (NO<sub>x</sub>), and several other elements or compounds in the form of heavy metals. Note that the main parameter as an indicator of pollution, especially the cause of global warming is carbon dioxide. Carbon dioxide is trapped in the earth's atmosphere, which causes solar radiation to be absorbed, giving rise to the phenomenon of a smog layer or air pollution layer consisting of a combination of smoke and fog containing carbon dioxide (CO<sub>2</sub>) and other pollutants.

According to Briefing [42] and Asian Development Bank (2020) [52], Indonesia's energy use consists in 2019 consisted of oil 35%, coal 37.3%, gas 18.5%, hydropower 2.5%, geothermal 1.7%, biofuel 3%, and biogas, solar, wind, and other renewables at nearly 2%. In 2013 regarding recoverable shale resources of Indonesia, a value of 8 Billion Barel. Indonesia has 72% of total coal production in other non-OECD Asian countries. Throughout the period ahead, Indonesia will continue to dominate regional coal production. According Climate Transparency Report (2020) The number of CO<sub>2</sub> emissions resulting from energy use in Indonesia is 581 MtCO<sub>2</sub> in

2019 [51]. To overcome this, every nation's agreement is needed to combat climate change, one of which is the Paris Convention. The Paris Convention aims to discuss the maximum limit for global warming of 2 to 1.5 °C concerning the conditions of the earth before the industrial revolution. Efforts to implement these long-term goals by minimizing Greenhouse Gas (GHG) emissions to 0 net.

Indonesia's NDC has an emission target based on Business As Usual (BAU) conditions in 2030 of 2,869 MtCO<sub>2</sub>e, while Indonesia's projected emissions in 2030 are 2,037 MtCO<sub>2</sub>e (29%) below the unconditional target and emissions as low as 1,693 MtCO<sub>2</sub>e below the conditional target. Efforts to achieve these goals require the government to implement priority actions to reduce climate change [43]. Reduce GHG emissions to 41% below BAU 2030 levels, subject to international assistance for finance, technology transfer and capacity building. This is not easy, but with the cooperation of all parties, the Net Zero Emission scenario can at least be fulfilled in 2060.

#### *Develop Green Conversion Technology in Various Sectors*

Development of environmentally friendly (green) conversion technology in the transportation, household and NRE sectors. Green technology in question is environmentally friendly and efficient technology both in terms of price and device efficiency. The development of green technology has been carried out for a long time but along with technological developments, technological development will not stop, development begins with the diversification of energy output, whether it is the result of chemical, physical, and biochemical reactions. This is in line with efforts to improve (1) high efficiency based on solar cells with surface functionalization methods as intelligent materials [44]. (2) Increase the efficiency of combustion/co-firing of the best biomass [45]. (3) Geothermal power plant technology developed with relatively inexpensive equipment [46]. (4) Finding windmill designs and a combination of both offshore and onshore windmills [47]. (5) The most efficient water turbine design in generating power output [48].

#### *Development of Hydrogen Fuel Cells Technology*

Green hydrogen is clean energy that has a very high calorific value (120 MJ/ almost 2.5 times higher than the calorific value of gasoline and LNG/CNG and is very flexible to be used in various energy sectors as well as raw materials for the chemical industry. On the other hand, H<sub>2</sub> has a low volumetric energy density, so it is necessary to be careful (in-depth study) in planning development, especially logistics planning (storage, transportation, and distribution). To achieve logistics that is more cost-effective and efficient, it is necessary to take into account further processes: H<sub>2</sub> to H<sub>2</sub> liquid and H<sub>2</sub> Carrier (Ammonia, MeOH, etc.) The scenario proposed in the implementation of GREEN HYDROGEN production is Power to H<sub>2</sub> or Power to X with electrolyzer technology where "X" is a variety of chemical products and synthetic fuels resulting from the further conversion of H<sub>2</sub>. The need for GREEN HYDROGEN is certain to increase drastically due to NZE requirements, so it is projected as a big business opportunity for energy sector business actors [49].

#### Opportunity:

1. H<sub>2</sub> as fuel produces clean emissions in the form of water (H<sub>2</sub>O) (clean energy)

2. H<sub>2</sub> is recognized worldwide as beyond/future energy” the main focus in mitigating climate change (Global Pathway to Net Zero Emissions)
3. Mitigation of carbon emissions in sectors that are harder to electrify”, for example, industry and transportation (Decarbonization Solution “Hard to abate Sector”)
4. Seasonal Storage Media (Seasonal Storage) H<sub>2</sub> stored can be converted into electricity to meet demand

Threat:

1. The electrolyzer system and the price of electricity from renewable sources is still relatively expensive (High Cost).
2. High requirement for storage & transport because of the low energy density of H<sub>2</sub>, it needs compression to 700 bar for storage/transport.; transport. long distances need conversion to H<sub>2</sub> carrier (e.g., Ammonia, MeOH)
3. Hydrogen only has 60% energy efficiency (High Energy Losses) from the production process to the final use.
4. Volatile and flammable so safety measures are required to prevent leakage and explosion (Safety Issues).

Fuel Cells technology has the potential to be applied in the defense sector because of its relatively small size, some fuel cells are quite light, have no emissions, have high specific energy, do not make noise, etc. Based on the context of the defense equipment application, the requirements can be a wearable, portable, or distributed power supply. Fuel Cell Powering unmanned aerial vehicles, ground vehicles and autonomous underwater vehicles form separate regimes. High levels of efficiency, reliability, reproducibility, durability to meet military standard environmental tests can be met so that the prerequisites for military hardware are almost completely met. A prominent and current issue of fuel cell technology is the design of air-independent propulsion (AIP) systems for submarines [50].

## Conclusion

Conversion technology will continue to evolve. These developments started from the industrial revolution 1.0 to the industrial revolution 4.0, but in these developments even though technology solves a problem, it has the potential to cause new problems such as environmental problems. Environmental problems that can occur starting from energy conversion that is not environmentally friendly as well as the use of several technologies that cause pollutants that are quite dangerous if high intensity can even cause health problems, acid rain and climate change. Therefore, currently, the development of energy conversion is environmentally friendly and besides that energy conservation is very important for energy saving and security for the community at large. Fuel cell technology has a high level of efficiency, reliability, reproducibility, durability. This is because the military standard environment is a very dangerous, steep and durable field in every environmental condition and temperature. For now, fuel cell technology is the design of the AIP system for high technology submarines.

## Acknowledgements

The authors express their deepest gratitude to the Indonesian Defense Research Council for providing research funding for preliminary research as a condition for submitting a thesis.

## Conflict of Interest

The authors declare that there is no conflict of interests regarding the publication of this paper.

## References

- [1] Fang, D., Shi, S., and Yu, Q. (2018). Evaluation of Sustainable Energy Security and an Empirical Analysis of China. *Sustainability*, 10(5), 1685. DOI: <https://doi.org/10.3390/su10051685>
- [2] Sapanji, R. V. T., and Hamdani, D. (2020). Perancangan Desain Sistem Informasi Geografis Pemetaan Desa Mandiri Energi Kec. Pangalengan Kab. Bandung. *Jurnal Manajemen Informatika (JAMIKA)*, 10(1), 96-109. DOI: <https://doi.org/10.34010/jamika.v10i1.2571>
- [3] Meilani, H., and Wuryandani, D. (2010). Potensi panas bumi sebagai energi alternatif pengganti bahan bakar fosil untuk pembangkit tenaga listrik di Indonesia. *Jurnal Ekonomi & Kebijakan Publik*, 1(1), 47-74. DOI: <http://dx.doi.org/10.22212/jekp.v1i1.74>
- [4] Davidson, D. J. (2019). Exnovating for a renewable energy transition. *Nature Energy*, 4(4), 254-256. DOI: 10.1038/s41560-019-0369-3
- [5] Seo, S. N. (2017). Beyond the Paris Agreement: Climate change policy negotiations and future directions. *Regional Science Policy & Practice*, 9(2), 121-140. DOI: <https://doi.org/10.1111/rsp3.12090>
- [6] Vicedo-Cabrera, A. M., Guo, Y., Sera, F., Huber, V., Schleussner, C.-F., Mitchell, D., Tong, S., Coelho, M. d. S. Z. S., Saldiva, P. H. N., Lavigne, E., Correa, P. M., Ortega, N. V., Kan, H., Osorio, S., Kyselý, J., Urban, A., Jaakkola, J. J. K., Rytí, N. R. I., Pascal, M., Goodman, P. G., Zeka, A., Michelozzi, P., Scortichini, M., Hashizume, M., Honda, Y., Hurtado-Diaz, M., Cruz, J., Seposo, X., Kim, H., Tobias, A., Íñiguez, C., Forsberg, B., Åström, D. O., Ragettli, M. S., Rööslí, M., Guo, Y. L., Wu, C.-f., Zanobetti, A., Schwartz, J., Bell, M. L., Dang, T. N., Do Van, D., Heaviside, C., Vardoulakis, S., Hajat, S., Haines, A., Armstrong, B., Ebi, K. L., and Gasparrini, A. (2018). Temperature-related mortality impacts under and beyond Paris Agreement climate change scenarios. *Climatic Change*, 150(3), 391-402. DOI: 10.1007/s10584-018-2274-3
- [7] Falkner, R. (2016). The Paris Agreement and the new logic of international climate politics. *International Affairs*, 92(5), 1107-1125. DOI: 10.1111/1468-2346.12708
- [8] Rogelj, J., den Elzen, M., Höhne, N., Fransen, T., Fekete, H., Winkler, H., Schaeffer, R., Sha, F., Riahi, K., and Meinshausen, M. (2016). Paris Agreement

- climate proposals need a boost to keep warming well below 2 °C. *Nature*, 534(7609), 631-639. DOI: 10.1038/nature18307
- [9] Razzaq, A., Sharif, A., Najmi, A., Tseng, M.-L., and Lim, M. K. (2021). Dynamic and causality interrelationships from municipal solid waste recycling to economic growth, carbon emissions and energy efficiency using a novel bootstrapping autoregressive distributed lag. *Resources, Conservation and Recycling*, 166, 105372. DOI: <https://doi.org/10.1016/j.resconrec.2020.105372>
- [10] Callan, S. J., and Thomas, J. M. (1999). Adopting a Unit Pricing System for Municipal Solid Waste: Policy and Socio-Economic Determinants. *Environmental and Resource Economics*, 14(4), 503-518. DOI: 10.1023/A:1008315305404
- [11] Lee, R. P., Keller, F., and Meyer, B. (2017). A concept to support the transformation from a linear to circular carbon economy: net zero emissions, resource efficiency and conservation through a coupling of the energy, chemical and waste management sectors. *Clean Energy*, 1(1), 102-113. DOI: 10.1093/ce/zkx004
- [12] Srigiri, S., and Reddy, M. V. (2012). Municipal solid waste—A potential latent resource for non-conventional energy in India: Needs and challenges. *Journal of Applied Geochemistry*, 14(3), 337-350.
- [13] Hemery, Y., Rouau, X., Lullien-Pellerin, V., Barron, C., and Abecassis, J. (2007). Dry processes to develop wheat fractions and products with enhanced nutritional quality. *Journal of Cereal Science*, 46(3), 327-347. DOI: <https://doi.org/10.1016/j.jcs.2007.09.008>
- [14] Parinduri, L., and Parinduri, T. (2020). Konversi biomassa sebagai sumber energi terbarukan. *JET (Journal of Electrical Technology)*, 5(2), 88-92.
- [15] Nemitallah, M. A., Rashwan, S. S., Mansir, I. B., Abdelhafez, A. A., and Habib, M. A. (2018). Review of Novel Combustion Techniques for Clean Power Production in Gas Turbines. *Energy & Fuels*, 32(2), 979-1004. DOI: 10.1021/acs.energyfuels.7b03607
- [16] So, P. Y. (2014). Implementasi kebijakan konservasi energi di Indonesia. *E-Journal Graduate Unpar*, 1(1), 1-13.
- [17] Gür, T. M. (2018). Review of electrical energy storage technologies, materials and systems: challenges and prospects for large-scale grid storage. *Energy & Environmental Science*, 11(10), 2696-2767. DOI: 10.1039/C8EE01419A
- [18] Onwuegbuzie, A. J., and Weinbaum, R. K. (2016). Mapping Miles and Huberman's Within-Case and Cross-Case Analysis Methods onto the Literature Review Process. *Journal of Educational Issues*, 2(1), 265-288.
- [19] Syamruddin, P., Saputra, J., and Rialmi, Z. A qualitative study of e-commerce growth during Corona virus disease (COVID-19) pandemic in Indonesia. In: *Proc., 11th Annual International Conference on Industrial Engineering and Operations Management, IEOM 2021*, pp: 3208-3216.
- [20] Caesaron, D., and Maimury, Y. (2017). Evaluasi dan Usulan Pengembangan Energi Terbarukan untuk Keberlangsungan Energi Nasional. *Jiems (Journal of Industrial Engineering and Management Systems)*, 7(2), 132-139. DOI: <http://dx.doi.org/10.30813/jiems.v7i2.116>
- [21] Zittel, W., Zerhusen, J., Zerta, M., and Arnold, N. (2013). *Fossil and nuclear fuels—the supply outlook*, Berlin: Energy Watch Group.

- [22] Wagner, H. L. (2009). *The Organization of the Petroleum Exporting Countries*, Infobase Publishing.
- [23] Höök, M., and Tang, X. (2013). Depletion of fossil fuels and anthropogenic climate change—A review. *Energy Policy*, 52, 797-809. DOI: <https://doi.org/10.1016/j.enpol.2012.10.046>
- [24] Abas, N., Kalair, A., and Khan, N. (2015). Review of fossil fuels and future energy technologies. *Futures*, 69, 31-49. DOI: <https://doi.org/10.1016/j.futures.2015.03.003>
- [25] Abas, N., Kalair, A., Khan, N., and Kalair, A. R. (2017). Review of GHG emissions in Pakistan compared to SAARC countries. *Renewable and Sustainable Energy Reviews*, 80, 990-1016. DOI: <https://doi.org/10.1016/j.rser.2017.04.022>
- [26] Pearson, R. J., Eisaman, M. D., Turner, J. W. G., Edwards, P. P., Jiang, Z., Kuznetsov, V. L., Littau, K. A., Marco, L. d., and Taylor, S. R. G. (2012). Energy Storage via Carbon-Neutral Fuels Made From CO<sub>2</sub>, Water, and Renewable Energy. *Proceedings of the IEEE*, 100(2), 440-460. DOI: 10.1109/JPROC.2011.2168369
- [27] Leung, D. Y. C., Caramanna, G., and Maroto-Valer, M. M. (2014). An overview of current status of carbon dioxide capture and storage technologies. *Renewable and Sustainable Energy Reviews*, 39, 426-443. DOI: <https://doi.org/10.1016/j.rser.2014.07.093>
- [28] Sifat, N. S., and Haseli, Y. (2019). A Critical Review of CO<sub>2</sub> Capture Technologies and Prospects for Clean Power Generation. *Energies*, 12(21), 4143.
- [29] Sun, W., Kherani, N. P., Hirschman, K. D., Gadeken, L. L., and Fauchet, P. M. (2005). A Three-Dimensional Porous Silicon p-n Diode for Betavoltaics and Photovoltaics. *Adv. Mater.*, 17(10), 1230-1233. DOI: <https://doi.org/10.1002/adma.200401723>
- [30] Yamegueu, D., Azoumah, Y., Py, X., and Zongo, N. (2011). Experimental study of electricity generation by Solar PV/diesel hybrid systems without battery storage for off-grid areas. *Renewable Energy*, 36(6), 1780-1787. DOI: <https://doi.org/10.1016/j.renene.2010.11.011>
- [31] Suyanto, M., Rusianto, T., and Subandi (2020). Development of a Household Solar Power Plant: System Using Solar Panels. *IOP Conference Series: Materials Science and Engineering*, 807(1), 012007. DOI: 10.1088/1757-899x/807/1/012007
- [32] Anagnostopoulos, J. S., and Papantonis, D. E. (2007). Pumping station design for a pumped-storage wind-hydro power plant. *Energy Conversion and Management*, 48(11), 3009-3017. DOI: <https://doi.org/10.1016/j.enconman.2007.07.015>
- [33] Kananda, K., Corio, D., Aziz, H., and Diah, A. (2019). Potential Analysis of Hydro Power Plants in Pesisir Barat District, Lampung Province. *Journal of Science and Applicative Technology*, 2(1), 100-106.
- [34] Pambudi, N. A. (2018). Geothermal power generation in Indonesia, a country within the ring of fire: Current status, future development and policy. *Renewable and Sustainable Energy Reviews*, 81, 2893-2901. DOI: <https://doi.org/10.1016/j.rser.2017.06.096>

- [35] Eliasson, E. T., Thorhallsson, S., and Steingrímsson, B. (2011). Geothermal power plants. *Short Course on Geothermal Drilling, Resource Development and Power Plants, Santa Tecla, El Salvador*.
- [36] Qurrahman, A. H., Wilopo, W., Susanto, S. P., and Petrus, H. T. B. M. (2021). Energy and Exergy Analysis of Dieng Geothermal Power Plant. *International Journal of Technology*, 12(1), 291-319. DOI: <https://doi.org/10.14716/ijtech.v12i1.4218>
- [37] Watson, S., Moro, A., Reis, V., Baniotopoulos, C., Barth, S., Bartoli, G., Bauer, F., Boelman, E., Bosse, D., Cherubini, A., Croce, A., Fagiano, L., Fontana, M., Gambier, A., Gkoumas, K., Golightly, C., Latour, M. I., Jamieson, P., Kaldellis, J., Macdonald, A., Murphy, J., Muskulus, M., Petrini, F., Pigolotti, L., Rasmussen, F., Schild, P., Schmehl, R., Stavridou, N., Tande, J., Taylor, N., Telsnig, T., and Wiser, R. (2019). Future emerging technologies in the wind power sector: A European perspective. *Renewable and Sustainable Energy Reviews*, 113, 109270. DOI: <https://doi.org/10.1016/j.rser.2019.109270>
- [38] Gebreegziabher, T., Oyedun, A. O., Luk, H. T., Lam, T. Y. G., Zhang, Y., and Hui, C. W. (2014). Design and optimization of biomass power plant. *Chemical Engineering Research and Design*, 92(8), 1412-1427. DOI: <https://doi.org/10.1016/j.cherd.2014.04.013>
- [39] Barz, M. (2014). Biomass Technology for Electricity Generation in Community. *Journal of Renewable Energy and Smart Grid Technology*, 3(1), 1-10.
- [40] Lele, U., and Goswami, S. (2017). The fourth industrial revolution, agricultural and rural innovation, and implications for public policy and investments: a case of India. *Agricultural Economics*, 48(S1), 87-100. DOI: <https://doi.org/10.1111/agec.12388>
- [41] Roberts, A., Brooks, R., and Shipway, P. (2014). Internal combustion engine cold-start efficiency: A review of the problem, causes and potential solutions. *Energy Conversion and Management*, 82, 327-350. DOI: <https://doi.org/10.1016/j.enconman.2014.03.002>
- [42] Briefing, U. S. (2013). International energy outlook 2013. *US Energy Information Administration*, 506, 507.
- [43] Wijaya, A., Chrysolite, H., Ge, M., Wibowo, C. K., Pradana, A., Utami, A. F., and Austin, K. (2017). How can Indonesia achieve its climate change mitigation goal? An analysis of potential emissions reductions from energy and land-use policies. *World Resources Institute. World Resour Inst Work Pap*, 1-36.
- [44] Wieszczycka, K., Staszak, K., Woźniak-Budyń, M. J., Litowczenko, J., Maciejewska, B. M., and Jurga, S. (2021). Surface functionalization – The way for advanced applications of smart materials. *Coordination Chemistry Reviews*, 436, 213846. DOI: <https://doi.org/10.1016/j.ccr.2021.213846>
- [45] Milićević, A., Belošević, S., Crnomarković, N., Tomanović, I., Stojanović, A., Tucaković, D., Lei, D., and Che, D. (2021). Numerical study of co-firing lignite and agricultural biomass in utility boiler under variable operation conditions. *International Journal of Heat and Mass Transfer*, 181, 121728. DOI: <https://doi.org/10.1016/j.ijheatmasstransfer.2021.121728>
- [46] Tozlu, A., Gençaslan, B., and Özcan, H. (2021). Thermoeconomic analysis of a hybrid cogeneration plant with use of near-surface geothermal sources in



- Turkey. *Renewable Energy*, 176, 237-250. DOI: <https://doi.org/10.1016/j.renene.2021.05.064>
- [47] Cahay, M., Luquiau, E., Smadja, C., and Silvert, F. (2011). Use of a Vertical Wind Turbine in an Offshore Floating Wind Farm. *Offshore Technology Conference* Houston, Texas, USA. DOI: 10.4043/21705-ms
- [48] Chen, J., Yang, H. X., Liu, C. P., Lau, C. H., and Lo, M. (2013). A novel vertical axis water turbine for power generation from water pipelines. *Energy*, 54, 184-193. DOI: <https://doi.org/10.1016/j.energy.2013.01.064>
- [49] Arefin, M. A., Nabi, M. N., Akram, M. W., Islam, M. T., and Chowdhury, M. W. (2020). A Review on Liquefied Natural Gas as Fuels for Dual Fuel Engines: Opportunities, Challenges and Responses. *Energies*, 13(22), 6127.
- [50] Narayana Das, J. Fuel Cell Technologies for Defence Applications. Springer Singapore, pp: 9-18.
- [51] Climate Transparency Report. 2020. Indonesia Climate Transparency Report Comparing G20 Climate Action and Responses to The COVID-19 Crisis. <https://www.climate-transparency.org/wp-content/uploads/2020/11/Indonesia-CT-2020-WEB.pdf>
- [52] Asian Development Bank. 2020. Indonesia Energy Sector Assessment, Strategy, and Road Map Update. <https://www.adb.org/sites/default/files/institutional-document/666741/indonesia-energy-asr-update.pdf>

**Article copyright:** © 2022 Abdi Manab Idris, Nugroho Adi Sasongko, Yanif Dwi Kuntjoro. This is an open access article distributed under the terms of the [Creative Commons Attribution 4.0 International License](https://creativecommons.org/licenses/by/4.0/), which permits unrestricted use and distribution provided the original author and source are credited.



# Life Cycle Assessment of a Coke Cleaning Agent

Yu Gong<sup>1</sup>, Changyan Yang<sup>1,2\*</sup>, Yinhang Qu<sup>1</sup>, Jiayi Li<sup>1</sup>, Bohan Yang<sup>1</sup>, Yigang Ding<sup>1</sup>, Bo Zhang<sup>1\*</sup>

1: Key Laboratory for Green Chemical Process of Ministry of Education, Hubei Key Laboratory of Novel Chemical Reactor and Green Chemical Technology, School of Chemical Engineering and Pharmacy, Wuhan Institute of Technology, Hubei, China

2: Hubei Key Laboratory for Processing and Application of Catalytic Materials, Huanggang Normal University, Hubei, China

Received February 28, 2022; Accepted March 18, 2022; Published March 20, 2022

The life cycle assessment of the coke cleaning agent developed by a university-enterprise cooperation project was conducted. This cleaning agent has the characteristics of phosphorus-free, environmentally friendly, and broad market prospects. The life cycle assessment of the established model showed that the GWP of producing 1kg of coke cleaning agent is 1.19 kg CO<sub>2</sub> eq, PED is 13.17 MJ, WU is 186.74 kg, AP is 3.63E-03 kg SO<sub>2</sub> eq, ADP is 7.75E-05 kg antimony eq, EP is 1.30E-03 kg PO43-eq, RI is 1.16E-03 kg PM2.5 eq, ODP is 4.63E-06 kg CFC-11 eq, and POFP is 1.85E-03 kg NMVOC eq. The uncertainty of the results is between 4.20% and 24.05%. The carbon footprint (GWP) analysis showed that the production process of isotridecanol polyoxyethylene ether, isopropanol, fatty alcohol polyoxyethylene ether M and isodecanol polyoxyethylene ether contributed significantly. The average sensitivity analysis showed that the most influential processes were sodium lauryl amphotacetate, isopropanol, and tripropylene glycol methyl ether.

*Keywords:* Life Cycle Assessment; Descaling Agent; Carbon Footprint; Coke; Production

## Introduction

As an important aspect of modern household, the hygiene level of the kitchen has been paid more and more attention by people [1]. During the cooking process, the edible oil and the grease in the food are vaporized under high temperature heating conditions for a long time, and then condense and adhere to the surface of the range hood, gas stove and other objects [2]. Then the dirt adsorbs the dust in the air to form the sticky kitchen dirt. These greasy dirt is often accompanied by odors and is difficult to be cleaned [3], [4]. As people have higher requirements for the removal of oil stains, cleaning agents are often needed to effectively remove them [5],[6].

Although the formula of ordinary cleaners is stable, they are not targeted and professional, and there are problems such as incomplete cleaning of dirt and environmental pollution [7]. At present, the main grease cleaning agents on the market are mostly formulated with high organic solvent content and high alkali, which contain harmful solvents and damage the surface of objects [8], [9]. In this paper, the life cycle of the production process of coke cleaning agent was studied. This product is a water-

based cleaning agent and has the characteristics of safety, high efficiency, low corrosion and environmental protection.

## Materials and Methods

### Goal and Scope Definition

The research object of this study is coke cleaning agent which is a water-based environment-friendly cleaning agent. In its formula, a variety of surfactants, organic solvents, and auxiliary agents are used. It has strong ability to remove tar scale and carbon deposits on the surface of kitchen utensils. It will not damage the surface of the utensils, and will maintain the original luster. The cleaning agent is also phosphorus-free with a very broad market prospect [10]. The product is a suspension, and the functional unit is 1 kg product. Time representation is 2021, and geographical representation is China

The system boundary of this study is from the cradle to the gate (out of factory), and the actual processes mainly include the production processes of sodium lauryl amphoacetate, isotridecanol polyoxyethylene ether, fatty alcohol polyoxyethylene ether M, isomeric ten alcohol polyoxyethylene ether, isopropanol, tripropylene glycol methyl ether, triethylene glycol butyl ether and disodium EDTA. Background processes include electrical grids, transportation and chemicals.

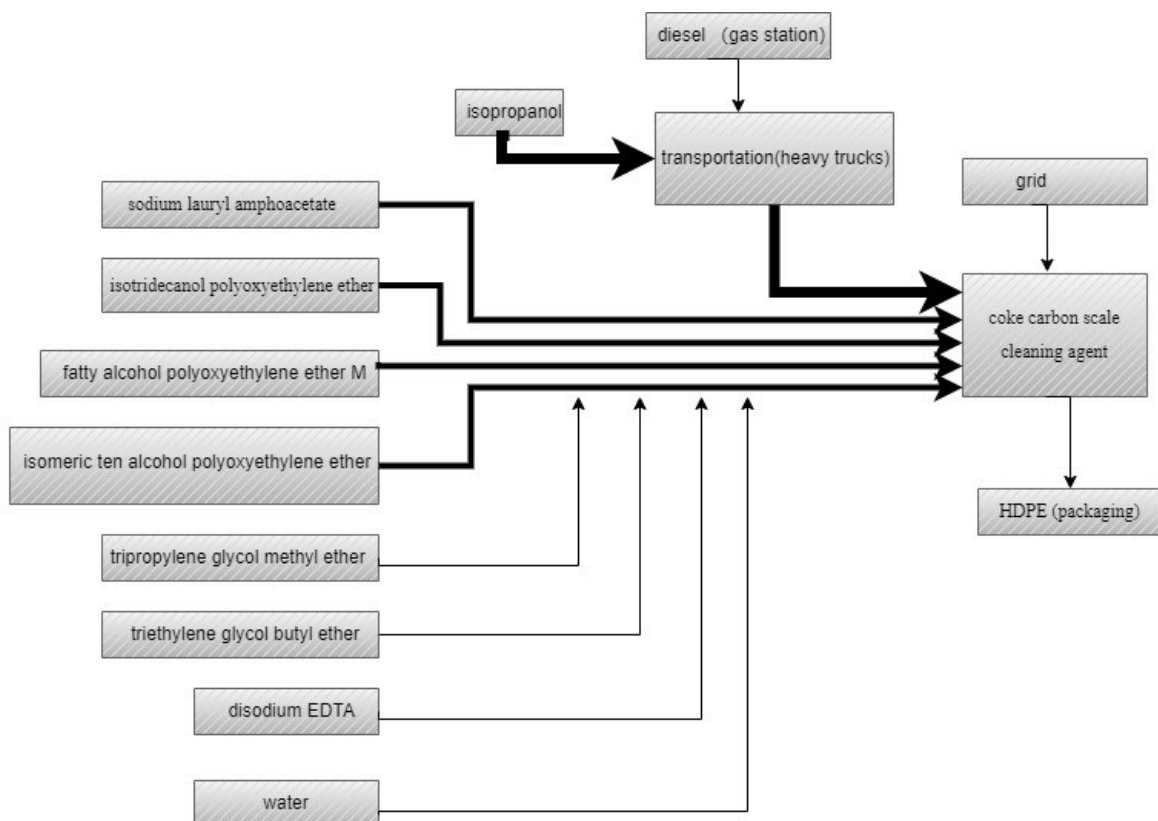


**Figure 1.** System boundary of the coke cleaning agent

## Selection Principle

The selection rule is based on the weight ratio of each raw material input to the product weight or the total process input. The specific rules are as follows:

- (1) When the weight of ordinary materials is less than 1% of the weight of the product, and the weight of materials containing rare or high-purity components is less than 0.1% of the weight of the product, the upstream production data of the material can be ignored. The total weight of ignored materials does not exceed 5%.
- (2) For low-value wastes as raw materials, such as fly ash, slag, straw, household waste, etc., the upstream production data can be ignored.
- (3) In most cases, production equipment, workshops and living facilities can be ignored.
- (4) Known emission data within the scope of the selected types of environmental impact should not be ignored.

## Types of Environmental Impact

**Table 1.** Types of environmental impact indicators

Environmental impact indicator	Unit	Main list substance
Climate change	kg CO <sub>2</sub> eq.	CO <sub>2</sub> , CH <sub>4</sub> , N <sub>2</sub> O...
Primary energy consumption	MJ	Hard coal, lignite, natural gas...
Abiotic resource consumption	kg antimony eq.	Iron, manganese, copper...
Water consumption	kg	Fresh water, surface water, groundwater...
Acidification	kg SO <sub>2</sub> eq.	SO <sub>2</sub> , NO <sub>x</sub> , NH <sub>3</sub> ...
Eutrophication	kg PO <sub>4</sub> <sup>3-</sup> eq.	NH <sub>3</sub> , NH <sub>4</sub> -N, COD...
Inhalable inorganic substances	kg PM <sub>2.5</sub> eq.	CO, PM <sub>10</sub> , PM <sub>2.5</sub> ...
Ozone depletion	kg CFC-11 eq.	CCl <sub>4</sub> , C <sub>2</sub> H <sub>3</sub> Cl <sub>3</sub> , CH <sub>3</sub> Br...
Photochemical ozone synthesis	kg NMVOC eq.	C <sub>2</sub> H <sub>6</sub> , C <sub>2</sub> H <sub>4</sub> ...

Note: eq is the abbreviation of equivalent.

## Data Quality Requirements

Data quality represents the difference between the target representativeness and the actual representativeness of the data of the LCA study. The China Life Cycle Basic Database (CLCD) method was adopted as the data quality assessment method. The CLCD method was used to evaluate the consumption and emission inventory data in the model from four aspects: ① inventory data sources and algorithms, ② time representativeness, ③ geographic representativeness, ④ technical representativeness. Using the method, the consumption of the background database was correlated and the uncertainty of its match with the upstream background process was assessed. After completing the inventory uncertainty assessment, the analytical formula method was used to calculate the uncertainty transfer and accumulation, and the uncertainty of the LCA results were obtained [11].

## Software and Database

In this study, the eFootprint software system was used to establish the life cycle model of the coke cleaning agent, and the LCA results were calculated. The eFootprint software system is online LCA analysis software developed by Yike Environmental Technology Co., Ltd. It supports the analysis of the whole life cycle process, and has built-in CLCD database, EU ELCD database and Swiss Ecoinvent database [12].

The CLCD used in the research process is an industry average database developed by Yike and based on the core model of China's basic industrial system life cycle. The CLCD database includes inventory datasets of major domestic energy, transportation, and basic raw materials. The background data sources used in this study are shown in Table 2:

**Table 2.** Coke cleaning agent [production] background data source

List name	Dataset name	Name database
Isotridecanol polyoxyethylene ether	Fatty alcohol polyoxyethylene ether sodium sulfate	LCAcontest4-39@ike-global.com 0.0
Fatty alcohol polyoxyethylene ether M	Fatty alcohol polyoxyethylene ether sodium sulfate	LCAcontest4-39@ike-global.com 0.0
Isomerized ten alcohol polyoxyethylene ether	Fatty alcohol polyoxyethylene ether sodium sulfate	LCAcontest4-39@ike-global.com 0.0
Isopropyl alcohol	Isopropyl alcohol	CLCD-China-ECER 0.8
Tripropylene glycol methyl ether	Dipropylene glycol monomethyl ether	Ecoinvent 3.1
Triethylene glycol butyl ether	Ethylene glycol dimethyl ether	Ecoinvent 3.1
Disodium EDTA, dihydrate	EDTA, ethylenediaminetetraacetic acid	Ecoinvent 3.1
Water	Tap water (industrial use)	CLCD-China-ECER 0.8
Electricity	East China Power Grid (to users)	CLCD-China-ECER 0.8

## Data Collection

### *Coke cleaning agent [Production]*

(1) Basic information of the process

Process Name: coke cleaning agent [production]

Process Boundaries: from cradle to gate

(2) Data representation

Main data sources: business surveys and literature[13][14]

Company: Jiangsu Biotechnology Co., Ltd.

Place of production: China

Base year: 2021

Process equipment: reactor, vacuum pump, condenser, heat exchanger

Main raw materials: organic raw materials

Main energy consumption: electricity

Production scale: 2000t/y

(3) Technical supplementary description:

The process simulation was carried out to obtain material balance and energy consumption balance for the production process. Figure 2 shows the flow chart. The water was injected into the reactor 1 through the pump 1, and then the main raw materials of the coke cleaning agent were sequentially added under the condition of 40°C under stirring condition. The raw materials include sodium lauryl amphoacetate, isotridecanol polyoxyethylene ether, fatty alcohol polyoxyethylene ether M, and isomeric ten alcohol polyoxyethylene ether. After being stirred for 20 minutes, disodium EDTA powder was added, and the mixture was further stirred for 10 minutes.

The mixed solution was pumped through the heat exchanger by the pump 2 to lower the temperature to 20°C. After the temperature was lowered to 20°C, the mixture entered the reactor 2, in which the organic solvents of isopropyl alcohol, tripropylene glycol methyl ether, and triethylene glycol butyl ether were added. The mixture was

stirred for 20 minutes to form a homogeneous solution, after which it can be taken out and canned through a packaging machine.

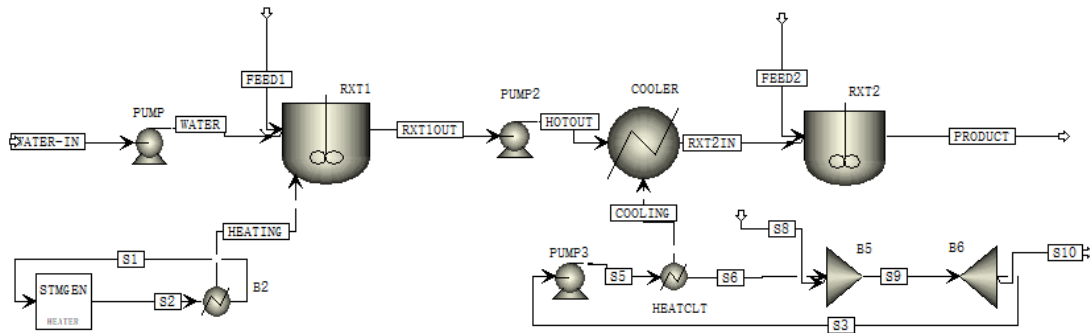


**Figure 2.** Coke cleaning agent production process

### *Sodium lauryl amphoacetate [Production]*

(1) Basic information of the process

Process Name: Sodium lauryl amphoacetate [Production]

Process Boundaries: From cradle to gate

(2) Data representation

Main data sources: business surveys and literature[15]

Place of production: China

Base year: 2020

Process equipment: reactor, vacuum pump, heat exchanger

Main raw materials: organic raw materials

Main energy consumption: electricity

Production scale: 2000 t/y

## Results and Discussion

### Life Cycle Impact Analysis

#### *LCA Results*

The LCA results of 1kg coke cleaning agent were calculated by using the eFootprint software, and the calculated environmental indicators were climate change (GWP), primary energy consumption (PED), water consumption (WU), acidification (AP), abiotic Resource consumption potential value (ADP), eutrophication potential value (EP), inhalable inorganic matter (RI), ozone depletion (ODP), and photochemical ozone synthesis (POFP). The results were shown in Table 3.

Table 3. LCA results of coke cleaning agent (1kg)

Environmental impact indicator	Unit	LCA result
GWP	kg CO <sub>2</sub> eq	1.19
PED	MJ	13.17
WU	kg	186.74
AP	kg SO <sub>2</sub> eq	3.63E-03
ADP	kg antimony eq	7.75E-05
EP	kg PO <sub>4</sub> <sup>3-</sup> eq	1.30E-03
RI	kg PM <sub>2.5</sub> eq	1.16E-03
ODP	kg CFC-11 eq	4.62E-06
POFP	kg NMVOC eq	1.85E-03

### Process Cumulative Contribution Analysis

The cumulative contribution of a process is the cumulative value of the direct contribution of the process and the contributions of all upstream processes (*i.e.*, contributed by the consumption of raw materials). Since the process usually contains multiple items of inventory data, the process contribution analysis is actually the accumulation of the sensitivity of multiple items of inventory data.

Table 4. LCA cumulative contribution results of coke cleaning agent

Process Name	GWP	PED	WU	AP	ADP
Coke cleaning agent [Production]	1.19	13.2	187	3.63E-03	7.75E-05
Electricity	4.73E-02	6.20E-01	1.85E-01	2.67E-04	5.58E-07
Sodium lauryl amphoacetate	0.146	2.58	176	5.02E-04	1.21E-05
Isotridecanol polyoxyethylene ether	0.235	0.12	3.59E-02	3.56E-04	1.08E-07
Fatty alcohol polyoxyethylene ether M	0.147	7.52E-02	2.24E-02	2.22E-04	6.77E-08
Isomerized ten alcohol polyoxyethylene ether	0.147	7.52E-02	2.24E-02	2.22E-04	6.77E-08
Isopropyl alcohol	0.213	3.50	9.83	6.98E-04	1.75E-05
Tripropylene glycol methyl ether	0.144	3.25	1.74E-03	7.80E-04	2.23E-05
Triethylene glycol butyl ether	6.76E-02	2.10	3.42E-04	3.62E-04	1.82E-05
EDTA, dihydrate	4.23E-02	0.843	3.90E-04	2.17E-04	6.54E-06
Water	1.28E-04	1.68E-03	0.683	6.71E-07	1.66E-09

Table 4. LCA cumulative contribution results of coke cleaning agent (continued)

Process Name	EP	RI	ODP	POFP
Coke cleaning agent [Production]	1.30E-03	1.16E-03	4.62E-06	1.85E-03
Electricity	1.66E-05	7.97E-05	1.21E-10	1.97E-05
Sodium lauryl amphoacetate	1.60E-04	1.27E-04	2.80E-11	6.86E-05
Isotridecanol polyoxyethylene ether	1.48E-04	6.72E-05	2.02E-06	2.56E-04
Fatty alcohol polyoxyethylene ether M	9.28E-05	4.20E-05	1.26E-06	1.60E-04
Isomerized ten alcohol polyoxyethylene ether	9.28E-05	4.20E-05	1.26E-06	1.60E-04
Isopropyl alcohol	1.74E-04	5.55E-04	1.50E-08	3.18E-04
Tripropylene glycol methyl ether	3.82E-04	1.52E-04	5.36E-08	5.15E-04
Triethylene glycol butyl ether	1.18E-04	5.61E-05	5.96E-09	2.31E-04
EDTA, dihydrate	1.19E-04	3.75E-05	9.08E-09	1.20E-04
Water	6.90E-08	2.06E-07	2.80E-13	5.11E-08

The obtained data was summarized and plotted to analyze the LCA results (Figures 3-11):

(1) For the climate change indicator (GWP), the four processes that contributed the most were the production of isotridecanol polyoxyethylene ether production (0.235 kg CO<sub>2</sub> eq),

isopropanol (0.213 kg CO<sub>2</sub> eq), fatty alcohol polyoxyethylene ether M(0.147 kg CO<sub>2</sub> eq) and isomerized ten alcohol polyoxyethylene ether (0.147 kg CO<sub>2</sub> eq).

(2) Primary energy consumption (PED): The three processes that contributed the most were the production of isopropanol (3.50MJ), tripropylene glycol methyl ether (3.25MJ), and sodium lauryl amphoacetate (2.58MJ).

(3) Water resource consumption (WU): The three processes that contributed the most were the production of sodium lauryl amphoacetate (176kg), isopropanol (9.83kg), and water (0.683kg).

(4) Acidification (AP): The three processes that contributed the most were the production of tripropylene glycol methyl ether (7.80E-04 kg SO<sub>2</sub> eq), isopropanol (6.98E-04 kg SO<sub>2</sub> eq), and sodium lauryl amphoacetate(5.02E-04 kg SO<sub>2</sub> eq).

(5) Abiotic resource consumption potential (ADP): The three processes that contributed the most were the production of tripropylene glycol methyl ether (2.23E-05 kg antimony eq), triethylene glycol butyl ether (1.82E-05 kg antimony eq), and isopropanol.(1.75E-05 kg antimony eq).

(6) Eutrophication potential (EP): The three processes that contributed the most were the production of tripropylene glycol methyl ether (3.82E-04 kg PO<sub>4</sub><sup>3-</sup>eq), isopropanol (1.74E-04 kg PO<sub>4</sub><sup>3-</sup>eq) and sodium lauryl amphoacetate (1.60E-04 kg PO<sub>4</sub><sup>3-</sup>eq).

(7) Inhalable inorganics (RI): The three processes that contributed the most were the production of isopropanol (5.55E-04 kg PM2.5eq), tripropylene glycol methyl ether (1.52E-04 kg PM2.5eq) and sodium lauryl amphoacetate (1.27E-04 kg PM2.5eq).

(8) Ozone depletion (ODP): The three processes with the largest contribution were the production of isotridecanol polyoxyethylene ether (2.02E-06 kg CFC-11eq), fatty alcohol polyoxyethylene ether M (1.26E-06 kg CFC-11eq) and isomeric ten alcohol polyoxyethylene ether (1.26E-06 kg CFC-11eq).

(9) Photochemical ozone synthesis (POFP): The three processes that contributed the most were the production of tripropylene glycol methyl ether (5.15E-4 kg NMVOC eq), isopropanol (3.18E-04 kg NMVOC eq) and isotridecanol polyoxyethylene ether (2.56E-04 kg NMVOC eq).

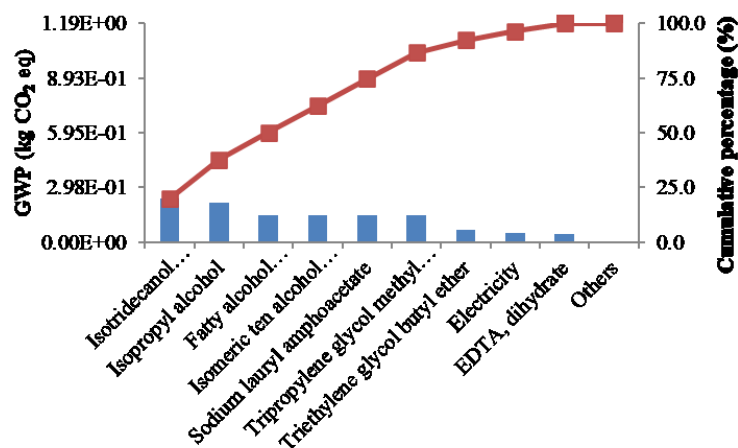


**Figure 3.** Climate change (GWP) results of coke cleaning agent



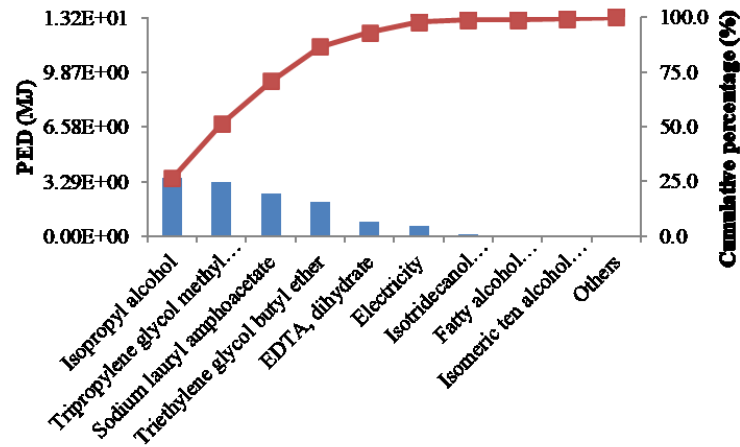


Figure 4. Primary energy consumption (PED) results of coke cleaning agent

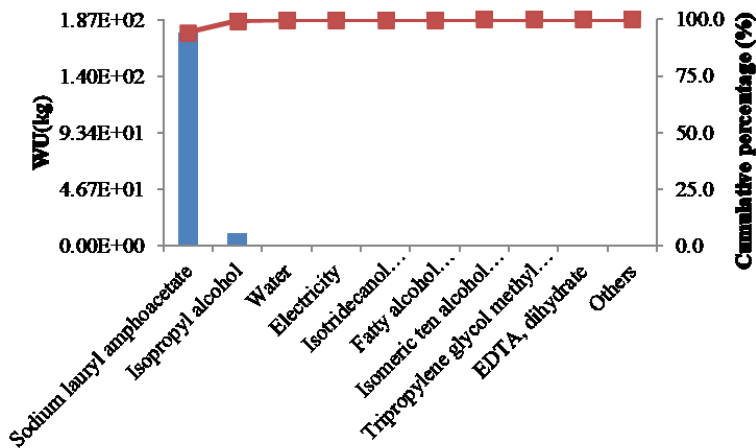


Figure 5. Water consumption (WU) results of coke cleaning agent

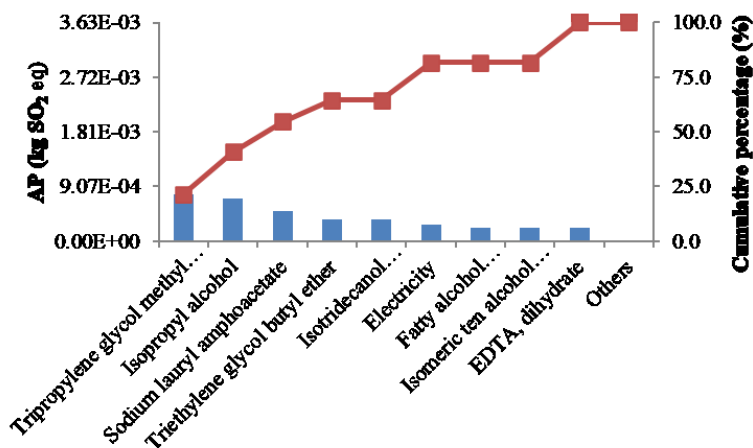


Figure 6. Acidification (AP) results of coke cleaning agent

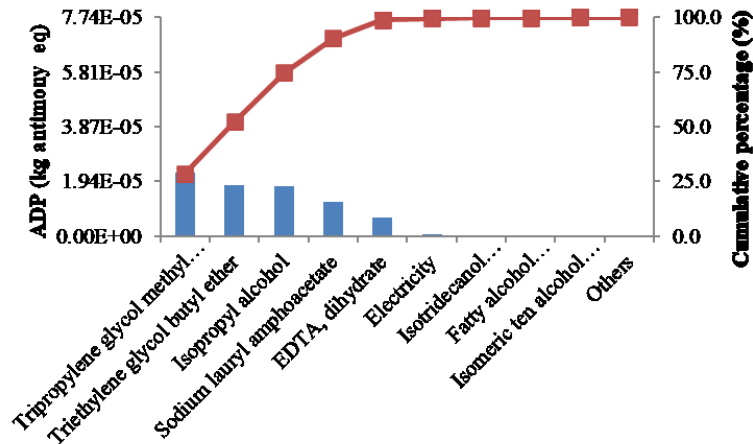


Figure 7. The results of abiotic resource consumption potential (ADP) of coke cleaning agent

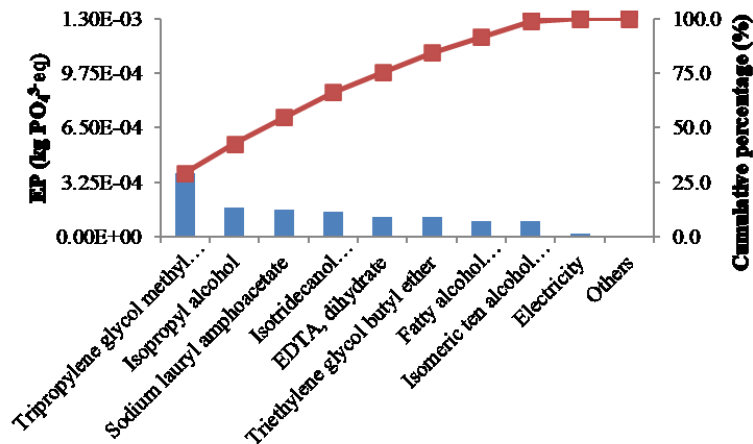


Figure 8. Eutrophication potential (EP) results of coke cleaning agent

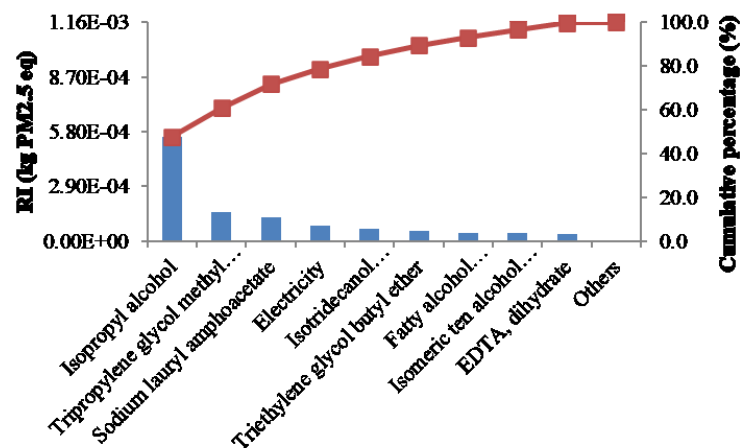


Figure 9. The results of inhalable inorganic matter (RI) of coke cleaning agent

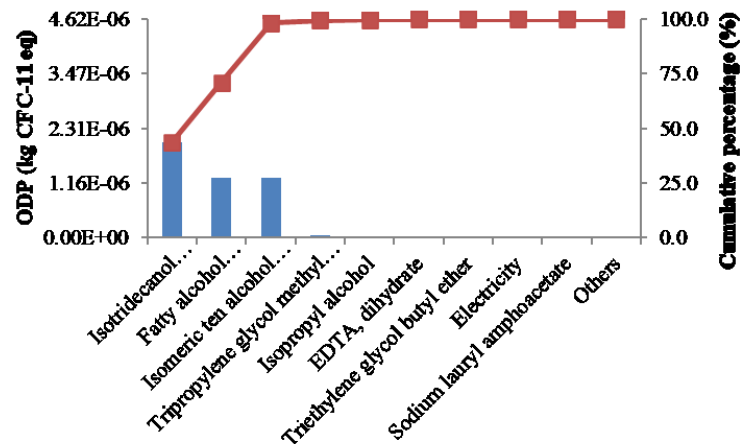


Figure 10. Ozone depletion (ODP) results of coke cleaning agent

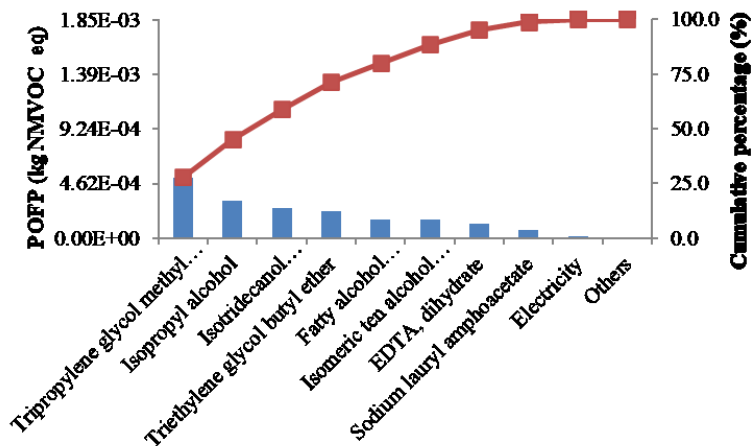


Figure 11. The results of photochemical ozone synthesis (POFP) of coke cleaning agent

### Inventory Data Sensitivity Analysis

Inventory data sensitivity refers to the corresponding indicator change rate caused by the unit change rate of inventory data. By analyzing the sensitivity of the inventory data to each indicator, and with the improvement of potential evaluation, the most effective improvement points can be identified.

The inventory data sensitivity of the coke cleaning agent and sodium lauryl amphotacetate are shown in Table 5 and Table 6, respectively.

According to the average sensitivity (contribution rate) analysis:

(1) The five processes with the highest average sensitivity were the production of sodium lauryl amphotacetate 20.27%, isopropanol 18.93%, tripropylene glycol methyl ether 17.62%, isotridecanol polyoxyethylene ether 11.70% and freshwater 10.46% in the process of sodium lauryl amphotacetate. The high water consumption in the production of sodium lauryl amphotacetate may be due to the fact that the last step in the production reaction requires the use of sodium hydroxide solution for acid-base neutralization. Dissolving the solid sodium hydroxide requires a large amount of water. The heat released by the neutralization reaction needs to be absorbed by a large amount of water.

**Table 5.** Table of inventory data sensitivity of coke cleaning agent

Process	GWP	PED	WU	AP	ADP
Sodium lauryl amphoacetate	12.23%	19.59%	94.23%	13.83%	15.67%
Isopropanol	17.93%	26.59%	5.26%	19.25%	22.61%
Tripropylene glycol methyl ether	12.13%	24.68%	9.34E-04%	21.51%	28.82%
Isotridecanol polyoxyethylene ether	19.77%	0.91%	0.02%	9.8%	0.14%
Triethylene glycol butyl ether	5.68%	15.97%	1.83E-04%	9.99%	23.43%
Fatty alcohol polyoxyethylene ether M	12.36%	0.57%	0.01%	6.13%	0.09%
Isomeric ten alcohol polyoxyethylene ether	12.36%	0.57%	0.01%	6.13%	0.09%
Disodium EDTA, dihydrate	3.55%	6.4%	2.09E-04%	5.98%	8.43%
Electricity	3.98%	4.7%	0.1%	7.36%	0.72%

**Table 5.** Table of inventory data sensitivity of coke cleaning agent (continued)

Process	EP	RI	ODP	POFP	Average sensitivity
Sodium lauryl amphoacetate	12.25%	10.93%	6.05E-04%	3.71%	20.27%
Isopropanol	13.35%	47.89%	0.32%	17.19%	18.93%
Tripropylene glycol methyl ether	29.29%	13.15%	1.16%	27.84%	17.62%
Isotridecanol polyoxyethylene ether	11.39%	5.8%	43.64%	13.85%	11.70%
Triethylene glycol butyl ether	9.08%	4.84%	0.13%	12.51%	9.07%
Fatty alcohol polyoxyethylene ether M	7.12%	3.63%	27.28%	8.66%	7.32%
Isomeric ten alcohol polyoxyethylene ether	7.12%	3.63%	27.28%	8.66%	7.32%
Disodium EDTA, dihydrate	9.12%	3.24%	0.2%	6.52%	4.83%
Electricity	1.27%	6.88%	2.62E-03%	1.07%	2.90%

Note: The average sensitivity of each component in the list is the average of the sensitivity of the 9 indicators, which are GWP, PED, WU, AP, ADP, EP, RI, ODP and POFP.

(2) In the carbon footprint (GWP), the top five processes with the highest sensitivity were the production of isotridecanol polyoxyethylene ether 19.77%, isopropanol 17.93%, isodecanol polyoxyethylene ether 12.36%, fatty alcohol polyoxyethylene ether M 12.36% and sodium lauryl amphoacetate 12.23%.

(3) Among the primary energy consumption (PED), the top five processes with the highest sensitivity were the production of isopropanol 26.59%, tripropylene glycol methyl ether 24.68%, sodium lauryl amphoacetate 19.59%, triethylene glycol butyl ether 15.97% and disodium EDTA, dihydrate 6.40%.

(4) Among water resources consumption (WU), the top five processes with the highest sensitivity were the production of sodium lauryl amphoacetate 94.23%, freshwater 94.18% and isopropanol 5.26%

(5) In acidification (AP), the top five processes with the highest sensitivity were the production of tripropylene glycol methyl ether 21.51%, isopropanol 19.25%, sodium lauryl amphoacetate 13.83%, triethylene glycol butyl ether 9.99% and isotridecanol polyoxyethylene ether 9.80%.

(6) In the non-biological resource consumption potential value (ADP), the top five processes with the highest sensitivity were the production of tripropylene glycol methyl ether 28.82%, triethylene glycol butyl ether 23.43%, isopropanol 22.61%, sodium lauryl amphoacetate 15.67% and natural gas 10.69%.

(7) Among the eutrophication potential value (EP), the top five processes with the highest sensitivity were the production of tripropylene glycol methyl ether 29.29%, isopropanol 13.35%, sodium lauryl amphoacetate 12.25%, isotridecanol polyoxyethylene ether 11.39% and disodium EDTA, dihydrate 9.12%.

**Table 6.** Table of inventory data sensitivity of sodium lauryl amphoacetate (unit:%)

Process	GWP	PED	WU	AP	ADP	EP	RI	ODP	POFP	Average sensitivity
Freshwater	0	0	94.18	0	0	0	0	0	0	10.46
Natural gas	0	6.4	0	0	10.69	0	0	0	0	1.90
Electricity	2.67	2.92	0.05	4.56	0.47	0.85	4.13	6.05 E-04	0.64	1.81
CO <sub>2</sub>	7.44	0	0	0	0	0	0	0	0	0.83
Nitrogen oxides	0	0	0	3.5	0	1.81	1.99	0	0	0.81
Crude	0	2.5	0	0	4.2	0	0	0	0	0.74
SO <sub>2</sub>	0	0	0	3.1	0	0	0.76	0	0.49	0.48
Nitrogen	0	0	0	0	0	4.1	0	0	0	0.46
Solar energy	0	4.07	0	0	0	0	0	0	0	0.45
Ammonia	0	0	0	2	0	1.04	0.4	0	0	0.38
PM2.5	0	0	0	0	0	0	3.08	0	0	0.34
Nitrate	0	0	0	0	0	2.35	0	0	0	0.26
Non-methane volatile organic compounds	0	0	0	0	0	0	0	0	1.92	0.21
Hard coal	0	1.2	0	0	0.17	0	0	0	0	0.15
Uranium	0	1.17	0	0	0	0	0	0	0	0.13
Phosphate	0	0	0	0	0	1.1	0	0	0	0.12
CO <sub>2</sub> (fossil source)	1.08	0	0	0	0	0	0	0	0	0.12
Lignite	0	0.9	0	0	0.12	0	0	0	0	0.11
N <sub>2</sub> O	0.39	0	0	0	0	0.27	0	0	0	0.07
CH <sub>4</sub>	0.65	0	0	0	0	0	0	0	0	0.07
NO	0	0	0	0.34	0	0	0.2	0	0	0.06

Note: The average sensitivity of each component in the list is the average of the sensitivity of the 9 indicators, which are GWP, PED, WU, AP, ADP, EP, RI, ODP and POFP.

(8) Among inhalable inorganic substances (RI), the processes with the highest sensitivity were the production of isopropanol 47.89%, tripropylene glycol methyl ether 13.15%, sodium lauryl amphoacetate 10.93%, electricity 6.88% and isotridecanol polyoxyethylene ether 5.80%.

(9) Among the ozone layer depletion (ODP), the processes with the highest sensitivity were the production of isotridecanol polyoxyethylene ether 43.64%, the production of isomeric ten alcohol polyoxyethylene ether 27.28%, and the production of fatty alcohol polyoxyethylene ether M 27.28%

(10) In photochemical ozone synthesis (POFP), the processes with the highest sensitivity were the production of tripropylene glycol methyl ether 27.84%, isopropanol 17.19%, isotridecanol polyoxyethylene ether 13.85%, triethylene glycol butyl ether 12.51%, fatty alcohol polyoxyethylene ether M 8.66%.

Through comprehensive analysis, the production of tripropylene glycol methyl ether, the production of isopropanol, the production of sodium lauryl amphoacetate and the production of isotridecanol polyoxyethylene ether have a significant impact on every LCA index. So they are the focuses of technology improvement.

#### *Product Improvement Project*

Isomeric ten alcohol polyoxyethylene ether, isotridecanol polyoxyethylene ether and fatty alcohol polyoxyethylene ether M account for the highest proportion in the formula, and are the necessary active ingredients in cleaning products as surfactants. It is

recommended to develop cleaner production processes or to partially replace such products with surfactants which have cleaner production processes.

Isopropyl alcohol and tripropylene glycol methyl ether also account for high proportion in the formula as organic solvents in the cleaning agent, which can speed up the penetration of the cleaning agent into the dirt. It is recommended to reduce the carbon footprint by appropriately reducing the amount of isopropanol through further research.

## Life Cycle Explanation

### *Assumptions and Limitations Statement*

In this study, the results of 9 indicators of the production process of the coke cleaning agent were calculated. Formulations are determined by this study and do not represent industry average emissions. The LCA study simplified the actual formulation, reducing the number of surfactants to 2, assuming similar emission data for the production processes of other surfactants in the original formulation.

The types of organic solvents were reduced to 2, assuming similar emission data for production processes of other organic solvents. When simulating the calculation process, only the energy consumption of the core equipment was calculated. It was assumed that when the number of the main equipment increased, only electricity was consumed, and the emissions of the process would not increase.

The data assumptions of each unit process model are described in table 7.

**Table 7.** Description of model assumptions

Process name	Model assumptions analysis
coke cleaning agent [Production]	The emission parameters of similar constituent compounds are similar, and the formulation is simplified. When the major equipment was added, only electricity was consumed, and the emissions of the process would not increase.
sodium lauryl amphoacetate [Production]	The technology with the same process and emissions was used, and the electricity consumption was localized.

### *Completeness Statement*

Strict mass balance and energy balance calculations were carried out in the production process of coke cleaning agent. Literature research was carried out on the emission data, and the average value of many literatures was used.

The dataset of sodium lauryl amphoacetate includes upstream raw material, energy and other data subsets and all emission data. To avoid double counting of emission data, all input data except electricity was ignored.

**Table 8.** Summary table of materials with missing or omitted data in the production process of sodium lauryl amphoacetate

Consumption name	Upstream data source	Quantity unit	Weight ratio	Test result
exhaust gas	negligible	0.3861kg	38.61%	Low-value waste from upstream, negligible
clay	negligible	6.2476E-05kg	0.01%	Comply with the selection rule
manganese	negligible	1.5903E-06kg	0%	Comply with the selection rule
dolomite	negligible	1.0391E-06kg	0%	Comply with the selection rule
crude potassium salt	negligible	0.0093kg	0.93%	Low-value waste from upstream, negligible
bauxite	negligible	4.8775E-06kg	0%	Comply with the selection rule
limestone	negligible	0.0028kg	0.28%	Low-value waste from upstream, negligible
chromium	negligible	2.865E-06kg	0%	Comply with the selection rule
fluorite	negligible	1.1383E-05kg	0%	Comply with the selection rule

Note: \* weight ratio = material weight \* quantity / product weight;

\* The weight ratio of total ignored materials = the weight ratio of missing data + the weight ratio that meets the selection rule.

#### Data Quality Assessment Results

The report adopted the CLCD quality assessment method and completed the uncertainty assessment of the model inventory data on the eFootprint system. The results of the data quality assessment are shown in Table 9.

**Table 9.** LCA data quality assessment results

Indicator name	Abbreviation (Unit)	LCA results	Result uncertainty	Upper and lower result limits (95% confidence interval)
Climate change	GWP(kg CO <sub>2</sub> eq)	1.158E+000	6.06%	[1.09,1.23]
Primary energy consumption	PED(MJ)	1.279E+001	6.31%	[11.98,13.6]
Water consumption	WU(kg)	1.866E+002	24.05%	[141.72,231.48]
Acidification	AP(kg SO <sub>2</sub> eq)	3.461E-003	4.65%	[3.30E-03,3.62E-03]
Abiotic resource consumption potential	ADP(kg antimony eq.)	7.716E-005	8.32%	[7.07E-05,8.35E-05]
Eutrophication potential	EP(kg PO <sub>4</sub> <sup>3-</sup> eq)	1.292E-003	4.78%	[1.23E-03,1.35E-03]
Inhalable inorganic substances	RI(kg PM2.5 eq)	1.110E-003	9.56%	[1.00E-03,1.22E-03]
Ozone depletion	ODP(kg CFC-11 eq)	4.637E-006	11.20%	[4.11E-06,5.15E-06]

The result uncertainty data was plotted, as shown in Figure 1-12, and the analysis showed that the result uncertainty was between 4.20% and 24.05%. The data source is credible. The results obtained from the analysis have a certain guiding effect on the design of the subsequent product as a real coke cleaning agent.

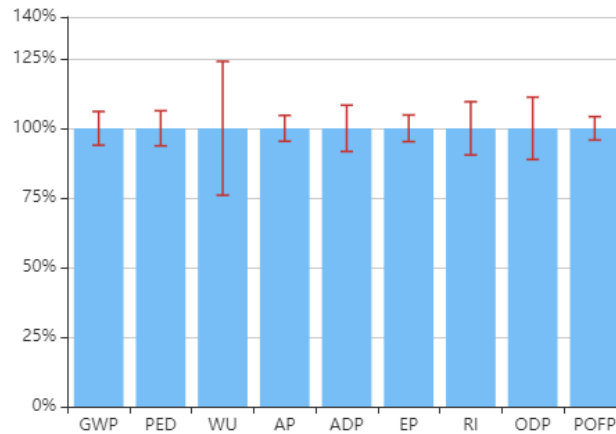


**Figure 12.** LCA result uncertainty

## CONCLUSIONS

In this study, the life cycle of the developed coke cleaning agent was analyzed. The technology is phosphorus-free and environmentally friendly, which has a very broad market prospect. The life cycle model is cradle-to-gate (out of factory), and the background database included power grids, transportation and chemicals. Computer simulation was used to carry out strict mass balance and energy consumption balance on the production process. The study combined production plant data and published literature to analyze emissions.

(1) The life cycle model analysis of the established model showed that the climate change (GWP) of producing 1kg of coke cleaning agent was 1.19kg CO<sub>2</sub> eq; the primary energy consumption (PED) was 13.17MJ; the water consumption (WU) was 186.74 kg; acidification (AP) was 3.63E-03 kg SO<sub>2</sub> eq; abiotic resource consumption potential (ADP) was 7.75E-05 kg antimony eq; eutrophication potential (EP) was 1.30E-03 kg PO<sub>4</sub><sup>3-</sup> eq; inhalable inorganic (RI) was 1.16E-03 kg PM<sub>2.5</sub> eq; ozone depletion (ODP) was 4.63E-06 kg CFC-11 eq; and photochemical ozone synthesis (POFP) was 1.85E-03 kg NMVOC eq. The uncertainty of the results was between 4.20% and 24.05%.

(2) Carbon footprint (GWP) analysis showed that isotridecanol polyoxyethylene ether, isopropyl alcohol, fatty alcohol polyoxyethylene ether M and isomeric ten alcohol polyoxyethylene ether contributed the most.

(3) The average sensitivity analysis showed that the most influential process were sodium lauryl amphoacetate, isopropanol, tripropylene glycol methyl ether. Therefore they were the focuses of improvement.

(4) It was recommended to reduce the amount of isopropanol through research and development, and at the same time surfactants with cleaner production processes should be used to partially replace polyoxyethylene ethers to reduce carbon footprint.



## ACKNOWLEDGMENTS

We are grateful for the support from the School of Chemical Engineering and Pharmacy at the Wuhan Institute of Technology.

## CONFLICTS OF INTEREST

The authors declare that there is no conflict of interests regarding the publication of this paper.

## REFERENCES

- [1] Zhang, M., and Wang, J.P. (2018). The current situation and development trend of domestic kitchen water-based cleaning agents. *Modern Salt Chemical Industry*, (03), 13-14. DOI: 10.19465/j.cnki.2095-9710.2018.03.007
- [2] Yan, Y., Li D.W., and Chen Y. (2013). Discussion on the formula design of kitchen grease and its cleaning agent. *Daily Chemical Science*, 36(12), 29-32. DOI: 10.13222/j.cnki.dc.2013.12.015
- [3] Yu, C.Y. (2000) Discussion on chemical cleaning of oil and scorch in industrial equipment. *Chemical Equipment and Anti-corrosion*, (01), 29-34.
- [4] Alargova, R. G., Kochijashky, I. I., Sierra, M.L., Kwetkat, K., and Zana, R. (2001) Mixed micellization of dimeric (Gemini) surfactants and conventional surfactants. *Journal of Colloid and Interface Science*. 235, 119-129. DOI: 10.1006/jcis.2000.7311
- [5] Pan, M.D., Chen, X.L., and Fan, H.L. (2019). Development of water-based high-efficiency brightening and rust-proof metal cleaning agent. *Plating and Finishing*, 38(5), 224-228. DOI: 10.19289/j.1004-227x.2019.05.008
- [6] Xiao, X. F., Liu, R. F., and Zheng, Y. Z. (2006). Characterization of hydroxyapatite /titania composite coatings codeposited by a hydrotherm al-electroche mical method on titanium. *Surface & Coatings Technology*, 200(14/15), 4406-4413. DOI: 10.1016/j.surfcoat.2005.02.205
- [7] Tao, Y., Zhang, W., and Wang, F.S. (2018). Application progress of alkyl glycosides in the field of water-based metal cleaners. *Cleaning World*, 34(1), 25-32.
- [8] Xiao, R., Xiao, G., Huang, B., Feng, J., and Wang, Q. (2016). Corrosion failure cause analysis and evaluation of corrosion inhibitors of ma huining oil pipeline. *Engineering Failure Analysis*, 68, 113-121. DOI: 10.1016/j.engfailanal.2016.05.029
- [9] Zhang, H. H., Gao, K. W., Yan, L. C., and Pang, X. L. (2017). Inhibition of the Corrosion of X70 and Q235 Steel in CO<sub>2</sub>-Saturated Brine by Imidazoline-Based Inhibitor. *Journal of Electroanalytical Chemistry*, 791, 83-94.
- [10] Wei, M., and Zhu, Y. (2007). Preparation of phosphorus-free water-based cleaning agent for metals. *Materials Protection*. DOI: 10.2514/1.26230
- [11] Finnveden, G., Hauschild, M. Z., Ekvall, T., J Guinée, and Suh, S. (2010). Recent developments in life cycle assessment. *Journal of Environmental Management*, 91(1), 1-21. DOI: 10.1016/j.jenvman.2009.06.018
- [12] Rebitzer, G., Ekvall, T., Frischknecht, R., Hunkeler, D., Norris, G., Rydberg, T., Schmidt, W.P., Suh, S., Weidema, B.P., and Pennington, D.W. (2004). Life cycle

- assessment part 1: framework, goal and scope definition, inventory analysis, and applications. *Environment International*, 30(5), 701-720. DOI: 10.1016/j.envint.2003.11.005
- [13] Hoof, G.V., Schowanek, D., and Feijtel, T.J.T. (2003). Comparative Life-Cycle Assessment of laundry detergent formulations in the UK. part I: Environmental fingerprint of five detergent formulations in 2001. *Tenside Surfactants Detergents*, 40(5), 266-275.
- [14] Saouter, E., Hoof, G.V., Feijtel, T.C.J., and Owens, J.W. (2002). The effect of compact formulations on the environmental profile of Northern European granular laundry detergents Part II: Life Cycle assessment. *The International Journal of Life Cycle Assessment*, 7(1), 27-38. DOI: 10.1007/BF02978907
- [15] Chen, M., and Cui, Q.F. (2007). Synthesis of sodium dodecyl sulfate by sulfamic acid. *Experimental Technology and Management*, 24(4), 3. DOI: 10.3969/j.issn.1002-4956.2007.04.011

**Article copyright:** © 2022 Yu Gong, Changyan Yang, Yinhang Qu, Jiayi Li, Bohan Yang, Yigang Ding, Bo Zhang. This is an open access article distributed under the terms of the [Creative Commons Attribution 4.0 International License](https://creativecommons.org/licenses/by/4.0/), which permits unrestricted use and distribution provided the original author and source are credited.





**CALL FOR PAPERS**

# Trends in Renewable Energy

ISSN Print: 2376-2136 ISSN online: 2376-2144

<http://futureenergysp.com/index.php/tre/>

Trends in Renewable Energy (TRE) is an open accessed, peer-reviewed semi-annual journal publishing reviews and research papers in the field of renewable energy technology and science. The aim of this journal is to provide a communication platform that is run exclusively by scientists. This journal publishes original papers including but not limited to the following fields:

- ✧ Renewable energy technologies
- ✧ Catalysis for energy generation, Green chemistry, Green energy
- ✧ Bioenergy: Biofuel, Biomass, Biorefinery, Bioprocessing, Feedstock utilization, Biological waste treatment,
- ✧ Energy issues: Energy conservation, Energy delivery, Energy resources, Energy storage, Energy transformation, Smart Grid
- ✧ Environmental issues: Environmental impacts, Pollution
- ✧ Bioproducts
- ✧ Policy, etc.

We publish the following article types: peer-reviewed reviews, mini-reviews, technical notes, short-form research papers, and original research papers.

*The article processing charge (APC), also known as a publication fee, is fully waived for the Trends in Renewable Energy.*

## Call for Editorial Board Members

We are seeking scholars active in a field of renewable energy interested in serving as volunteer Editorial Board Members.

### Qualifications

Ph.D. degree in related areas, or Master's degree with a minimum of 5 years of experience.

All members must have a strong record of publications or other proofs to show activities in the energy related field.

If you are interested in serving on the editorial board, please email CV to

[editor@futureenergysp.com](mailto:editor@futureenergysp.com).